Ju Lee Kim

Differentiation of mouse germline stem cells into meiotic germ cells

2013

Biologie

Differentiation of mouse germline stem cells into meiotic germ cells

Inaugural-Dissertation

zur Erlangung des Doktorgrades

der Naturwissenschaften im Fachbereich Biologie

der Mathematisch-Naturwissenschaftlichen Fakultät

der Westfälischen Wilhelms-Universität Münster

vorgelegt von

Ju Lee Kim

aus Seoul

-2013-

Dekan:	Prof. Dr. Dirk Prüfer
Erster Gutachter:	Prof. Dr. Hans R. Schöler
Zweiter Gutachter:	Prof. Dr. Martin Bähler
Tag der mündlichen Prüfung:	21.10.2013
Tag der Promotion:	25.10.2013

Table of contents

1. Summary 1

2. Introduction 3

2.1 Germ cell development 3

2.1.1 Spermatogonial stem cells 4

2.1.2 Spermatogenesis 6

2.2 *In vitro* culture of spermatogonial stem cells 10

2.2.1 Role of growth factors in spermatogonial stem cell proliferation 11

2.2.2 Restoration of spermatogenesis by spermatogonial stem cell transplantation 13

2.3 Reprogramming of germline stem cells 14

2.4 Differentiation of germline stem cells 15

3. Aim 19

4. Material and methods 21

4.1 Animals 21

4.2 Generation and culture of different cells 21

4.2.1 Derivation of mouse germline stem cells 21

4.2.2 Derivation of mouse embryo fibroblasts 22

4.2.3 Culture of mouse embryo fibroblasts 22

4.2.4 Culture of mouse germline stem cells 23

4.2.5 Culture of mouse embryonic stem cells 23

4.2.6 Culture of mouse germline-derived pluripotent stem cells 24

4.2.7 Culture of OP9 cells 24

4.2.8 Culture of human embryonic stem cells 25

4.2.9 Culture of Sertoli cells 25

4.2.10 Differentiation of mouse germline-derived pluripotent stem cells into endothelial cell-like cells 26

4.2.11 *In vitro* differentiation of germline stem cells into meiotic germ cells....26

4.3 Characterization of mouse germline-derived pluripotent stem cells 27

4.3.1 Alkaline phosphatase staining....27

4.3.2 *In vitro* differentiation of germline-derived pluripotent stem cells 28

4.3.3 Teratoma formation 28

4.3.4 Chimera formation....28

4.3.5 Analysis for potency and functionality of mouse germline stem cells 29

4.3.5.1 Testicular transplantation....29

4.4 Analyses....29

4.4.1 Messenger RNA expression....29

4.4.1.1 RNA isolation 29

4.4.1.2 Complementary DNA synthesis 30

4.4.1.3 RT-PCR analysis....30

4.4.1.4 Real-time RT-PCR analysis....32

4.4.1.5 Micro array analysis....34

4.4.1.5.1 Whole genome expression analysis 34

4.4.1.5.2 Microarray data processing....34

4.4.2 Protein expression....34

4.4.2.1 Flow cytometry 34

4.4.2.2 Immunocytochemistry 35

4.4.2.3 Immunocytochemistry of spermatocytes with synaptonemal complex protein 3 35

4.4.3 Transmission electron microscopy 36

4.4.4 Round spermatid injection 36

4.4.5 Derivation of embryonic stem cell lines 37

4.4.6 Karyotyping of round spermatid injection-derived embryonic stem cell lines...37

4.4.7 Genotyping of round spermatid injection-derived embryonic stem cell lines....38

4.4.8 DNA methylation analysis.....38

5. Results.....40

5.1 Derivation of germline stem cells.....40

5.1.1 Derivation of germline stem cells form mouse testes.....40

5.1.2 Derivation of germline stem cells from human testicular biopsies.....42

5.2 Conversion of unipotent germline stem cells into pluripotent germline-derived stem cells.....48

5.2.1 Conversion of germline stem cells from autologous testicular biopsy into germline-derived pluripotent stem cells.....48

5.2.2 Characterization of germline stem cells from autologous testicular biopsy into germline-derived pluripotent stem cells.....49

5.2.3 Differentiation ability of germline-derived pluripotent stem cells 60

5.2.3.1 *In vitro* and *in vivo* differentiation ability analysis 60

5.2.3.2 Differentiation of germline-derived pluripotent stem cells into endothelial cell-like cells 62

5.3 *In vitro* differentiation of germline stem cells 70

5.3.1 Differentiation of germline stem cells into meiotic cells.....70

5.3.2 Characterization of meiotic cells 71

5.3.2.1 Flow cytometry analysis of *in vitro*-generated cells.....71

5.3.2.2 Immunofluorescence staining 73

5.3.2.3 Transmission electron microscopy 75

5.3.2.4 Real-time RT-PCR analysis.....81

5.3.2.5 Round spermatid injection, embryo transfer, and derivation of embryonic stem cells 82

5.3.2.6 Flow cytometry analysis 85

5.3.2.7 Karyotyping 86

5.3.2.8 Methylation analysis 86

5.3.2.9 Characterization of round spermatid injection-derived *Acrosin* embryonic stem cells 87

5.4 Derivation of germline stem cells from OG2 x *Acrosin EGFP* mouse testes 88

6. Discussion 90

6.1 Characteristics of germline stem cells 90

6.1.1 Potency and functional analysis of germline stem cells 91

6.1.2 Self-reprogramming ability of germline stem cells into pluripotent cells 92

6.1.3 Differentiation ability of germline-derived pluripotent stem cells into endothelial-like cells 92

6.2 *In vitro* spermatogenesis of germline stem cells 94

7. References 100

8. Abbreviations 111

9. List of figures 115

10. List of tables 118

11. Appendix 119

11.1 Companies 119

1. Summary

During spermatogenesis, spermatogonial stem cells (SSCs) continuously give rise to mature male germ cells, which contain the genetic information that is transmitted to the next generation. SSCs, also known as germline stem cells (GSCs), can be cultured and maintained *in vitro* without significant loss of their typical characteristics, such as grape-like morphology, expression of specific marker genes including *Oct4*, *Tex18*, *Piwil2*, *Vasa*, *Dazl*, *Utf1*, and *Fragilis* at molecular level and CD9, CD90, integrin alpha6, integrin beta1, and Vasa at the protein level. *In vivo* these stem cells are unipotent as they normally only give rise to sperm. The possibility to sustain GSCs *in vitro* could provide research models to study the molecular mechanisms involved in reprogramming and differentiation of GSCs as well as application of these models in different fields e.g.- potential clinical application, drug development, or gene correction therapy.

Recently germline-derived pluripotent stem cells (gPSCs) were generated from fetal or adult GSCs. Under specific culture conditions, without activation through exogenous transcription factors, pluripotency could be induced in otherwise unipotent GSCs. These gPSCs are very similar to other pluripotent stem cells, such as embryonic stem cells (ESCs). Pluripotency of gPSCs was confirmed *in vitro* by their ESC-like morphology, gene expression profile, and differentiation ability into three germ layers, *in vivo* by chimera formation, germline contribution, and germline transmission.

In the present thesis, gPSCs were evaluated as a source for the derivation of one kind of somatic cells, namely endothelial (EC)-like cells. The gPSC-derived EC-like cells showed cobblestone morphology, typical of endothelial cells. They were characterized at molecular and cellular level and revealed expression of endothelial cell-specific markers including Tie2, CD31, VE-Cadherin, vWF, Flk1, Flt1, and Icam2. In addition, *in vitro* functionality of the EC-like cells was confirmed by Dil-conjugated acetylated low-density lipoprotein (LDL) uptake and tube formation assay, when cultured on matrigel.

Another study described in the present thesis is the stepwise generation of different types of spermatogenetic cells from established GSCs. The initial step of *in*

vitro spermatogenesis, namely differentiation of GSCs into meiotic cells is associated with changes in c-kit protein expression. The developmental status of GSCs into premeiotic cells was determined by c-kit protein expression in a time course during differentiation using flow cytometry analysis. At the beginning of *in vitro* differentiation, nominal levels of c-kit were detected, while c-kit expression was upregulated during the period of the first differentiation step. Upregulation was followed by subsequent downregulation, indicating that GSCs enter the first wave of spermatogenesis known as spermatocytogenesis. The transition of mitosis to meiosis, which is defined by the occurrence of DNA recombination, was confirmed by immunofluorescence staining for synaptonemal complex protein 3 (Scp3), a specific maker for meiotic cells in the first meiotic division. Typical staining of spermatocytes at various stages of meiosis I was distinguishable either by their punctuated or elongated form. The derivation of primary spermatocyte-like cells from GSCs was further confirmed by gene expression analysis of the premeiotic marker *Oct4* and the meiotic markers *Stra8*, *Dmc1*, and *Scp3*.

This *in vitro* system using GSCs will help elucidate the underlying processes and mechanisms required for the first wave of spermatogenesis, as well as the study of spermatocytogenesis and the onset and progression of meiosis. Further steps will be required to develop an *in vitro* culture system to obtain even later stages of spermatogenesis

2. Introduction

2.1 Germ cell development

Primordial germ cells (PGCs) are the precursors of gametes that differentiate in gonads. During embryogenesis, PGCs form clusters within the extra-embryonic mesoderm and increase in number, when they are in the midline extra-embryonic mesoderm posterior to the primitive streak. The specification of germ cells to PGCs is induced under the control of pathways of bone morphogenetic proteins (BMP) and members of the transforming growth factor beta (TGF-b) super family BMP4 and 8b are expressed in the extra-embryonic ectoderm posterior to the primitive streak and play a role in the induction of PGCs from the proximal epiblast and formation of PGC precursors. BMP signaling is transduced through decapentaplegic homolog proteins (SMAD) including SMAD1 and 5, other types of the TGF-b super family, which are expressed in the proximal cells of the epiblast. In addition, it has been suggested that B-lymphocyte-induced maturation protein 1 (Blimp1, also known as Prdm1) is also required to induce PGCs. Blimp1 starts to be expressed in the epiblast, subsequently in the proximal layer of the epiblast and eventually its expression is restricted to the founder population of PGCs (Ko and Schöler, 2006; Ying et al., 2002).

At 6.0 days post coitum (dpc), also termed embryonic day 6.0 (E6.0), PGC precursors are set aside from the epiblast and at 7.25 dpc form a cluster of about 40 founder cells located in the extra-embryonic region of the primitive streak. At 8.0 dpc, PGCs are located at the base of the allantois. The cells migrate along the hindgut around 9.5 dpc, the dorsal mesentery at 10.5 dpc and enter the genital ridges at 11.5 dpc. Subsequently, at 12.5 dpc, most cells have reached the gonads, where they continue to actively proliferate. Until 13.5 dpc, the number of PGCs rises to 25.000 cells. Between 13.5 dpc and 14.5 dpc, female PGCs (now called oogonia) enter prophase I of meiosis and undergo meiotic arrest at the diplotene stage around birth (Ginsburg et al., 1990; McLaren, 2003; Molyneaux et al., 2001; Saitou, 2009; Sasaki and Matsui, 2008), while male germ cells are arrested until birth and become prospermatogonia also known as gonocytes in the postnatal testis. They enter meiosis around postnatal day (PND) 3 giving rise to spermatogonia (McLaren, 2003).

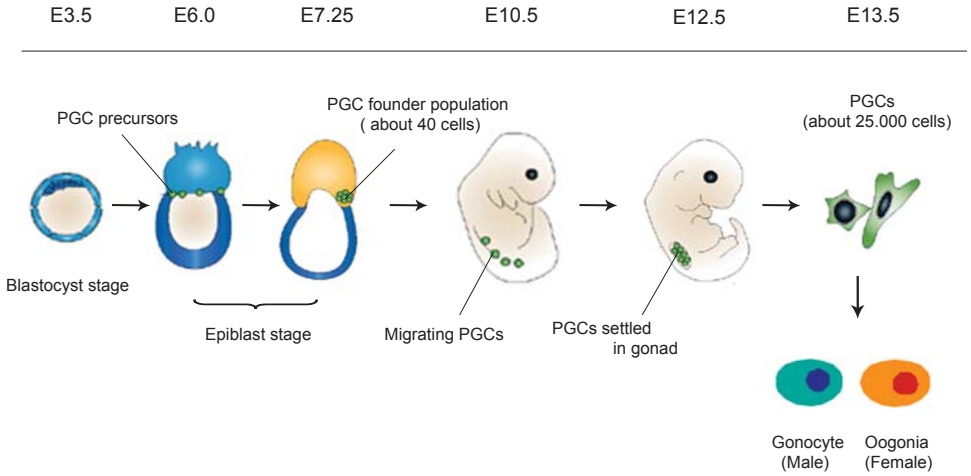

Figure 1. Germ cell development (figure modified from Sasaki *et al*, *Nature Reviews Genetics*, 2008). At embryonic day 3.5 (E3.5), the inner cell mass is formed, afterwards becoming epiblast. PGC precursors appear at around E6.0 and develop into PGC founder population (about 40 cells) at around E7.25, which are located in the extra-embryonic region of the primitive streak. PGCs start to migrate from the allantois through hindgut and mesentery, finally reaching the genital ridge and settle at E12.5. At E13.5, the number of PGCs increases to about 25.000 cells and in the male, PGCs enter mitotic arrest, while in the female, PGCs enter meiosis.

2.1.1 Spermatogonial stem cells

SSCs are male GSCs and localized on the basement membrane of seminiferous tubules in the testis. They can either renew themselves to maintain the stem cell pool or differentiate into mature spermatogenetic cells in order to transit the genetic information to the next generation. The balance of self-renewal and differentiation *in vivo* is controlled precisely. Mouse testes contain undifferentiated spermatogonial population including type A_{single}, A_{paired}, $A_{aligned\text{-}4}$, $A_{aligned\text{-}8}$, $A_{aligned\text{-}16,}$ and differentiating spermatogonial population including type A_1, A_2, A_3, A_4, intermediate spermatogonia, and type B spermatogonia. In particular, type A_{single} spermatogonia can be identified as self-renewing stem cells. In primates, type A_{dark} and A_{pale} spermatogonia are considered to be undifferentiated spermatogonial populations, namely resting (A_{dark}) and active (A_{pale}) SSC populations. They divide further into differentiating spermatogonial populations including type B_1, B_2, B_3, and B_4 spermatogonia (Oatley and Brinster, 2012).

Two ways of proliferation have been suggested in terms of mitotic division of spermatogonial populations: in one case division is symmetric, in the other it is asymmetric. In the case of symmetric division, one self-renewing spermatogonium results in two identical self-renewing spermatogonia, whereas another spermatogonium produces two committed daughter cells that during spermatogenesis differentiate into sperm. In case of an asymmetric division, one self-renewing spermatogonium divides into a self-renewing spermatogonium and a committed progenitor spermatogonium through the transient amplifying progenitor (de Rooij and Russell, 2000).

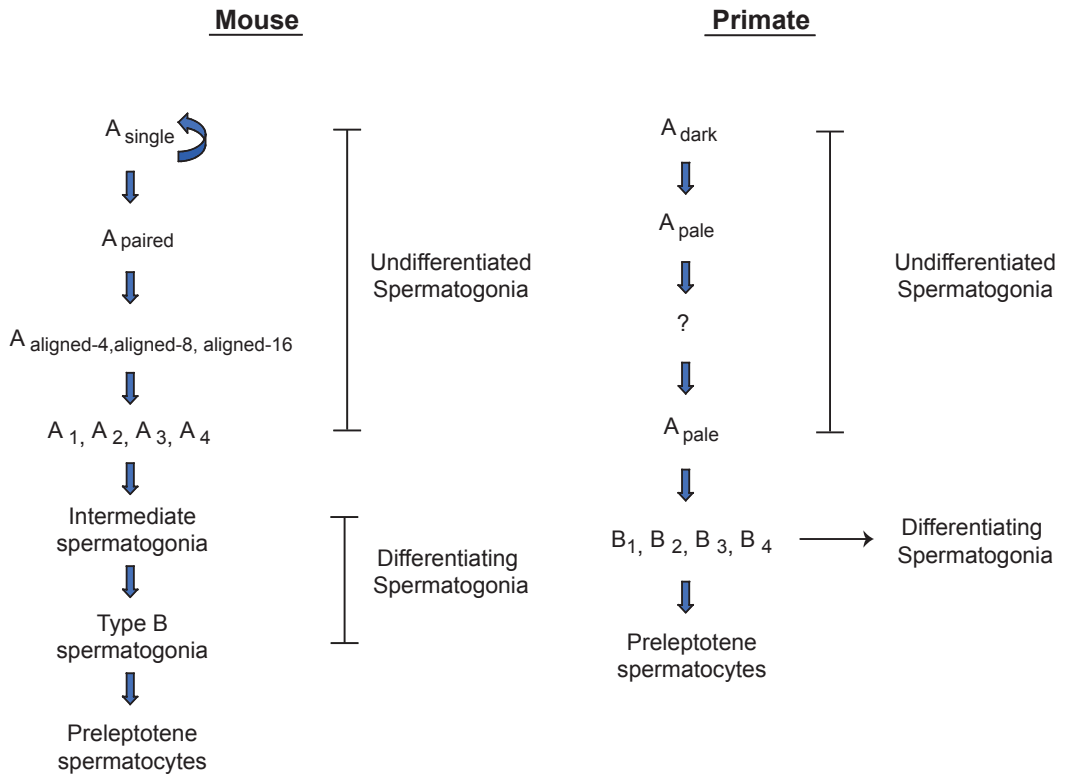

Figure 2. Mitotic division of spermatogonia in mouse and primate (figure modified from Oatley and Brinster, *Physiol Rew*, 2012). There are two types of spermatogonia in spermatogonial development-i.e. undifferentiated spermatogonia and differentiating spermatogonia. The number of mitotic cell divisions is species-dependent and it has not yet been exactly known in primate, in contrast to other species including mouse.

2.1.2 Spermatogenesis

Spermatogenesis is a multi-step process and can be distinguished in three major phases: spermatocytogenesis, meiosis, and spermiogenesis.

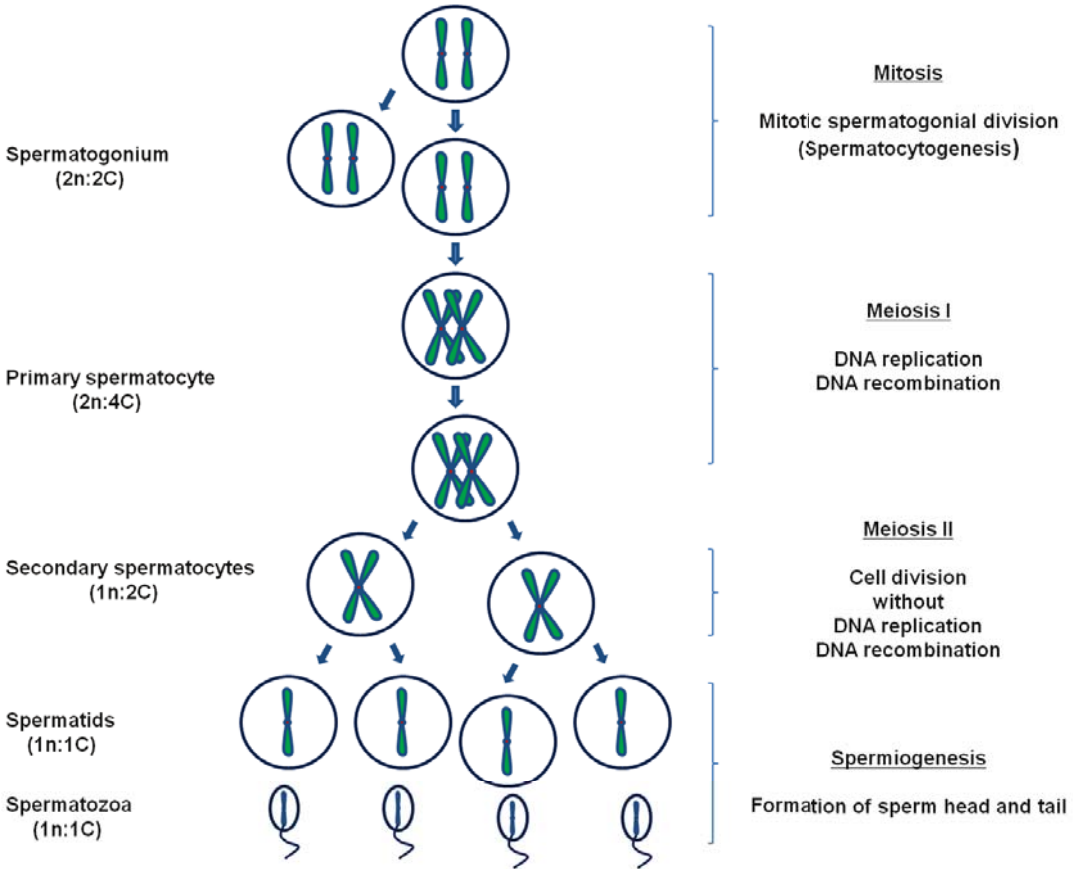

Figure 3. Schematic description of spermatogenesis (figure modified from Wolgemuth, *Nature Genetics*, 2006). At the beginning of spermatogenesis, the proliferative spermatogonia divide through other subtypes of spermatogonia into preleptotene spermatocytes. Subsequently, they undergo two meiotic phases and during these phases, primary and secondary spermatocytes are generated. Finally after completion of meiosis, spermatids differentiate into spermatozoa, a process known as spermiogenesis. Abbreviation: n = ploidy; 2n = diploid; 1n = haploid; C = chromatid.

During spermatocytogenesis, A_{single} (undifferentiated type A_s) spermatogonia are identified as spermatogonial stem cells, which develop through the differentiating type A and B spermatogonia into preleptotene primary spermatocytes. The number of mitotic spermatogonial divisions from type A spermatogonia to preleptotene primary spermatocytes occur for instance nine to eleven times in mice and rat, in human (and other primates), although not precisely known, certainly lower than in mice and rat (de Rooij, 2001; de Rooij and Russell, 2000). Thereafter, these cells enter meiosis and proceed through two meiotic divisions, thus reducing the sets of chromosomes (Wolgemuth, 2006). When the preleptotene primary spermatocytes enter the S-phase of the cell cycle, their chromosomes will be duplicated and form two sister chromatids.

Meiosis differs from mitosis, in which the cells divide twice after a single DNA replication, first by separating homologous chromosomes and then by separating sister chromatids. Meiosis I can be divided into four stages: prophase, metaphase, anaphase, and telophase. Prophase I of meiosis is the longest stage in the first meiotic division and exhibits most of the defining events that are unique to meiosis, in which homologous pairs, double stranded break forms, and DNA recombination begins between homologues chromosomes. DNA recombination also known as crossover is defined as the exchange of genetic information between chromosomes of different parental origin. It results in generation of genetically different cells and leads to increased genetic variability in offspring. Therefore, DNA recombination is a crucial step in meiosis and the elementary purpose of the specialized events of meiotic prophase I.

The prophase I is further divided into five developmental stages: leptotene, zygotene, pachytene, diplotene, and diakinesis. A meiosis-specific structure known as the synaptonemal complex (SC) is formed during prophase I. It is composed of two lateral elements (LE) forming along the entire length of each sister chromatid, and one central element (CE) connecting the two lateral elements and thus linking the two homologous chromosomes in a process called synapsis. The various stages of prophase I are defined by the degree the SC is formed. This is shown in Figure 4 and can be visualized by immunostaining of SC components, including the LE protein, synaptonemal complex protein 3, and the CE protein, synaptonemal complex protein 1 (Lee and Hirano, 2011).

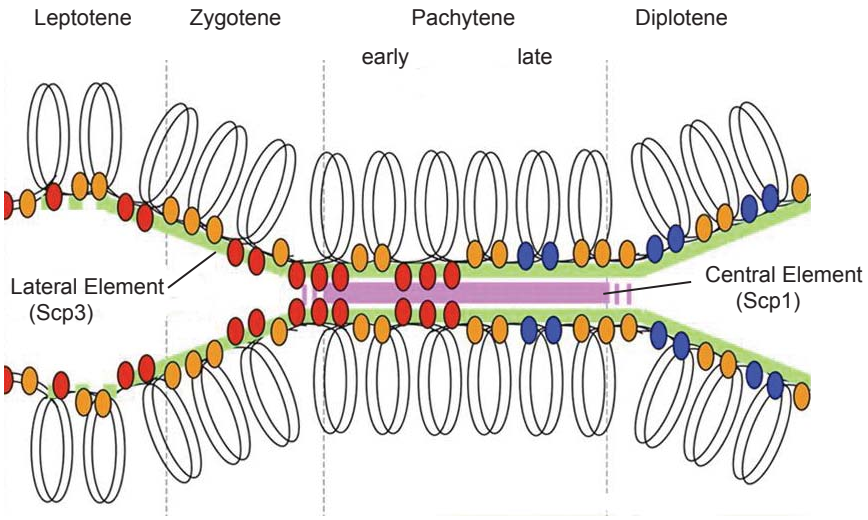

Figure 4. Different stage in prophase I of meiosis (figure modified from Lee *et al, J Cell Biol,* 2011). Synaptonemal complex is formed during prophase I of first meiotic division. In leptotene, lateral elements (synaptonemal complex protein 3; Scp3) associates with two sister chromatids of each chromosome. As prophase I progresses, in zygotene, the lateral elements are linked by central elements (synaptonemal complex protein 1; Scp1), the process known as synapsis. In pachytene, the chromosomes are completely synapsed, thereafter, central elements are dissociated in diplotene.

After prophase I follow metaphase I, anaphase I, and telophase I. During metaphase I, pairs of homologous chromosomes align opposite each other on the metaphase plate and then separate into different daughter cells during anaphase I. The second meiotic division depicts a cell division like mitosis, without DNA replication or recombination, in which the sister chromatids are separated, termed anaphase II. During meiosis II, the chromosome number is reduced by half and results in four haploid cells containing a single copy of each chromosome. Therefore, cells in the first meiotic division are tetraploid primary spermatocytes, while those after the first meiotic division are diploid secondary spermatocytes that have two sets of chromosomes. One primary spermatocyte gives rise to two secondary spermatocytes. They divide further in the second meiotic division to produce haploid round spermatids with a single set of chromosomes, which then undergo a series of complex molecular and morphological events known as spermiogenesis. During this process, cell divisions do not occur and the haploid cells finally differentiate into sperm.

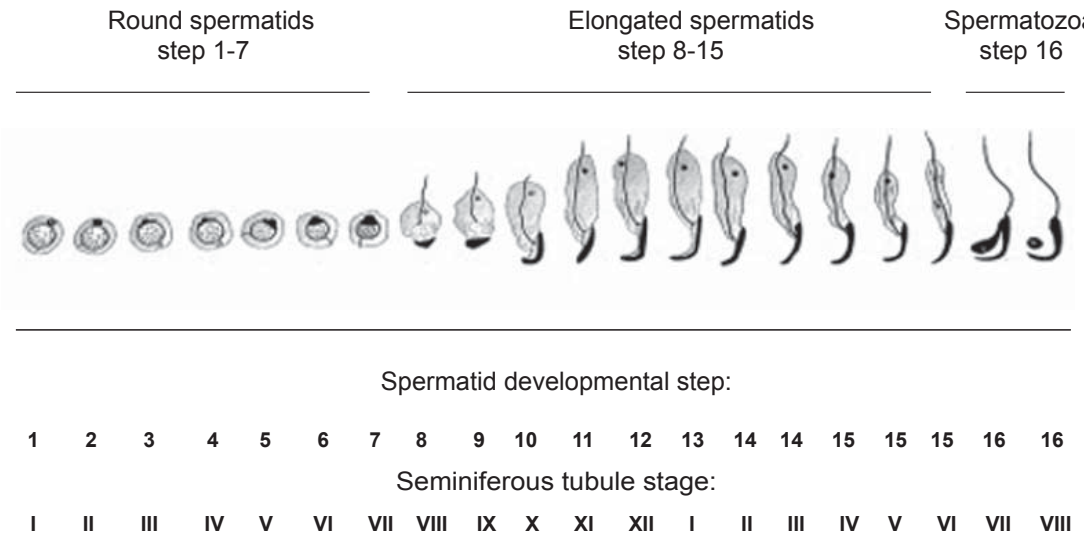

Figure 5. The multiple steps in the mouse spermiogenesis (figure modified from Yan *et al, Molecular and cellular Endocrinology*, 2009). Mouse spermiogenesis is composed of 16 steps, which are labeled with 1-16 and stages of the seminiferous epithelial cycles categorized by roman numerals I-XI are demonstrated.

The last phase in spermatogenesis, named spermiogenesis, can be divided into three phases; Golgi phase, Cap phase (development of acrosome, nuclear condensation), and Maturation phase (formation of flagella) (Yan, 2009). The Golgi apparatus has an important role in the early steps of spermiogenesis, since the formation of the acrosome is dependent on their ability to produce vesicles and granules containing the enzymatic components of the acrosomic structure covering the developing sperm nucleus. Thus, in the Golgi phase, the number of Golgi apparatuses increases. They get in contact with the nuclear membrane that secretes factors essential for membrane fusion. Step 1 spermatids show a small, perinuclear Golgi region without an acrosomic vesicle or granule. They differentiate further into step 2 and step 3 spermatids. Spermatids have proacrosomal vesicles and granules within the Golgi apparatus, forming a single, large acrosomal granule within a larger vesicle that will indent the nucleus.

In the cap phase, the acrosomal cap is formed. As the cap is formed, chromatin compaction progresses, thus forming a condensed nucleus. The acrosomic granule of step 4 and 5 round spermatids extends to the nuclear envelope and the vesicle begins to flatten into a small cap over the nuclear surface. Subsequently, in steps 6 and 7 round spermatids, the acrosomic vesicle is getting thinner and the granule spreads out.

In step 8 round spermatids, the acrosome covers approximately one third of the nuclear surface and the nuclei begin to change their shape. In steps 9 to 14 spermatids, the acrosomal structure moves over the ventral surface of the elongating spermatid nucleus and the migration of the acrosome is completed approximately by step 14 spermatids. During these spermatid steps, condensation of the chromatin occurs, as the chromosomes are packed more tightly.

In the maturation phase, step 15 and 16 spermatids show fewer changes in their nuclear shape and acrosomal migration. The nucleus continues to condense and the acrosome matures further and flattens almost all the nucleus, apart from that portion linked to the tail structure. Excess cytoplasm is displaced, afterwards prominent cytoplasmic lobes and residual bodies are formed, which contain mitochondria, ribosome, lipids, vesicles, and other cytoplasmic components. Finally, the flagellum is formed with the capacity for motility (Eddy, 2002).

2.2 *In vitro* culture of spermatogonial stem cells

The two major characteristics, namely self-renewal and differentiation, are differently regulated in neonate and adult testis. The neonate or prepubertal testicular microenvironment support the self-renewal of SSCs to establish the stem cell population, while the adult testes harbors self-renewing SSCs as well as differentiating ones. Many studies have been done with respect to interaction between SSCs and somatic cells, such as the effect of the niche during development of SSCs upon transplantation into different species, impact of colonization activity of SSCs, aging effect of somatic cells on SSCs, and correction of defective genes *in vitro*. The findings from those reports reveal the importance of an appropriate microenvironment during postnatal development in male testis. In fact, it has been shown that a reduced SSC activity and production of mature spermatogenetic cells is caused primarily by impairment of the niche rather than by stem cells themselves (Kubota and Brinster, 2006; Oatley and Brinster, 2012; Ryu et al., 2006; Schmidt et al., 2011).

The self-renewal and differentiation potential of SSCs can be maintained under defined *in vitro* culture conditions, which make the SSCs an attractive and available source for *in vitro* experiments. SSC populations can be obtained from either neonate or adult mouse testes and are termed germline stem cells once cultured *in vitro*.

In comparison to neonate testicular cells that contain more mitotically dividing spermatogonial cells, adult testes contain only 0.01-0.03% of undifferentiated spermatogonial cells, which jeopardizes experimental analyses and thus raised interest in developing cultivation procedures *in vitro*. To date, many reports have demonstrated the *in vitro* culture of mouse GSCs under different conditions. Cells were cultured on different kinds of feeder cells, among them mouse embryonic fibroblasts (MEFs), which turned out to be the most effective supporting cell type for maintenance and proliferation of SSCs. Under feeder-free culture conditions, GSCs can be grown on various types of proteins including laminin, collagen, and matrigel. The medium compositions differ slightly, but commonly contain glial cell line-derived neurotrophic factor (GDNF), basic fibroblast growth factor 2 (FGF2), and leukemia inhibitory factor (LIF) under both, serum-containing and serum-free culture conditions (Kanatsu-Shinohara et al., 2005; Kanatsu-Shinohara et al., 2003; Ko et al., 2009).

2.2.1 Role of growth factors in spermatogonial stem cell proliferation

In order to study the biological activity of SSCs, either combinations of cytokines or individual cytokines were added to the culture medium and their effect on survival and growth of SSCs was documented. It has been suggested that GDNF, FGF2, epidermal growth factor (EGF), insulin-like growth factor 1 (IGF1), and LIF are essential factors to support the survival and proliferation of SSCs by blocking differentiation and thus maintaining SSC self-renewal potential under defined *in vitro* culture conditions (Kanatsu-Shinohara et al., 2007; Kubota et al., 2004; Nagano et al., 2003). BMP4 and Neuregulin1 on the other hand influence differentiation of SSCs (Nagano et al., 2003; Pellegrini et al., 2003).

In particular, GDNF has been shown to be a crucial regulator to sustain the function of SSCs-i.e. self-renewal capability *in vivo*. Supplementation of GDNF enables the long-term survival and maintenance of undifferentiated spermatogonia populations *in vitro*; however, it is unclear whether GDNF has an effect on proliferation of SSCs (Meng et al., 2000; Yomogida et al., 2003). Nevertheless, the combinations of growth factors like FGF2 or EGF together with GDNF support the expansion of SSCs.

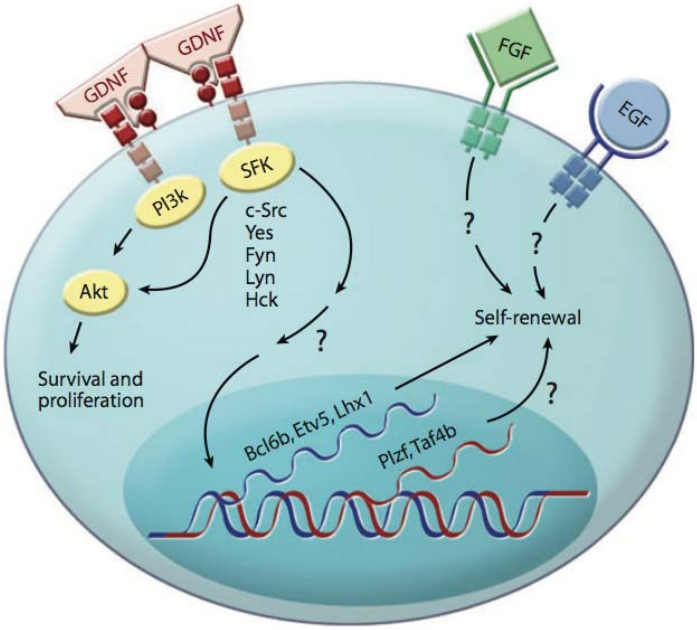

Figure 6. Signaling pathway in spermatogonial stem cells (figure from Oatley *et al, Annu. Rev. Cell Dev. Biol,* 2008). Schematic presentation of signaling cascades, which play a role in the regulation of survival, proliferation, and self-renewal of SSCs.

As shown in Figure 6, the binding of GDNF to its receptor complex, c-Ret and the glycosylphosphatidylinositol (GPI)-anchored binding molecule GDNF family receptor alpha 1 (Gfrα1), initiates the signaling cascade of phosphoinositide 3-kinase (PI3K) and Src family kinase (SFK). This initiation leads to the downstream activation of the serine-threonine kinase AKT (also known as protein kinase-B) signaling, which has an influence on the survival and proliferation of SSCs *in vivo*. SSCs accordingly express *c-Src* (Rous sarcoma oncogene), *Yes* (Yamaguchi sarcoma viral oncogene), *Fyn* (fyn proto-oncogene), *Lyn* (Lyn tyrosinase kinase), and *Hck* (hematopoietic cell kinase). In addition, SFK signaling regulates *bcl6b* (B cell CLL/lymphoma 6, member B; also known as *baz*f), *etv5* (Ets variant gene 5; also known as *erm*), and *lhx1* (Lim homeobox protein 1 or *lim1*), which are known to be crucial to sustain the self-renewal potential of SSC in *in vitro* culture. Although the important role of *Plzf* and *Taf4b* in the self-renewal of SSCs *in vivo* has been suggested, an essential role of these genes in the self-renewal of *in vitro* cultured SSCs through supplementation of the growth factor GDNF has not been demonstrated yet. Furthermore, the role of the cytokines EGF and FGF2 in survival and self-renewal has not yet been documented (Braydich-Stolle et al., 2007; Lee et al., 2007; Oatley et al., 2007).

2.2.2 Restoration of spermatogenesis by spermatogonial stem cell transplantation

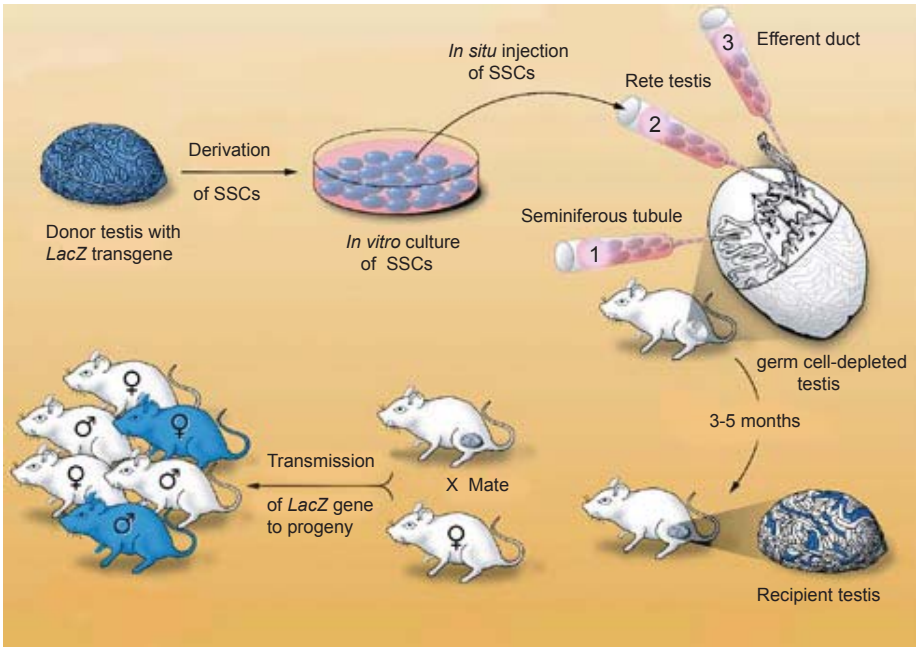

Figure 7. Testicular transplantation (figure modified from Kubota *et al, Nat Clin Pract Endocrino Metabol,* 2006). Testicular cells can be obtained from donor testes that express *LacZ* or *GFP*. SSCs can be cultured *in vitro* and restore spermatogenesis upon injection into endogenous germ cell-depleted recipient mice. Donor genes get transmitted to the next generation, thereby confirming the functionality of the injected donor spermatogonial stem cell populations.

To identify the spermatogonial stem cells and examine their biological activity or functionality, transplantation techniques were developed utilizing different species (Brinster et al., 2003; Kubota and Brinster, 2006; Ogawa et al., 1997). Among them, the mouse model depicts the most studied animal model. The donor cells are collected from fertile mice and are microinjected into seminiferous tubules of recipient infertile mice. To reduce or destroy the endogenous spermatogenesis in recipient male, several methods are used including radiation, chemotherapeutic drugs, and production of transgenic mice like homozygous W mice carrying a c-kit point mutation in the white spotting locus or vitamin A deficient mice. The commonly used method is busulfan treatment of males, which leads to the disappearance of endogenous germ cells from the tubule lumen of recipient mice. The donor cells express reporter transgenes e.g.- *LacZ* or *GFP* that enable identification of donor cells after transplantation.

There are three methods to introduce donor cells into the seminiferous tubules of recipients. The first method is a direct injection of donor cell suspensions into the seminiferous tubules. The cells flow through the rete testis and fill each tubule individually. Various site injections can be required to fill a large number of tubules. The second method is injection of cells directly into the rete testis, to which all tubules are connected. Injection via one site will therefore fill all tubules. The third method is injection of donor cells into the fine efferent ducts running from the rete testis to the head of the epididymis, thereby filling the rete testis and subsequently the tubules. After transplantation, the donor-derived cells are located on the basement membrane of the seminiferous tubules and start to proliferate, subsequently differentiating into other types of germ cells and filling the tubules from the basement membrane towards the lumen. Collectively, all these methods result in a similar donor cell-derived colony formation rate in recipient infertile males, thereby restoring the spermatogenesis throughout the life of the recipient males.

2.3 Reprogramming of germline stem cells

To date, several pluripotent stem cell types, including induced pluripotent stem cells (iPSCs), embryonic germ cells (EGCs), and gPSCs have been generated using different strategies. The best-studied pluripotent stem cell population is ESCs, which are derived from the inner cell mass (ICM) of the blastocyst. Recently, reprogramming of fibroblast somatic cells into iPSCs was accomplished through ectopic expression of defined transcription factors-e.g. *Oct4*, *Sox2*, *Klf4*, and *c-Myc* (Takahashi et al., 2007; Takahashi and Yamanaka, 2006). Thereafter, many independent experiments were performed to introduce selected sets of reprogramming factors into different kinds of somatic cells using various delivery methods to generate pluripotent stem cells (Eminli et al., 2009; Hanna et al., 2008; Heng et al., 2010; Kim et al., 2009a; Kim et al., 2009b; Kim et al., 2008; Okita et al., 2007). Moreover, other types of pluripotent stem cells such as EGCs and ESC-like cells have been generated from unipotent germline cells-i.e. PGCs and GSCs, respectively (Kanatsu-Shinohara et al., 2004; Matsui et al., 1992; Resnick et al., 1992). Compared to iPSCs, the conversion of GSCs occurs under defined culture conditions without delivery methods. These ESC-like cells were termed gPSCs and were first generated from GSCs isolated from neo-

natal mouse testis and subsequently also from testis of adult *Oct4-GFP* transgenic mice (Ko et al., 2010; Ko et al., 2009; Ko et al., 2011). gPSCs depict a valuable tool to study the mechanisms underlying the induction of certain states of pluripotency in GSCs.

iPSCs, EGCs, and gPSCs are morphologically similar to ESCs and express transcription factors regulating pluripotency of ESCs including *Oct4*, *Sox2*, *Klf4*, *c-Myc*, *Nanog*, or *Lin 28*. Once the cells are converted to pluripotent stem cells, they demonstrate the unlimited self-renewal potential and differentiation ability to cell types of the three germ layers ectoderm, mesoderm, endoderm, and the germline. These converted cells are proven to be pluripotent by teratoma formation, generation of chimeras, and germline transmission.

2.4 Differentiation of germline stem cells

The important feature of GSCs is their capability to produce the mature spermatozoa, the process called spermatogenesis, which occurs in seminiferous tubules of testis. The testis is composed of two major parts, seminiferous tubules and interstitial tissues. The seminiferous tubules contain Sertoli cells that provide the physical support and nutrient for different types of spermatogenetic cells. The interstitial tissues contain other somatic cells, like myoid cells, that provide physical support and contractile motion. Leydig cells secret the androgen hormone testosterone for the maturation process in spermatogenesis (Cooke and Saunders, 2002; Maekawa et al., 1996; Mendis-Handagama, 1997; Oatley and Brinster, 2012).

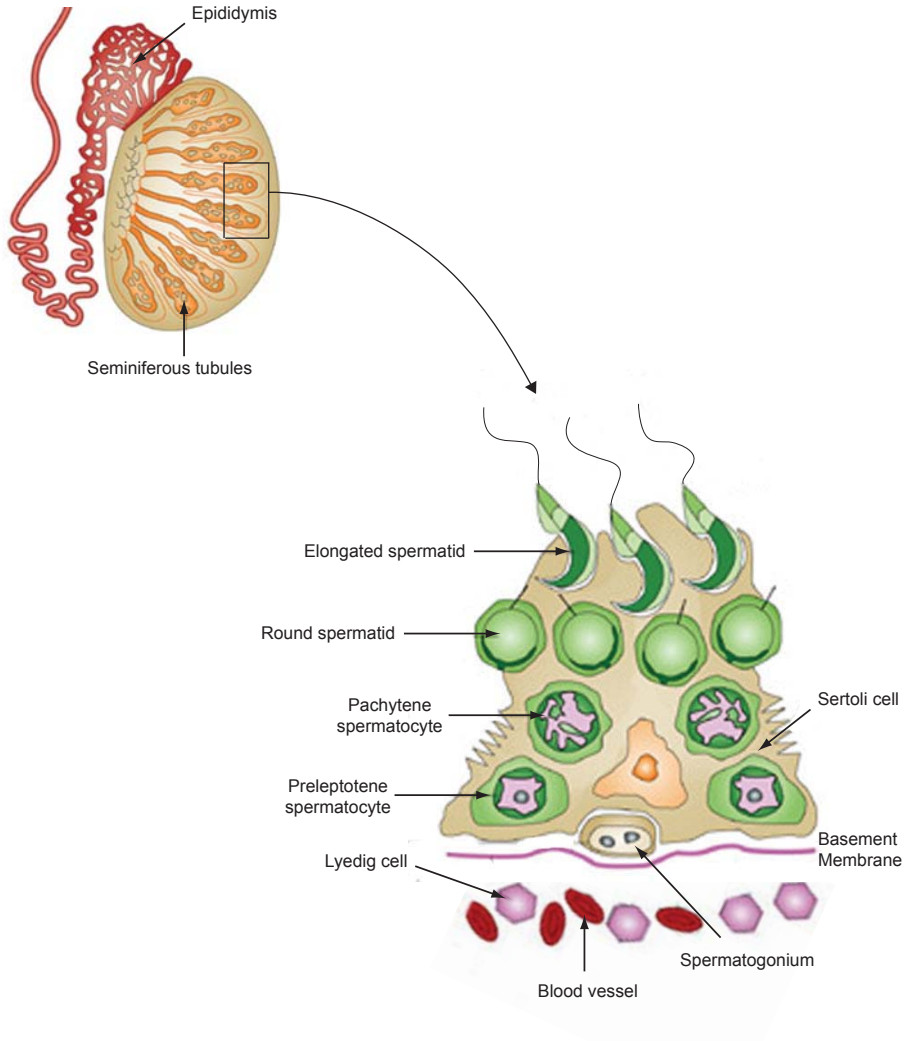

Figure 8. Schematic illustration of seminiferous tubules in testis (figure modified from Cooke *et al*, *Nature Reviews Genetics*, 2002). The testis consists of seminiferous tubules and interstitial tissues. Within seminiferous tubules, germ cells are directly associated with Sertoli cells that secret various cytokines to support germ cell maturation. Maturation begins with spermatogonia at the basal lamina and continues toward the lumen over primary spermatocytes, secondary spermatocytes, round spermatids, elongated spermatids, and to spermatozoa. The interstitial tissues lie between seminiferous tubules and contain clusters of Leydig cells and blood vessels.

To understand how each step of spermatogenesis is regulated, studies (Aflatoonian et al., 2009; Feng et al., 2002; Geijsen et al., 2004; Marh et al., 2003; Zhu et al., 2012) focused on either mutant animal models or on the establishment of *in vitro* culture systems to generate meiotic germ cells or haploid cells from different cell types, such as testicular cells or embryonic stem cells. More recently, functional sperm have been produced using organ culture methods, round spermatid injection

(ROSI), and intracytoplasmic sperm injection (ICSI) (Sato et al., 2011). However, in spite of intense efforts and different approaches at generating different types of spermatogenetic cells including functional spermatozoa, to date how each step of spermatogenesis is actually regulated still remains elusive.

In the present study, *in vitro* spermatogenesis from GSCs in a stepwise culture system has been demonstrated (Ko et al., 2010; Ko et al., 2009; Ko et al., 2011). Morphological analysis, gene expression profiling, immunofluorescence staining, and flow cytometry revealed the characteristic properties of GSCs. Moreover, when transplanted into infertile mouse testis, GSCs were able to restore spermatogenesis, thereby confirming their identity and full functional capacity.

For *in vitro* differentiation, GSCs were co-cultured with Sertoli cells in the presence of defined factors. The potential of GSCs to differentiate into meiotic cells was determined by assessing the pattern of c-kit protein expression in a time-course analysis by flow cytometry. It is known that expression of c-kit is not found in undifferentiated spermatogonia type A_s, but onset of expression occurs in differentiating spermatogonia and c-kit downregulation is seen upon entry into meiosis (Yoshinaga et al., 1991). In accordance with this finding, in our study, c-kit expression was strongly upregulated and subsequently downregulated during culture in a subset of cells, suggesting that these cells had initiated differentiation and then entered meiosis.

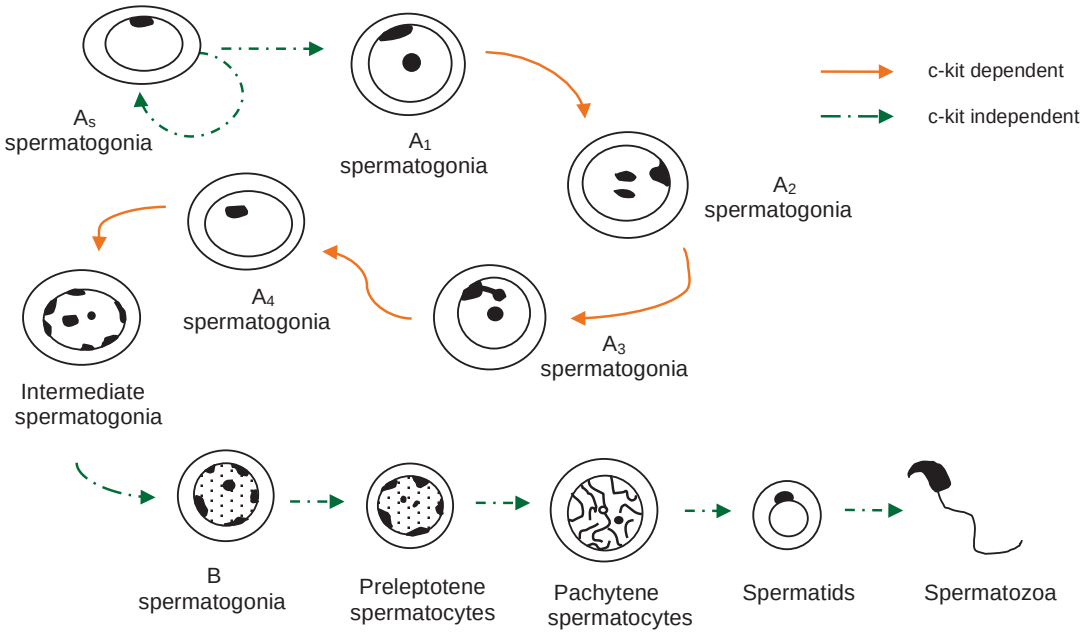

Figure 9. c-kit expression in different types of spermatogenetic cells (figure modified from Yoshinaga *et al*, Development, 1991). The type A_s spermatogonia classify as stem cells and do not express of c-kit. The mitotic proliferation phase from different subtypes of A spermatogonia to intermediate spermatogonia is categorized as c-kit dependent phase. The following phase during spermatogenesis, including meiosis and spermiogenesis, categorizes as c-kit independent phase. Arrows in orange indicate the c-kit dependent pathway and the dotted arrows in green indicate the c-kit independent pathway.

To confirm meiotic entry and to determine the stage of the first meiotic division, where DNA recombination occurs, immunocytochemistry was performed using an antibody against Scp3, a marker widely used for meiotic prophase I. Additionally, gene expression analysis was performed using the premeiotic cell marker *Oct4* and meiotic cell markers *c-kit*, *Stra8*, *Dmc1*, and *Scp3*.

Finally, transmission electron microscopy was conducted of *in vitro*-generated germ cells and compared with *in vivo*-isolated testicular cells. Even though differences in the cell structure-i.e. nucleus, cytoplasmic components, and membranes-were observed between *in vivo* and *in vitro* cells, synaptonemal complexes were detected in the culture-derived germ cells. Synaptonemal complexes are exclusively formed in meiotic germ cells and unequivoqually mark prophase I of meiosis.

Taken together, the observations described above clearly demonstrate that GSCs differentiated *in vitro* into meiotic cells of different stages of meiosis

3. Aim

GSCs are the only adult tissue-specific stem cells that can be maintained as self-renewing population *in vitro* for long periods of time. Their biological activity can be proven by ability of reestablishment of spermatogenesis in infertile males after transplantation of donor cells. This capability or availability allows studies to find crucial extrinsic factors influencing GSC function and to understand how processes involved in self-renewal, differentiation of GSCs, and conversion of GSCs into gPSCs are regulated. A large number of animal models, especially the mouse model, have been established to study the control of spermatogenesis by ablation or over-expression of related genes. Spermatogenetic failures have been observed, such as loss of SSCs, arrest during meiosis, or inadequate spermiogenesis. In addition, previous *in vitro* studies have identified the role of specific genes in the regulation of proliferation and differentiation of GSCs into various stage-specific cells during spermatogenesis such as *bcl6b*, *Oct4*, *c-kit*, *LDH-C4*, and *Acr3*. (Feng et al., 2002; Oatley et al., 2006).

In the present thesis, GSC lines were used as a starting source to study processes involved in reprogramming and differentiation as summarized in Figure 10. Although the developmental ability of GSCs towards mature germ cells under the current *in vitro* differentiation procedure is limited, this system can be utilized to study the first steps of spermatogenesis and how they are regulated. Furthermore, the findings from this study provide hints for future studies of how to overcome obstacles during *in vitro* differentiation through establishment of optimized culture conditions or the necessity of a supporting microenvironment for the successful *in vitro* spermatogenesis.

Additionally, it has been shown that reprogrammed gPSCs are able to differentiate into somatic cells-e.g. endothelial cell-like cells. gPSCs are therefore a valuable new source of pluripotent cells for drug development and toxicity testing for clinical applications in the future.

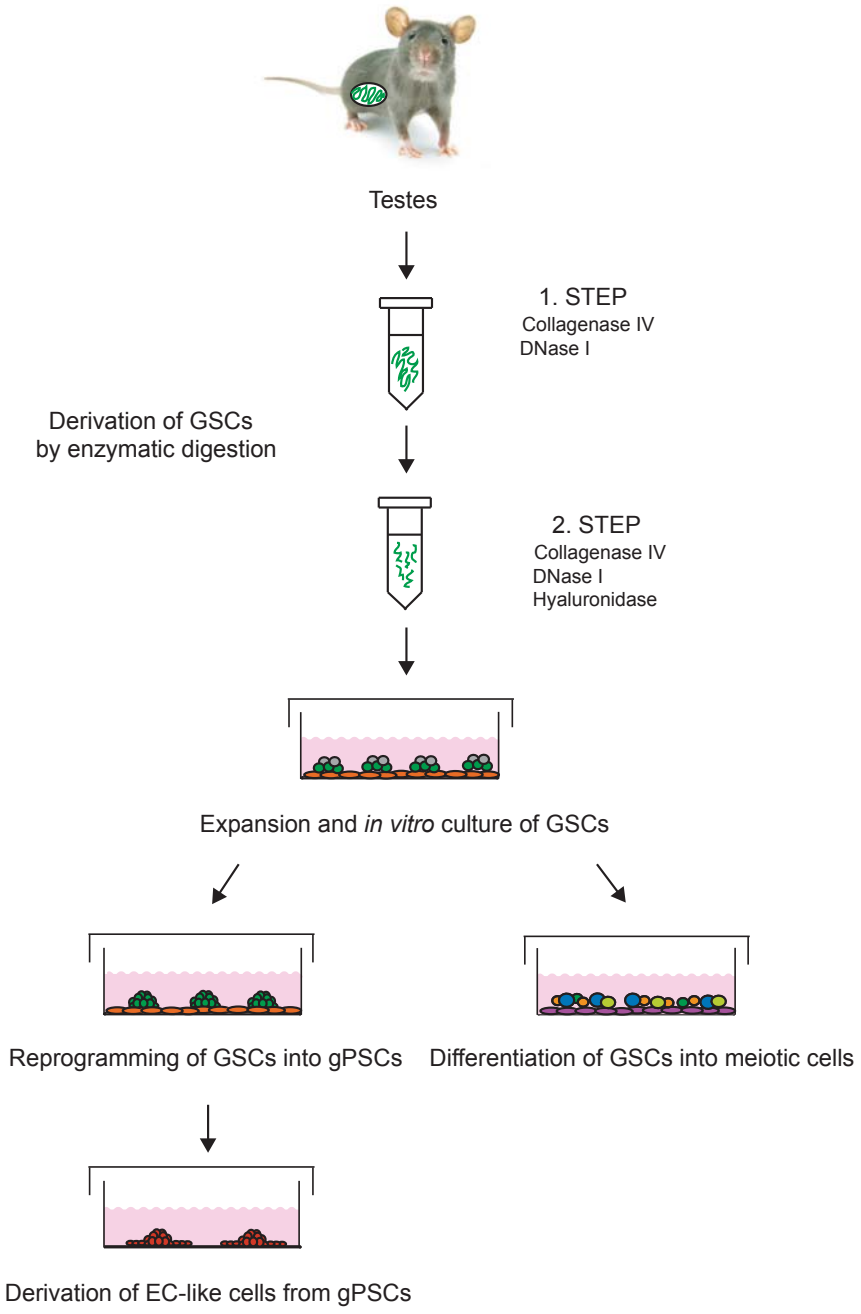

Figure 10. Schematic presentation of studies performed on GSCs in this thesis. GSCs were derived from mouse testis and maintained *in vitro* for long-term culture. The GSCs were used for the generation of gPSCs, as well as for differentiation experiments into meiotic germ cells. Furthermore, endothelia-like cells (EC-like cells) were generated from gPSCs

4. Material and methods

4.1 Animals

The transgenic mice including *Oct4-GFP* (OG2), *Oct4-GFP*-Rosa26, and *Acrosin-EGFP* were raised in a temperature and humidity controlled animal facility with a 12 h light-dark cycle controlled environment at a temperature of 22±1 °C and 35±5% humidity. All animal procedures and experiments were conducted under protocols approved by the committee on animal care and use of the Max-Planck-Institute for Molecular Biomedicine.

4.2 Generation and culture of different cells

4.2.1 Derivation of mouse germline stem cells

Testes were taken from different adult (5-7 weeks) *Oct4-GFP* transgenic mice (OG2 or OG2Rosa26) or pubertal (PND 6-7), OG2*AcrosinEGFP*, or *Acrosin-EGFP* transgenic mice. For the derivation of GSCs, testes from 5-7 weeks old *Oct4-GFP* transgenic mice (OG2 or OG2Rosa26) were used. The seminiferous tubules were digested either by a one-step digestion or a two-step digestion. The digestion solution consisted of 1 mg/ml of collagenase IV, 0.5 mg/ml of DNase I, and 0.5 mg/ml of hyaluronidase in DMEM/F12 medium, in which dulbecco's minimal eagle's medium (DMEM) and Ham's F12 medium are mixed at a ratio of 1:1. For the one-step digestion, all three enzymes were used at the same time, while for the two-step digestion, the tubules were first digested with 1 mg/ml of collagenase IV, 0.5 mg/ml of DNase I, washed once with fetal bovine serum (FBS) containing medium, then further digested with 1 mg/ml of collagenase IV, 0.5 mg/ml of DNase I, and 0.5 mg/ml of hyaluronidase. The tubules were incubated in a 37 °C water bath for 15-30 min and gently tapped every 2-3 min to facilitate the digestion. To stop the digest, FBS containing medium was added and the testicular cells were gently triturated to generate a single-cell suspension. After washing twice with FBS containing medium, the cell suspension isolated from testes of pubertal mice (PND 6-7) was plated at a density of

120.000 cells/cm^2 onto 0.1% gelatin-coated tissue culture dishes to remove somatic cells (2 h minimum). Depending on the amount of somatic cells still present in the supernatant, this procedure was repeated two to three more times until no spindle-shaped cells were found on the plate anymore. Subsequently, the cell supernatant was transferred onto mouse MEFs and cultured in GSC medium described in section 3.2.4 at 37 °C in 5% CO_2 in a humidified incubator. After 8-10 days, GSC colonies could be observed.

4.2.2 Derivation of mouse embryo fibroblasts

MEFs were generated from E12.5 dpc embryos of C57BL/6, C3H, or CF1 mice. The pregnant female mice were sacrificed by cervical dislocation and extra-embryonic membranes and placentas were removed and placed in PBS. The uteri were isolated and the embryos were removed and immersed in PBS. After decapitation of the embryos, heart, and liver as well as the extremities were removed and the remaining embryos were placed in DMEM medium (4.5 g/l glucose) supplemented with 10% (v/v) heat-inactivated FBS, L-glutamine/penicillin/streptomycin (1x), 10 µM β-mercaptoethanol, and 1% (v/v) non-essential amino acids (NEAA) stock solution (1x). The embryos were cut into small pieces with scissors and digested with 0.05% Trypsin/EDTA for 4 min at 37 °C. The tissue was further digested with a 4 to 1 dilution of 0.05% Trypsin/EDTA with MEF medium. Subsequently, the digests were filtered through a 100-µm cell strainer and the cell suspension was centrifuged at 200 xg for 5 min and then plated onto gelatinized plates at a density of two to three embryos per 15-cm tissue culture dish. The cells were incubated at 37 °C in 5% CO_2 in a humidified incubator.

4.2.3 Culture of mouse embryo fibroblasts

MEFs were cultivated on 0.1% gelatin-coated tissue culture dishes at a density of 12.000 cells/cm^2 in MEF medium described in section in 3.2.2. For passaging, a sub-confluent cell layer was rinsed with PBS and then digested with Accutase for 5 min at room temperature (RT). Fifteen percentage FBS containing medium was added to stop the digestion. After centrifugation at 200 xg for 5 min at RT, cells were ex-

panded at a dilution of 1:3 to 1:5 every other day, when the cell layer had reached confluency. Medium was changed every 2 days. Before use of MEFs for stem cell cultures, cells were mitotically inactivated by γ-irradiation or mitomycin C treatment. The cell were irradiated for 35-45 min at 1 gy/min at RT or incubated with 10 μg/ml of mitomycin C for 2-3 h at 37 °C in 5% CO_2 in a humidified incubator followed by three times washing in PBS. MEFs were cultured at 37 °C in 5% CO_2 in a humidified incubator.

4.2.4 Culture of mouse germline stem cells

GSCs were cultivated on inactivated MEFs at a density of 12.000 cells/cm^2 in Stem Pro-34 SFM medium supplemented with 2% (v/v) heat-inactivated FBS (56 °C for 30 min), 5 mg/ml of BSA fraction V solution, L-glutamine/penicillin/streptomycin (1x), 10 μM β-mercaptoethanol, 6 mg/ml of D-(+)-glucose, 0.085 % (w/v) DL-lactic acids, minimum essential medium (MEM) vitamins (1x), 1% (v/v) NEAA stock solution (1x), 1 mM sodium pyruvic acid stock solution, N2 supplement (1x), 20 ng/ml of mouse recombinant EGF, 10 ng/ml of human FGF2, 10 ng/ml of human GDNF, 30 ng/ml of β-estradiol, 60 ng/ml of progesterone, and 20 ng/ml of LIF. To passage GSCs, cells were mechanically dislodged by tapping the culture dish and transferred to a conical tube. After centrifugation at 200 xg for 5 min, cells were digested with Accutase for 1-5 min at RT. Subsequently, 15% FBS containing medium was added to stop the digest. After centrifugation at 200 xg for 5 min, cells were plated onto MEFs. Cultures were expanded every 4-7 days at a dilution of 1:2 to 1:10, depending on confluency and colony size of the GSCs. The medium was changed every 3-4 days. GSCs were cultured at 37 °C in 5% CO_2 in a humidified incubator.

4.2.5 Culture of mouse embryonic stem cells

ESCs were maintained on inactivated MEFs at a density of 4.000 cells/cm^2 in DMEM medium (4.5 g/l glucose) supplemented with 15% (v/v) heat-inactivated FBS, L-glutamine/penicillin/streptomycin (1x), 10 μM β-mercaptoethanol, 1% (v/v) NEAA stock solution (1x), and 20 ng/ml of LIF. For passaging, cells were washed once with PBS and incubated with Accutase for 2-5 min at RT. After centrifugation at 200 xg

for 5 min, cells were plated onto MEFs at a dilution of 1:2 to 1:5 every 2-7 days, depending on confluency and colony size. The medium was changed every 2-3 days. ESCs were incubated at 37 °C in 5% CO_2 in a humidified incubator.

4.2.6 Culture of mouse germline-derived pluripotent stem cells

gPSCs were cultivated on inactivated MEFs at a density of 4.000 cells/cm^2 in DMEM (4.5 g/l glucose) medium supplemented with 15% (v/v) heat-inactivated FBS, L-glutamine/penicillin/streptomycin (1x), 10 µM mercaptoethanol, 1% (v/v) NEAA stock solution (1x), and 20 ng/ml of LIF. For passaging, cells were washed once with PBS, digested with Accutase for 2-5 min at RT. After adding FBS containing medium and centrifugation at 200 xg for 5 min, the cell suspension was replated at a density of 4.000 cells/cm^2 onto inactivated MEFs. gPSCs were replated every 2-3 days, depending on confluency and colony size. The medium was changed every 2 days. gPSCs were incubated at 37 °C in 5% CO_2 in a humidified incubator.

4.2.7 Culture of OP9 cells

OP9 cells were cultivated on 0.1% gelatin-coated tissue culture dishes at a density of 12.000 cells/cm^2 in alpha-minimum essential medium (MEM) supplemented with 20% (v/v) heat-inactivated FBS and L-glutamine/penicillin/streptomycin (1x). For passaging, OP9 cells were washed once with PBS, incubated with 0.05% Trypsin/EDTA for 2-5 min, inactivated with 15% FBS containing medium and centrifuged at 200 xg for 5 min. The cell suspension was replated and expanded at a dilution of 1:2 to 1:4 every 4-7 days, depending on confluency of cells. The medium was changed every 2-3 days. OP9 cells were incubated at 37 °C in 5% CO_2 in a humidified incubator.

4.2.8 Culture of human embryonic stem cells

Human embryonic stem cells (hESCs) were cultivated on inactivated MEFs at a density of 17.000 cells/cm^2 in Knockout (KO) DMEM/Ham's medium, in which KO DMEM medium and Ham's F12 medium are mixed at a ratio of 1:1, supplemented with 20% (v/v) KO serum replacement (KOSR), L-glutamine/penicillin/streptomycin (1x), 10 µM β-mercaptoethanol, 1% (v/v) NEAA stock solution (1x), 1% (v/v) GlutaMax-I, and 4 ng/ml of human FGF2. For passaging of hESCs, the cells were incubated with 1 mg/ml of collagenase IV for 10-15 min at 37 °C and colonies were mechanically dissected using a 23-gauge needle. The cells were collected in a conical tube and centrifuged at 200 xg for 5 min. The cells were replated depending on confluency and colony size at a dilution of 1:2 to 1:5 every 5-7 days. The medium was changed everyday. To prepare human embryonic stem cell conditioned medium (hCM), mouse CF1 MEFs were cultured 24 h in the presence of hESC medium. The medium was filtered through a 0.2-µm filter and 4 ng/ml of FGF2 was added prior to use of the medium. hESCs were incubated at 37 °C in 5% CO_2 in a humidified incubator.

4.2.9 Culture of Sertoli cells

Sertoli cells were cultured on 0.1% gelatin-coated tissue culture dishes at a density of 12.000 cells/cm^2 in DMEM/F12 medium supplemented with 2.5% (v/v) heat-inactivated FBS, 5% (v/v) horse serum, 1.2 g/l of sodium bicarbonate, 15 mM HEPES, L-glutamine/penicillin/streptomycin (1x), and 1 mM sodium pyruvic acid stock solution. For expansion, cells were washed once with PBS, incubated with 0.05% Trypsin/EDTA for 2-5 min at RT and inactivated with 15% FBS containing medium. After centrifugation at 200 xg for 5 min, the cells were replated at a dilution of 1:2 to 1:5 every 2-7 days depending on confluency. The medium was changed every 2-3 days. Sertoli cells were incubated at 37 °C in 5% CO_2 in a humidified incubator.

4.2.10 Differentiation of mouse germline-derived pluripotent stem cells into endothelial cell-like cells

To induce differentiation, embryoid bodies (EBs) were generated by suspension culture. On day 0 of differentiation, gPSCs were seeded at a density of 30.000 cells/cm^2 in 10-cm bacteriological dishes for the generation of EBs in differentiation medium consisting of iscove's modified dulbecco's medium (IMDM) supplemented with 15% (v/v) heat-inactivated FBS, L-glutamine/penicillin/streptomycin (1x), 10 µM β-mercaptoethanol, and 1% (v/v) NEAA stock solution (1x). On day 2 of differentiation, EBs were transferred at a 1:3 ratio in 10-cm bacteriological dishes for further culture. On day 5 of differentiation, EBs were digested with Accutase to create a single-cell suspension. CD31-positive cells were isolated from the cell suspension by fluorescence-activated cell sorting (FACS) using a phycoerythrin (PE)-conjugated anti-CD31 antibody. Subsequently, CD31-positive cells were plated at a density of 1.200-2.500 cells/cm^2 onto OP9 cells and maintained in alpha-MEM medium supplemented with 10%(v/v) heat-inactivated FBS, L-glutamine/penicillin/streptomycin (1x), 10 µM β-mercaptoethanol, and 50 ng/ml of recombinant mouse vascular endothelial growth factor (VEGF). EC-like colonies were then plated onto 5 µg/ml of collagen IV-coated tissue culture dishes and maintained in the above-mentioned medium. To passage the cells, cells were washed with PBS and incubated with Accutase for 2-5 min at RT. Subsequently, the cells were collected by pipetting or using cell scrapers. After centrifugation at 200 xg for 5 min, cells were plated onto collagen IV-coated tissue culture dishes and passaged every 2-5 days, depending on their confluency at a dilution of 1:2 to 1:10. The medium was changed every 2-4 days. Differentiation cultures were maintained at 37 °C in 5% CO_2 in a humidified incubator.

4.2.11 *In vitro* differentiation of germline stem cells into meiotic germ cells

For *in vitro* differentiation, GSCs were cultured on inactivated Sertoli cells at a density of 1.200-2.500 cells/cm^2 in differentiation medium consisting of DMEM/F12 medium supplemented with 2% (v/v) heat-inactivated FBS, 5 mg/ml of BSA fraction V solution, L-glutamine/penicillin/streptomycin (1x), 10 µM β-mercaptoethanol, 6 mg/ml of D-(+)-glucose, 0.085% (w/v) DL-lactic acids, insulin-transferrin-selenium-A solution (1x), MEM vitamins (1x), 1% (v/v) NEAA stock so-

lution (1x), and 1mM sodium pyruvic acid stock solution. Cultures were monitored for c-kit expression by FACS and qPCR and were supplemented with 100 ng/ml of recombinant mouse stem cell factor (SCF), when high c-kit expression could be detected and the *Oct4-GFP* signal declined. Cultures were treated with 10^{-6} M retinoic acid (RA) in differentiation medium at day 8 for 2-3 days when c-kit expression declined. Subsequently, 10 ng/ml of mouse recombinant EGF, 10 ng/ml of mouse recombinant IGF1, and 45 ng/ml of human growth hormone (hGH) were added for another 10-12 days in differentiation medium. Media was changed every 2-3 days. To promote further differentiation, 100 ng/µl of follicle-stimulating hormone (FSH) and 10^{-7} M testosterone (T) were added to a 3:7 mixture of conditioned medium and differentiation medium. The cells were cultivated for 3-5 days before analysis. Conditioned medium was prepared from adult mouse testes of C57BL6, CD1, or C57BL6 x CD1 as described previously (Aflatoonian et al., 2009). Briefly, seminiferous tubules were isolated from mouse testes and digested in 1 mg/ml of collagenase IV in DMEM/F12 to remove the basement membrane. Tubules were then embedded in 6 mg/ml of agarose in DMEM/F12 medium and placed in differentiation medium. Twenty-four to fourty-eight hours later the medium was collected and filtered through a 0.2-µm filter. Media was stored at -20 °C until use. Differentiation cultures, as well as cultures for conditioned medium were maintained at 32 °C in 5% CO_2 in a humidified incubator.

4.3 Characterization of mouse germline-derived pluripotent stem cells

4.3.1 Alkaline phosphatase staining

The cells were washed with PBS and fixed with 4% paraformaldehyde (PFA) for 1 min at RT, washed three times with PBS and incubated with staining solution (0.4 mg/ml of naphthol phosphate and 1 mg/ml of Fast Red TR salt in 25 mM Tris-maleate buffer, pH 9) for 15-30 min at RT in the dark. Cells were washed twice with PBS. Colonies expressing alkaline phosphatase (AP) turn red and are indicative of pluripotent cells.

4.3.2 *In vitro* differentiation of germline-derived pluripotent stem cells

As shown in previous reports (Ko et al., 2009; Ko et al., 2011), gPSCs can differentiate *in vitro* and *in vivo* into derivatives of the three germ layers ectoderm, mesoderm, and endoderm. In this thesis, we demonstrate that gPSCs can differentiate *in vitro* into the ectodermal lineage via spontaneous EB formation. For this, gPSCs were plated at a density of 30.000 cells/cm^2 in DMEM/F12 medium supplemented with L-glutamine/penicillin/streptomycin (1x), 1% (v/v) NEAA stock solution (1x), N2 supplement (1x), 30 ng/µl of 3,3,5-tri-iodothyronine, and 100 µM ascorbic acid. Cultures were analyzed by immunocytochemistry for the neuron specific marker TuJ1. The mouse monoclonal anti-TuJ1 primary antibody and Alexa 568-conjugated anti-mouse IgG secondary antibody (1:1000 dilution) were used for immunfluorescence detection of positive-stained cells.

4.3.3 Teratoma formation

For teratoma formation analysis, 1-2 million gPSCs were subcutaneously injected into severe immunodeficient disorder (SCID) mice. About 4-5 weeks later, mice were sacrificed through cervical dislocation and the teratomas were dissected and fixed in Bouin's Solution overnight. The tumors were dehydrated in an ascending ethanol series and then embedded into paraffin. Samples were sectioned into 5-10 µm serial slices and stained with hematoxylin and eosin before evaluation.

4.3.4 Chimera formation

Aggregation of gPSCs with zona-free embryos was performed according to a previously described method (Wu et al., 2011). Briefly, clumps of loosely connected ten to twenty gPSCs were collected from briefly trypsin-treated day-2 cultures and transferred into microdrops of potassium simplex optimized medium (KSOM) medium containing 10% FBS under mineral oil in microplates with a depression. In the meantime, batches of thirty to forty eight-cell morula stage embryos were incubated in acidified Tyrode's solution until the zona pellucida had disintegrated. Subsequently, a single embryo was placed on top of the cell clump in a microdrop. All aggregates

were gathered in the above-mentioned way and cultured overnight at 37 °C in 5% CO_2 in a humidified incubator. After 24 h of culture, most of the aggregates had formed blastocysts. Eleven to fourteen aggregated embryos were transferred into the uterine horn of each pseudo-pregnant mouse.

4.3.5 Analysis for potency and functionality of mouse germline stem cells

4.3.5.1 Testicular transplantation

To analyze the functionality of the derived cell populations from testes, a testicular transplantation approach was used with slight modifications (Brinster et al., 2003; Kubota and Brinster, 2006; Ogawa et al., 1997). Briefly, to deplete the testes of endogenous germ cells, male mice were intraperitoneally injected with 40 mg/kg of busulfan. Intratesticular transplantation was performed through the efferent duct, 28 days after busulfan treatment with 0.3 million GSCs/testis (100-150 µl). Three months after transplantation, the seminiferous tubules of recipient mice were analyzed for restored spermatogenesis by dissociation with collagenase and microscopic examination for *Oct4-GFP* expression or by LacZ staining.

4.4 Analyses

4.4.1 Messenger RNA expression

4.4.1.1 RNA isolation

Total RNA was isolated with a RNeasy mini or micro Kit depending on the cell number, according to the manufacturer's recommendations. Briefly, cells were lysed in 350 µl of lysis buffer containing 1% ß-mercaptoethanol and homogenized using a shredder spin column. After centrifugation for 2 min at 16.000 xg, 350 µl of 70% ethanol was added to the lysate and mixed without centrifugation. This mixture was transferred onto the RNeasy column for binding of total RNA and washed once with 350 µl of wash buffer. The silica gel membrane of the column was treated with 70 µl of DNase solution containing 10 µl of DNase I for 15 min at RT to digest the DNA. The column was washed with 350 µl of wash buffer and then with 500 µl of

wash buffer. Subsequently, 500 µl of 80% ethanol was added to the column and centrifuged for 5 min at 16.000 xg to dry the column. Finally to elute the RNA, at least 14 µl of RNase-free water was added to the column and centrifuged for 1 min at 16.000 xg for elution.

4.4.1.2 Complementary DNA synthesis

The high capacity cDNA Reverse Transcription Kit was used to synthesize cDNA in a 20-µl reaction volume containing 50-100 ng of total RNA. The reaction mix consisted of 2 µl of 10x RT buffer, 2 µl of 10x Random hexamer, 0.8 µl of 25x dNTP (100 mM), 1 µl of MultiScribe RT (50 U/µl), 1 µl of mRNA, and 3.2 µl of water. The mixture was incubated at 25 °C for 10 min, 37 °C for 2 h, and kept at 4 °C.

4.4.1.3 RT-PCR analysis

Total RNA was extracted using the RNeasy Mini or Micro Kit and reverse transcribed using the high capacity cDNA Reverse Transcription Kit as described in the above sections 3.4.1.1 and 3.4.1.2. For a 25-µl PCR reaction, 2.5 µl of 10x PCR buffer, 0.2 µl of dNTP (25 mM), 0.5 µl of forward primer (final concentration 0.2 µM), 0.5 µl of reverse primer (final concentration 0.2 µM), 0.2 µl of Taq polymerase (5 U/µl), 1 µl of cDNA, and 20.7 µl of water were used. PCR was performed as follows: 94 °C for 2 min (1 cycle), 94 °C for 30 s, 55 °C for 30 s (annealing), 72 °C for 30 s (extension) (35 cycles), 72 °C for 5 min (final extension), and 4 °C incubation. The PCR products were mixed with DNA loading dye and loaded on a 1-2% agarose gel to separate amplicons at 100 V for 30 min-1 h.

Table 1. Sequences of oligonucleotide primers for RT-PCR

Gene	Primer sequence
beta-actin	F: 5’-CGT GCG TGA CAT CAA AGA GAA GC-3’ R: 5’-ATC TGC TGG AAG GTG GAC AGT GAG-3’
Oct4	F: 5’-CTG AGG GCC AGG CAG GAG CAC GAG-3’ R: 5’-CTG TAG GGA GGG CTT CGG GCA CTT-3’
Tex18	F: 5’-GGG GAG GGA GTA GTA CCT GTT T-3’ R: 5’-CCA CAC CCT GGA TAC TTC ACT-3’
Piwil2	F: 5’-CCT CCT GTA ACT GGG AAC TTG G-3’ R: 5’-GCA CCA CAA CAC CCT ACT ATG A-3’
Vasa	F: 5’-CTT GCA GAG ATG TTC AGC AGA C-3’ R: 5’-CTC CAA GAG CTT GCT CTC TCT C-3’
Dazl	F: 5’-GCA CTC AGT CTT CAT CAG CAA C-3’ R: 5’-CTA TCT TCT GCA CAT CCA CGT C-3’
Fragilis	F: 5’-GGA AGA ATA TGA GGT GGC TGA G-3’ R: 5’-GTG CTG ATG TTC AGG CAC TTA G-3’
Nanog	F: 5’-AGG GTC TGC TAC TGA GAT GCT CTG-3’ R: 5’-CAA CCA CTG GTT TTT CTG CCA CCG-3’
Utf1	F: 5’-CTC AAG GAC AAA CTC CGA GAC T-3’ R: 5’-AGA CTT CGT CGT GGA AGA ACT G-3’
Cripto	F: 5’-ATG GAC GCA ACT GTG AAC ATG ATG TTC GCA-3’ R: 5’-CTT TGA GGT CCT GGT CCA TCA CGT GAC CAT-3’
Fgf4	F: 5’-CAG CGA GGC GTG GTG AGC ATC TTC GGA-3’ R: 5’-CTT CTT GGT CCG CCC GTT CTT ACT GAG-3’

4.4.1.4 Real-time RT-PCR analysis

Total RNA was extracted using the RNeasy Mini or Micro Kit and reverse transcribed using a high capacity cDNA Reverse Transcription Kit as described in section 3.4.1.1 and 3.4.1.2. Amplification was performed on the ABI prism 7300 Fast Sequence Detection System according to the manufacturer's instructions. Real-time RT-PCR was carried out for each sample in triplicates. *Gapdh* was used as an internal control. Relative gene expression values were calculated by normalizing Ct (threshold cycle) values of the target genes with the housekeeping gene (*Gapdh*) value using the ΔΔCt method. The primer sequences used for real-time RT-PCR are listed below. For a 20-µl reaction, 10 µl of iTaq SYBR Super mix with ROX for SYBR green, 1 µl of forward primer (final concentration 0.2 µM), 1 µl of reverse primer (final concentration 0.2 µM), 1 µl of cDNA, and 9 µl of water were used. Real-time PCR was performed as follows: 50 °C for 2 min (1 cycle), 95 °C for 10 min (1 cycle), 95 °C for 15 s, 60 °C for 1 min (45 cycles), 95 °C for 15 s, 60 °C for 1 min, and 95 °C for 15 s (1 cycle).

Table 2. Sequences of oligonucleotide primers for Real-time RT-PCR

Gene	Primer sequence
Gapdh	F: 5'-TGG TTC CAG TAT GAC TCC ACT CAC-3' R: 5'-GAT GAC AAG CTT CCC ATT CTC G-3'
Oct4	F: 5'-CTG AGG GCC AGG CAG GAG CAC GAG-3' R: 5'-CTG TAG GGA GGG CTT CGG GCA CTT-3'
c-kit	F: 5'-TCA ACG ACC TTC CCG AAG GCA CCA-3' R: 5'-CTG GTG GTT CAG AGT TCC ATA GAC-3'
Stra8	F: 5'-CCA GTC TGA TAT CAC AGC CTC A-3' R: 5'-TTC CTT GAC CTC CTC TAA GCT G-3'
Dmc1	F: 5'-GGG AAT TGG TAC AGA CTG CTT C-3' R: 5'-CCC AAT ACC TAC AGG CAC ATT T-3'
Scp3	F: 5'-ACA TCT AAA GAT GGT GCC TGG T-3' R: 5'-GAT GTC AGC TCC AAA TTT TTC C-3'
Tie2	F: 5'-TTG AAG TGA CGA ATG AGA T-3' R: 5'-ATT TAG AGC TGT CTG GCT T-3'
VE-Cadherin	F: 5'-ACG GGA TGA CCA AGT ACA GC-3' R: 5'-ACA CAC TTT GGG CTG GTA GG-3'
CD31	F: 5'-GTC ATG GCC ATG GTC GAG TA-3' R: 5'-CTC CTC GGC GAT CTT GCT GAA-3'
Flt1	F: 5'-CTC TGA TGG TGA TCG TGG-3' R: 5'-CAT GCG TCT GGC CAC TTG-3'
vWF	F: 5'-AGG GCT GGA GTG TGC TAA GA-3' R: 5'-TAC CAA TGG CAG ATG CAA GTG-3'
Icam2	F: 5'-ACT CCA CAG ACC CCA CAG AC-3' R: 5'-ATG GCA AAA GAA GAC CGT GT-3'
Flk1	F: 5'-CAC CTG GCA CTC TCC ACC TTC-3' R: 5'-GAT TTC ATC CCA CTA CCG AAA G-3'

4.4.1.5 Micro array analysis

4.4.1.5.1 Whole genome expression analysis

Four hundred nanograms of total RNA (DNA-free) isolated as described in section 3.4.1.1 was used per sample as input for a linear amplification protocol from Ambion, which involved synthesis of T7-linked double-stranded cDNA and 12 h of *in vitro* transcription incorporating biotin-labeled nucleotides. The hybridization of purified and labeled cRNA was carried out for 18 h using MouseRef-8 v2 expression Bead Chips from Illumina. Chips were stained with streptavidin-Cy3 and scanned using the iScan reader from Illumina and accompanying software. Samples were hybridized as biological replicates.

4.4.1.5.2 Microarray data processing

The bead intensities were mapped to gene information using Bead Studio 3.2 from Illumina. To correct the background, Affymetrix robust multi-array analysis background correction model was conducted (Irizarry et al., 2003). Variance stabilization was carried out using the log2 scaling and gene expression normalization was calculated with the method implemented in the lumi package of R-Bioconductor. Data post-processing and graphics was performed with in-house developed functions in Matlab. Hierarchical clustering of genes and samples was performed with one minus correlation metric and the unweighted average distance linkage method.

4.4.2 Protein expression

4.4.2.1 Flow cytometry

For flow cytometry analysis, at least 0.1 millions cells were stained with antibodies at a final concentration 1-2 µg/ml in 100 µl of FACS buffer (PBS with 3% FBS). Cells were incubated with antibody for 20 min on ice, centrifuged at 200 xg for 5 min, and then washed twice with 500 µl of FACS buffer. Cells were resuspended in 400 µl of FACS buffer, and analyzed on a FACS Aria cell sorter. The following con-

jugated antibodies were used: allophycocyanin (APC)-conjugated anti-c-kit, PE-conjugated anti-SSEA1, PE-conjugated anti-CD31, PE-conjugated anti-Flk1, and PE-conjugated IgG control. In addition, the following first and secondary antibodies were used: anti-TRA1-81 and PE-conjugated anti-mouse IgM antibody; anti-VE-Cadherin, anti-Tie2, anti-vWF, rat IgG control, and Alexa 488-conjugated anti-rat IgG antibody.

4.4.2.2 Immunocytochemistry

Cells were fixed in 4% PFA for 10 min and permeabilized with 0.1% Triton-X-100 for anti-SSEA1 or 0.5% Triton-X-100 for anti-VE-Cadherin, or anti-vWF, respectively for 5-10 min at RT. The fixed cells were washed three times with PBS and incubated with 3% BSA in PBS for 30 min to block non-specific binding. Cells were stained with the primary antibodies anti-SSEA1, anti-VE-Cadherin, or anti-vWF at a concentration of 1-2 mg/ml for 1 h at RT. After washing the cells three times with PBS, bound primary antibodies were visualized using the Alexa 568 conjugated anti-mouse IgG secondary antibody for SSEA1 (1:1000 dilution) and Alexa 488-conjugated anti-rat IgG secondary antibody (1:1000 dilution) for VE-Cadherin and vWF. Incubations with the secondary antibody were carried out for 1 h at RT. The stained cells were mounted with 4'-6-Diamidino-2-phenylindole (DAPI)-containing mounting medium and then examined using a Leica DMI6000B fluorescence microscope (Leica, Germany).

4.4.2.3 Immunocytochemistry of spermatocytes with synaptonemal complex protein 3

The cells were incubated in hypoextraction buffer composed of 15 mM Tris, 50 mM sucrose, 20 mM citrate, 5 mM EDTA, 0.1 M DTT, and 10 mg/ml of PMSF for 5-15 min at RT, pelleted at 200 xg for 5 min and gently resuspended in 10 mM sucrose solution. Fifteen microliters of cell suspension were dropped from ca. 1-m height onto a slide with a thin film of freshly prepared fixative solution containing 2% PFA and 0.5% Triton X-100 in PBS. Cells were fixed overnight at RT in a humidified chamber. For staining, slides were washed twice with PBS and rinsed once in 1:250 diluted photoflo. After drying in air, slides were incubated with blocking solution containing 10% FBS and 0.05% Triton X-100 for 30 min at RT to block non-specific

binding. The slides were then stained with anti-Scp3 primary antibody for 1 h at RT. Bound antibodies were visualized after incubation with Alexa 488-conjugated goat anti-rat IgG secondary antibody (1:1000 dilution) for 1 h at RT. The stained cells were mounted with DAPI-containing mounting medium and then examined using a Leica DMI6000B fluorescence microscope (Leica, Germany).

4.4.3 Transmission electron microscopy

For transmission electron microscopy (TEM), the testicular cells were isolated from testes as described in section 3.2.1. One million testicular cells were incubated with 4 μg/ml of Hoechst for 20 min in 37 °C water bath and subjected to FACS sorting. The cells were sorted for haploid (1C), diploid (2C), and tetraploid (4C) cell populations. Thereafter cells were fixed with 2.5% glutaraldehyde in 0.1 M sodium cacodylate buffer, pH 7.4, post-fixed in 1% aqueous osmium tetroxide, dehydrated stepwise in a graded ethanol series and embedded in Epon 812. Ultrathin (70-nm) sections were prepared with an ultramicrotome (Leica, Germany), stained first with 1% uranyl acetate and then with 3% lead citrate, and subsequently examined under a Zeiss EM 109 electron microscope (Zeiss, Germany). Images were taken on 70-mm films.

4.4.4 Round spermatid injection

The female B6C3Fa mice (7-10 weeks) were superovulated by injection of 7.5 IU of equine chorionic gonadotropin and by injection of 7.5 IU of human chorionic gonadotropin 48 h later. After 15-17 h of hCG injection, mature metaphase II oocytes were collected from the oviducts and cumulus cells were removed by treatment with 0.1% hyaluronidase in potassium modified simplex optimization medium (KSOM). Subsequently, the oocytes were transferred to fresh KSOM medium and incubated at 37 °C in 5% CO_2 in a humidified incubator for up to 90 min before ROSI.

ROSI was carried out using a piezo-driven micromanipulator. The cover of a plastic dish was used as a microinjection chamber. Several small drops (~ 4 μl) of BSA-free HEPES-buffered KSOM (HEPES-KSOM), with or without 10% polyvi-

nylpyrrolidone (PVP), were placed on the bottom of the plate and covered with mineral oil. For activation, the oocytes were treated with Ca^{2+}-free KSOM containing 2.5 mM $SrCl_2$ for 20 min at 37 °C, then washed once to remove Ca^{2+}. Ten minutes later, the nuclei of round spermatids were injected into enucleated oocytes (one nucleus/oocyte). Injected oocytes were maintained in KSOM at 37 °C in 5% CO_2 in a humidified incubator up to morula or blastocyst stage.

4.4.5 Derivation of embryonic stem cell lines

The mouse embryos generated using ROSI were cultured to obtain embryonic day E2.5, eight-cell morula or E3.5 blastocysts. Zonae pellucidae were removed by incubation of morula or E3.5 blastocysts in acidic Tyrode's solution. The zona-free embryos were transferred onto inactivated MEFs in ESC medium as described in section 3.2.5 and cultured for 4-5 days at 37 °C in 5% CO_2 in a humidified incubator. The ICM outgrowth was picked with a drawn-out glass pipette and transferred into 30 µl of 0.25% Trypsin/EDTA in a 96-well plate. After 5-10 min incubation at RT, 30 µl of FBS containing ESC medium was added. To obtain a single cell suspension, cells were gently triturated and transferred into a well of a 4-well plate in ESC medium. After 4-7 days of culture, cells were passaged and expanded at a ratio of 1:3 to 1:6, depending on the colony size. Thereafter, cultures were expanded regularly every 2-3 days.

4.4.6 Karyotyping of round spermatid injection-derived embryonic stem cell lines

Established ESCs were cultured in a 3-cm tissue culture dish on MEFs for 2 days. The medium was changed 12-24 h before trypsinization of the cells into single cell suspensions. MEFs were removed by preabsorption on a gelatinized tissue culture dish for about 40 min. ESCs from the supernatant were collected and cultured in 2 ml of DMEM medium containing 0.5 µg/ml of nocodazole for 2 h in a 15-ml conical tube, followed by centrifugation at 200 xg for 4 min. One hundred microliters of medium was kept to resuspend the cell pellet by gentle flicking. Subsequently, 3 ml of prewarmed 0.56% KCl were added dropwise and the suspension was then incubated for 12 min at 37 °C in water bath. After centrifugation at 200 xg for 5 min, the cells

were resuspended in 100 µl of KCl and fresh fixative solution (Methanol: acetic acid 3:1) was added slowly. After fixation at RT for 30 min, cells were washed with 3 ml of fixative solution and resuspended in 50-300 µl of fixative solution. After a minute to let big aggregates settle, one drop of solution was dropped on a dry slide. The slides were stained with DAPI and mounted using mounting medium after the drop had dried (minimum 30 min). The slides were examined for metaphase plates; twenty to thirty cells were counted for each line. Normal diploid cell should have forty chromosomes.

4.4.7 Genotyping of round spermatid injection-derived embryonic stem cell lines

To genotype the ROSI-derived ESC lines, PCR analysis was performed using the following primers:

Table 3. Sequences of oligonucleotide primers for genotyping

Gene	Primer sequence
GFP	F: 5'-TGC AGT GCT TCA GCC GCT AC-3' R: 5'-TCG CCC TCG AAC TTC ACC TC-3'
Sry	F: 5'-TGG GAC TGG TGA CAA TTG TC-3' R: 5'-GAG TAC AGG TGT GCA GCT CT-3'
Il2	F: 5'-CTA GGC CAC AGA ATT GAA AGA TCT-3' R: 5'-GTA GGT GGA AAT TCT AGC AGC ATC ATC-3'
ROSA L221	5'-CTT GTG ATC CGC CTC GGA GTA TT-3'
ROSA L238	5'-CGC GCC GCT GTA AAG TGT TAC GT-3'
ROSA R316	5'-GGA GCG GGA GAA ATG GAT ATG-3'

PCR conditions: 95 °C for 2 min (1 cycle), 94 °C for 30 s, 56 °C for 45 s, 72 °C for 75 s (35 cycles), and 4 °C incubation.

4.4.8 DNA methylation analysis

Genomic DNA was prepared using the EpiTect Bisulfite Kit from Quiagen according to the manufacturer's protocol. DNA was treated with bisulfite mix in DNA

protection buffer. Bisulfite DNA conversion was performed under the following conditions: 99 °C for 5 min, 60 °C for 25 min, 99 °C for 5 min, 60 °C for 85 min, 99 °C 5 min, 60 °C for 175 min, and 20 °C incubation. Five hundred sixty microliters of BL buffer containing 10 µg/ml of carrier RNA was added to the DNA and the reaction was loaded onto an EpiTech spin column, then centrifuged at 16.000 xg for 1 min. The column was washed with 500 µl of BW wash buffer and then desulfonated with 500 µl of BD desulfonation buffer. After centrifugation and another wash with BW buffer, 20 µl of EB buffer was added to the column and centrifuged for 1 min at 16.000 xg to elute the purified DNA. The differentially methylated regions of the *H19* and *Igf2r* genes were amplified with the below listed primer sequences. For subcloning of PCR products, PCR 2.1-TOPO vectors were used and the cloned PCR products were sequenced according to the protocol of GATC Biotech AG.

Table 4. Sequences of oligonucleotide primers for DNA methylation analysis

Gene	Primer sequence
H19 1st	F: 5'-TAA GGA GAT TAT GTT TTA TTT TTG GA-3' R: 5'-CCC CCT AAT AAC ATT TAT AAC CCC-3'
H19 2nd	F: 5'-AAG GAG ATT ATG TTT TAT TTT TGG A-3' R: 5'-AAA CTT AAA TAA CCC ACA ACA TTA CC-3'
Igf2r 1st	F: 5'-GTA GAG TTT TTT GAA TTT TTT TGT T-3' R: 5'-TAA ACT ATA ATT CTA ATT ATA CCA AAT TAC-3'
Igf2r 2nd	F: 5'-TGG TAT TTT TAT GTA TAG TTA GGA TAG-3' R: 5'-AAA AAT TCT ATA ATC AAA ACC AAC-3'

5. Results

5.1 Derivation of germline stem cells

5.1.1 Derivation of germline stem cells form mouse testes

GSCs were established from testes of adult *Oct4-GFP* mice. Seminiferous tubules from OG2 (C57BL/6) or OG2/LacZ Rosa26 (C57BL/6 x129sv) mice were enzymatically digested with a mixture of collagenase IV, DNase I, and hyaluronidase. After removal of somatic cell populations via preabsorption on gelatinized culture plates, cell suspensions were plated onto MEFs to obtain GSC colonies. Once GSC colonies appeared, they were maintained under GSC culture conditions as described in section 3.2.4.

Figure 11 illustrates that GSCs form grape-like colonies that grow loosely attached on the supporting MEF layer. Notably, not all of the GSCs expressed *Oct4-GFP*, even though *Oct4* is a well-known maker for GSCs (Pesce et al., 1998). *Oct4-GFP* expression was heterogeneous in *in vitro* cultures with single cells, all cells or only cells at the boundaries of colonies positive for *GFP*. Flow cytometry analysis for *Oct4-GFP* and c-kit expression confirmed the above observation (Figure 12).

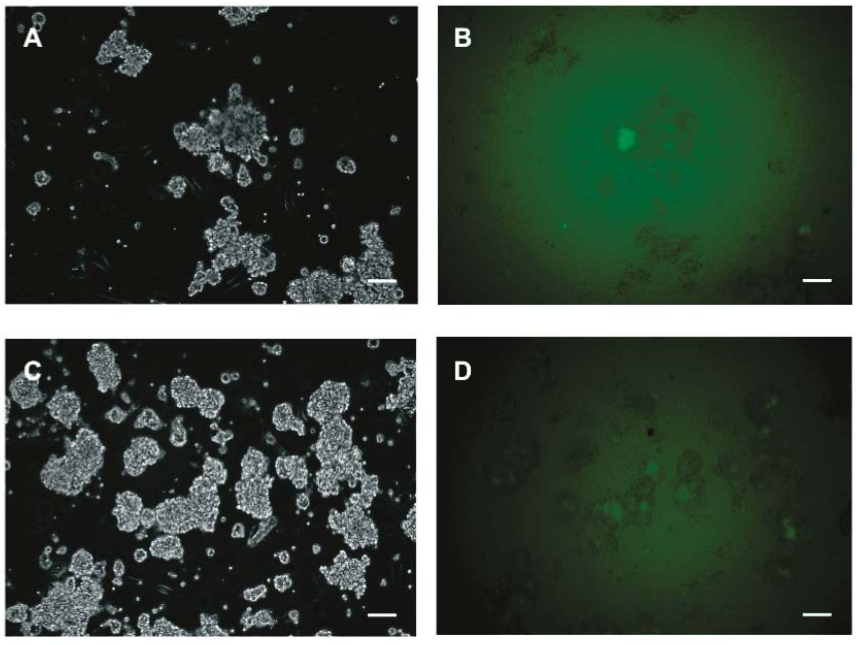

Figure 11. Morphology of *Oct4-GFP* GSCs at passage 42. A-D. GSC colonies exhibited a typical grape-like morphology (A, B). GSC colonies from *Oct4-GFP* testes (C, D) demonstrated heterogeneous *GFP* expression. *GFP*-positive as well as *GFP*-negative subpopulations were detected within the same culture. Scale bar indicates 100 µm.

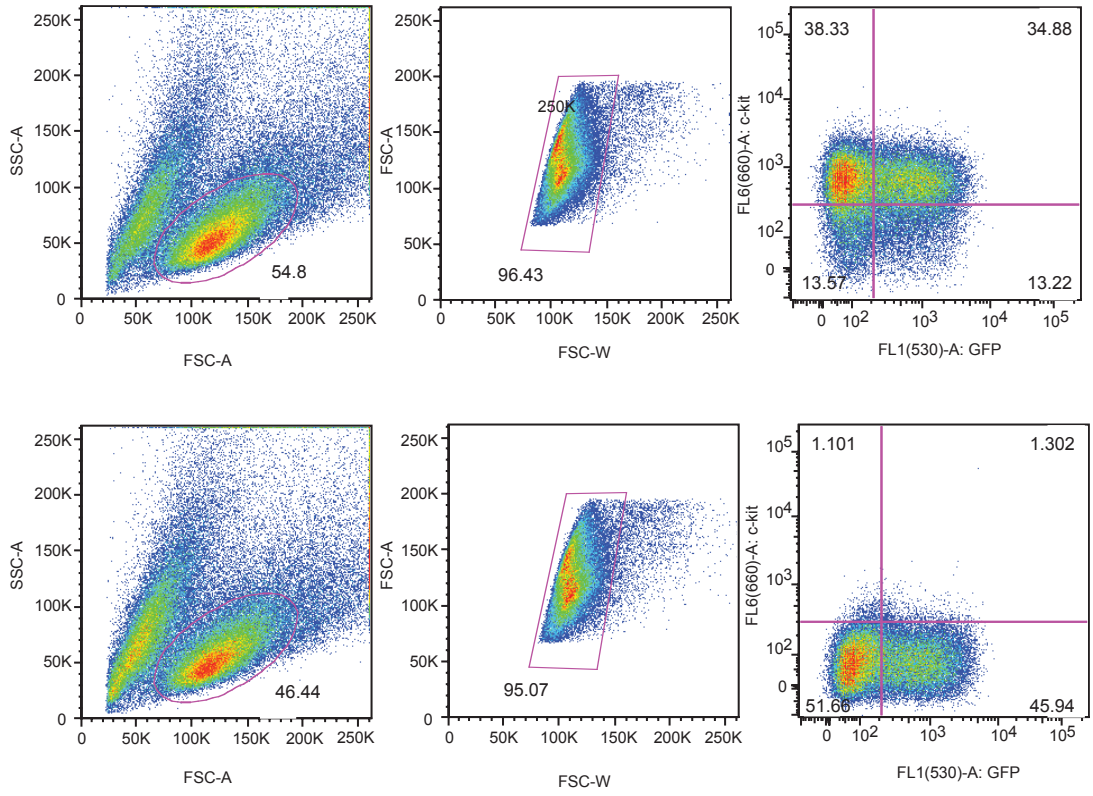

Figure 12. Flow cytometry analysis of *in vitro* cultured GSCs. GSCs (passage 42) were stained for the surface antigen c-kit and sorted for *GFP* and c-kit. The different expression pattern of *Oct4-GFP* and c-kit protein (upper panel) is shown in comparison to unstained GSCs (lower panel).

Within this study, we were unable to find an explanation for the appearance, disappearance and reappearance of *Oct4-GFP* signal within long-term *in vitro* cultures of GSCs. According to a previous report, early passages GSCs exhibit high *Oct4-GFP* expression in almost all cells of the GSC colonies (Ko et al., 2010; Ko et al., 2009; Ko et al., 2011). Additional studies addressing this phenomenon are needed to better understand *Oct4* expression during GSC derivation and *in vitro* culture.

5.1.2 Derivation of germline stem cells from human testicular biopsies

To derive human GSCs, each human testicular biopsy was digested with the enzyme mixture that was also used for digestion of mouse testes. Single cell suspensions were plated onto differently precoated tissue culture dishes at different cell densities. The culture methods of human testicular cells are summarized in Table 5.

To deplete fibroblast-like cells, human testicular cells were first plated on protein (gelatin, collagen IV, matrigel, or laminin)-coated wells after digestion and then transferred onto either protein coated-wells or MEFs (C3H or CF1) for further culture. The cells were maintained either under mouse GSC culture conditions in mouse GSC medium (mGSC) or human ESCs culture conditions with conditioned medium prepared from CF1 MEFs (hCM) as described in section 3.2.8. Medium compositions were slightly changed in case of biopsy number 7, 8, and 9; mouse GSC medium was made without LIF and with KOSR instead of serum. For biopsy number 12, human ESC conditioned medium and mouse GSC medium was mixed at a 1:1 ratio. Serial dilutions of the cell suspensions were performed before seeding onto protein-coated wells or MEFs at a ratio of 1:2 to 1:10 for biopsy number 5 and 6. The cells were maintained at 37 °C except biopsy number 11 that was cultured at 34 °C for the first 4 days to enhance cell survival and then transferred to 37 °C. The biopsy number 12 was maintained at 34 °C.

Table 5. Culture of human testicular biopsies under various conditions

Biopsy	Coating/Feeder	Medium	Temperature (°C)
1	gelatin	hCM & mGSC	37
2	collagen IV, C3H MEF	hCM & mGSC	37
3	gelatin, CF1 MEF	hCM & mGSC	37
4	gelatin, Matrigel	hCM & mGSC	37
5	gelatin, matrigel, CF1 MEF	hCM & mGSC serial dilution	37
6	gelatin, matrigel, CF1 MEF	hCM, serial dilution	37
7	gelatin, matrigel	hCM &mGSC without LIF	37
8	gelatin, matrigel	hCM &mGSC without LIF and with KOSR	37
9	gelatin, collagen IV	hCM &mGSC without LIF and with KOSR	37
10	gelatin, collagen IV	hCM	37
11	gelatin, laminin, C3H MEF	hCM & mGSC	34 (4 days) → 37
12	CF1 MEF	Mix of hCM and mGSC without LIF at a ratio of 1:1	34

Abbreviation: hCM = conditioned medium for culture of human embryonic stem cells; mGSC = medium for culture of mouse germline stem cells; KOSR = knockout serum replacement.

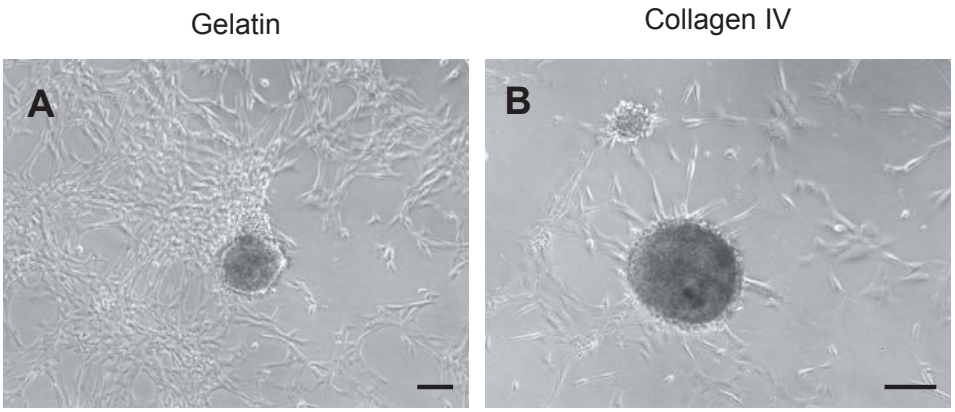

Figure 13. Morphology of human testicular cells grown on gelatin- or collagen IV-coated well. Cells isolated from human testis biopsies were cultured on gelatin-coated tissue culture dishes (A) or on collagen IV-coated tissue culture dishes (B). Scale bars indicate 100 μm in A and 75 μm in B.

The attached cells first exhibited a short spindle and irregular morphology and upon further cultivation a long spindle morphology resembling fibroblast cells. These cells formed different sized compact clumps, distinct from the typical flat morphology of human ESC colonies (Figure 15) after cultivation in human ESC conditioned medium at different time intervals. Different sized, round floating cells that did not attach to gelatin- or collagen IV-coated wells disappeared during culture, most probably due to medium change or apoptosis. The compact colonies survived up to 1 month in culture.

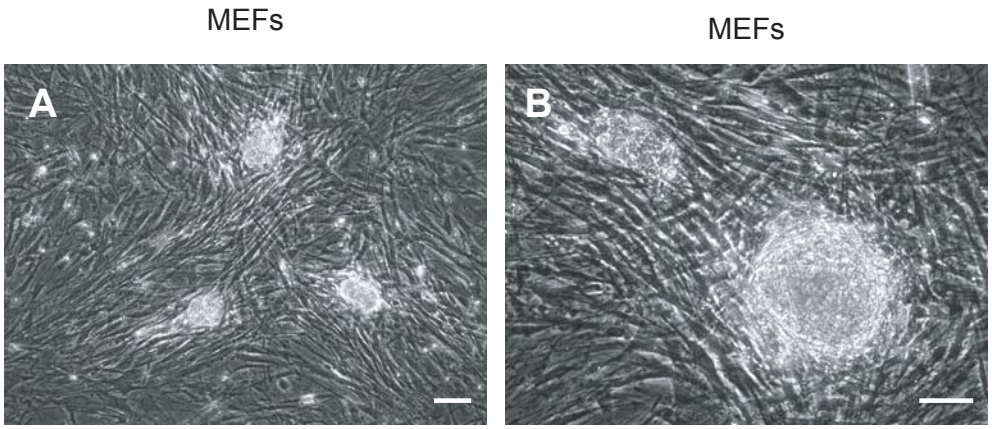

Figure 14. Morphology of human testicular cells grown on MEFs. The representative micrographs show small compact colonies (A) or large colonies (B) within a culture. These colonies differed morphologically significantly from typical human ESC colonies. Scale bars indicate 100 μm in A and 75 μm in B.

The human testicular cells were cultured on gelatin-coated tissue culture dishes with human ESC conditioned medium. Subsequently, the cells were transferred onto C3H MEF and incubated at 34 °C for 4 days. After this they were maintained at 37 °C for the following weeks. The cell supernatants attached to MEF cells and first showed short spindle or irregular morphology. Upon further culture they exhibited long spindle-like morphology similar to fibroblast cells. These cells were distinguishable from MEFs, since inactivated MEFs were plated at a confluent density as shown in A and B and survived up to 1 month under above-mentioned culture condition. The fibroblast-like cells grew rapidly and formed different sized compact colonies in different time intervals. Once the compact colonies had formed, they survived up to about 1 month in culture. The floating cells that did not attach to MEFs disappeared during further culture, most likely due to changing medium or apoptosis.

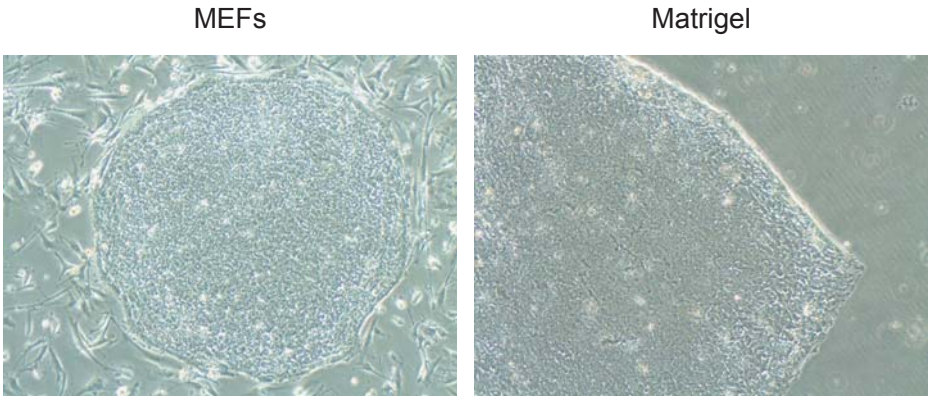

Figure 15. Morphology of human embryonic stem cells (WA09/H9) grown on MEFs and matrigel-coated well. Human ESCs (WA09/H9) were cultured on CF1 MEFs with human ESC medium and on matrigel-coated wells in human ESC conditioned medium.

Under all conditions tested, fibroblast-like human testicular cells attached to the protein-coated dishes. They grew rapidly under mouse GSC culture conditions and human ESC culture conditions in the presence or absence of feeder cells. Regardless of the culture condition (medium, feeder cells, coating, plated cell density, culture temperature, or duration of culture period), we observed formation of compact colonies (Figure 13 and 14), which morphologically differed from typically flat and large human ESC colonies (WA09/H9) (Figure 15).

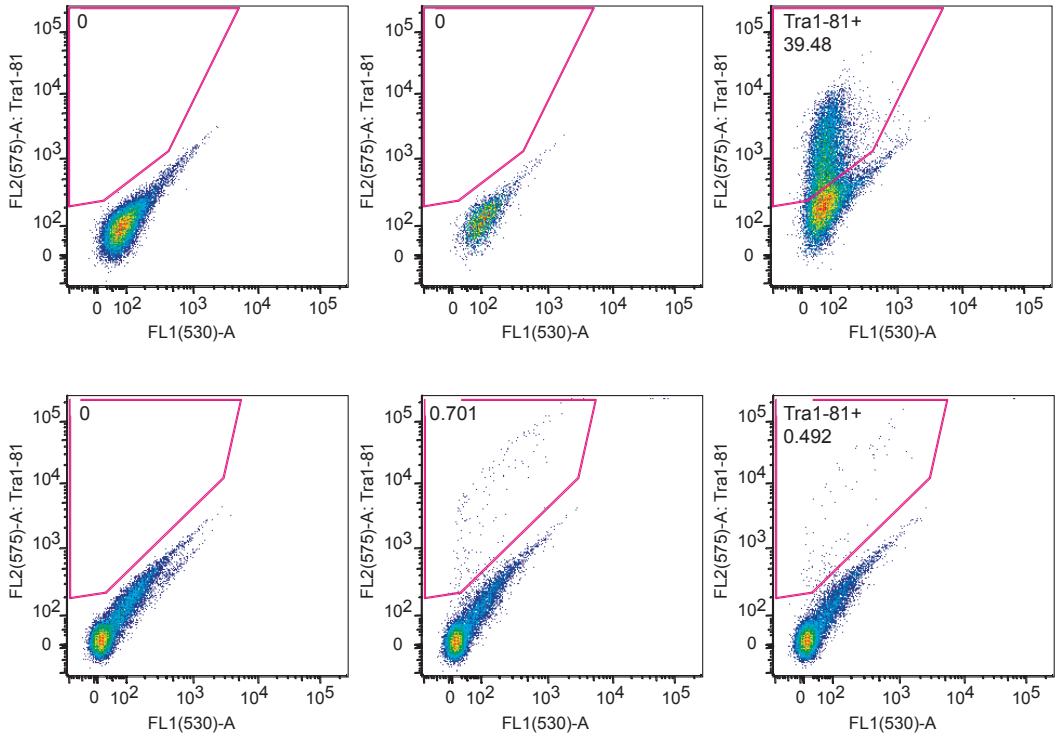

Figure 16. Flow cytometry analysis of the TRA1-81 surface antigen. Cell surface staining of human ESCs (WA09/H9) (upper row) and human testicular cells (lower row) for the human pluripotent cell marker TRA1-81 (first panel: unstained cells; second panel: secondary antibody only; third panel: TRA1-81 and PE conjugated anti mouse IgM). In contrary to the human ESC control that stained positive for TRA1-81 (upper row, third panel), freshly isolated human testicular cells stained only sporadically, most probably due to unspecific binding of the secondary antibody (lower row, second panel).

To further characterize the colonies formed from human testicular cells, flow cytometry analysis was performed using a TRA1-81 antibody. TRA1-81 is one of the widely used surface markers for characterization of human ESCs (Draper et al., 2002). TRA1-81 was readily detected on human ESCs (WA09/H9) as shown in Figure 16, while only sporadic expression was detected on human testicular cells. We attribute this low TRA1-81 expression to unspecific binding of the secondary antibody, since the signal for the PE-conjugated TRA1-81 staining was lower than the signal detected in staining with only the secondary antibody. These data suggest the absence of human ESC-like cells in the human testicular cell population. To identify the cell types in the colonies, the compact colonies (Figure 13 and 14) were collected, digested, and replated onto new plates. Neither GSC-like nor ESC-like cells could be

detected in these cultures, while the compact colonies outlined above formed again. They resembled the initial colonies used for morphological analysis (Figure 13 and 14) and most likely depict fibroblast-like cells.

5.2 Conversion of unipotent germline stem cells into pluripotent germline-derived stem cells

5.2.1 Conversion of germline stem cells from autologous testicular biopsy into germline-derived pluripotent stem cells

In order to convert unipotent GSCs into a pluripotent state, defined numbers of GSCs were plated and maintained 2-6 weeks in GSC medium until ESC-like colonies became obvious. Afterwards, ESC-like colonies were cultured in ESC medium and characterized using various methods to proof their pluripotent phenotype. The established cell lines were termed germline-derived pluripotent stem cells (Ko et al., 2010; Ko et al., 2009; Ko et al., 2011). Figure 17 illustrates the derivation procedure of autologous GSCs and gPSCs from *Oct4-GFP* transgenic mice. The cell lines established from OG2 mice are referred to as OG2 GSCs and gPSCs, and from OG2Rosa 26 mice as OG2Rosa GSCs and gPSCs.

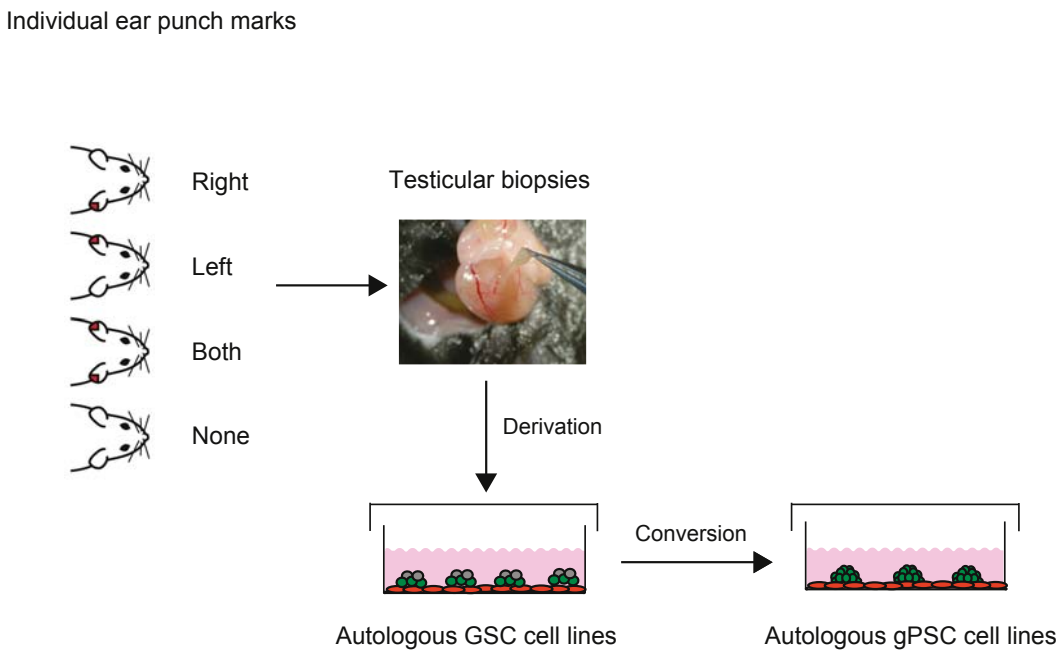

Figure 17. Derivation of autologous GSC cell lines and their conversion into gPSC cell lines. The testicular biopsies were taken from OG2 and OG2Rosa26 mice,

which were marked using ear clips to identify each biopsy. The autologous GSCs were derived from biopsies and maintained as cell lines, which were in turn converted into corresponding autologous gPSC cell lines. Abbreviation: R = right ear clip; L = left ear clip; B = both ear clips; none = without ear clips.

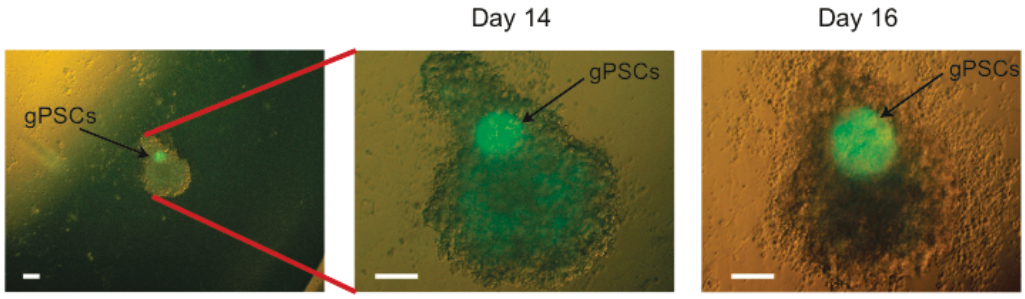

Figure 18. Reprogramming of GSCs into gPSCs (figure from Ko *et al*, *Nature Protocols*, 2010). The conversion of GSCs into gPSCs occurs within GSCs colonies. After about 2 weeks of culture, *Oct4-GFP* positive colonies appeared (left and middle picture) and increased in size by 16 days of culture (right picture). Scale bars indicate 200 µm.

As shown in Figure 18, *Oct4-GFP* was used as a first indicator to monitor the conversion process of GSCs into gPSCs. Once the subpopulation of *Oct4-GFP* positive GSCs converted into gPSCs, colonies with high levels of *GFP* were observed. These colonies closely resembled ESC colonies.

5.2.2 Characterization of germline stem cells from autologous testicular biopsy into germline-derived pluripotent stem cells

The morphological analysis of autologous OG2 and OG2Rosa26 GSCs shown in Figure 19 and 20 revealed formations of chain- and cluster-like colonies during *in vitro* culture. The *Oct4-GFP* expression of GSCs and LacZ-positive GSC colonies demonstrated in Figure 19 and 20 confirm the identity and origin of GSC lines.

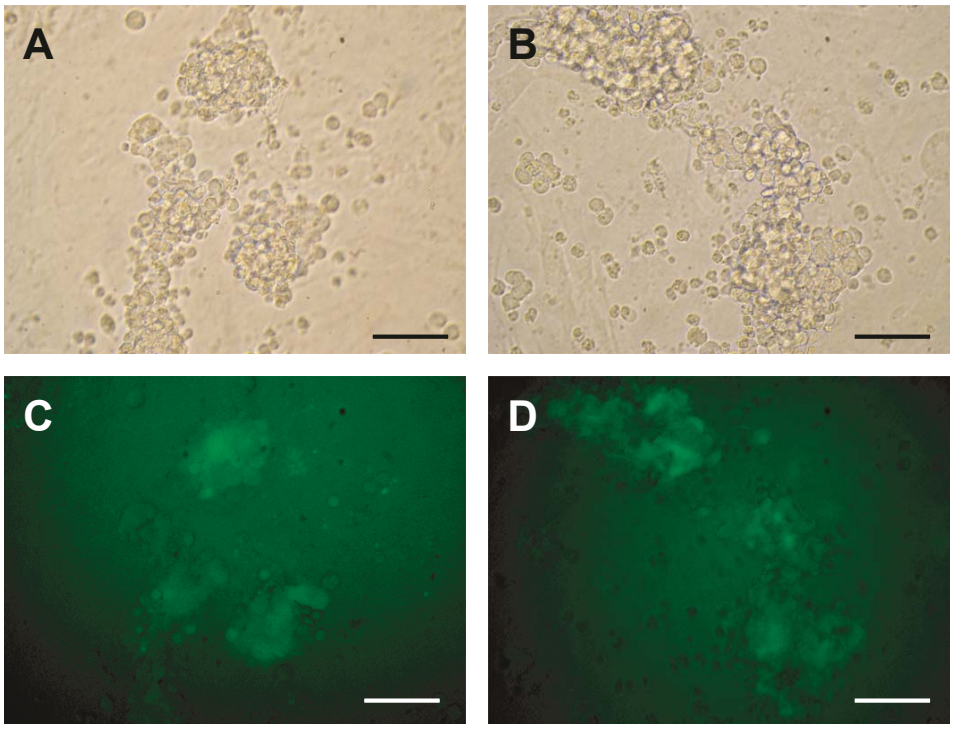

Figure 19. Morphology and *Oct4-GFP* expression within GSC colonies (figures from Ko *et al, Stem cells Rev and Rep,* 2011). OG2 GSCs show a grape-like structure (A, B) and express *Oct4-GFP* (C, D). Scale bars indicate 50 μm.

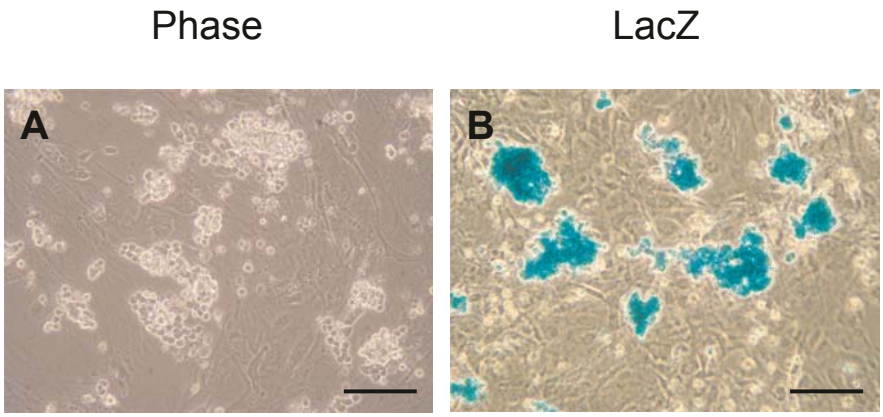

Figure 20. LacZ staining of GSCs (figures from Ko *et al, Stem cells Rev and Rep,* 2011). OG2Rosa26 form grape-like colonies (A) and stained positive for LacZ (B). Scale bars indicate 2 mm.

The established GSC lines were characterized at the RNA level using selected GSC-specific markers. Both GSC lines expressed *Oct4, Tex18, Piwil2, Vasa, Dazl,* and *Fragilis,* whereas MEFs did not express these genes indicating the successful

generation of autologous GSCs from testicular biopsies of OG2 and OG2Rosa 26 mice.

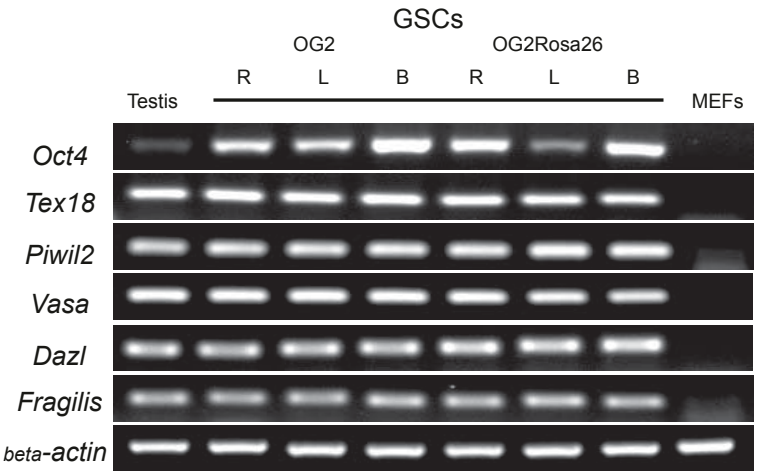

Figure 21. RT-PCR analysis of GSCs (figure from Ko *et al, Stem cells Rev and Rep*, 2011). OG2 and OG2Rosa GSCs were characterized by RT-PCR analysis using GSC-specific makers. The cells were generated from mice marked with right, left, and both ear clips. Abbreviation: R = right ear clip; L = left ear clip; B = both ear clips.

Furthermore, to prove cell identity and the unipotency of the *in vitro*-isolated and cultured GSCs, they were transplanted into infertile mouse testis. As expected, the transplanted cells restored spermatogenesis *in vivo* without teratoma formation.

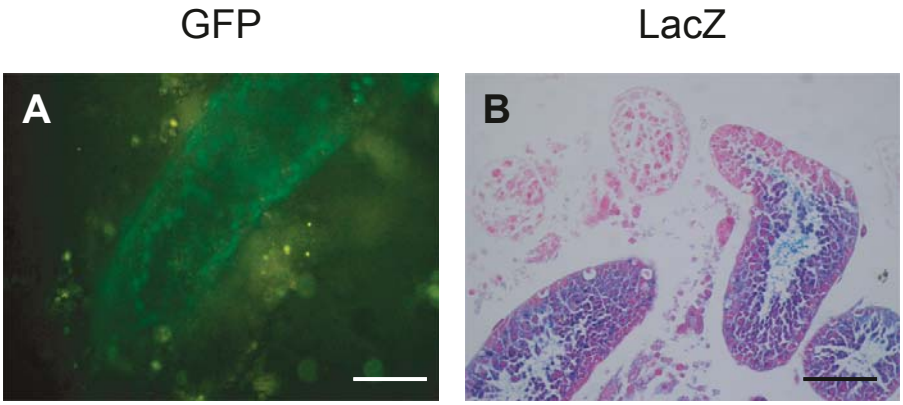

Figure 22. Testicular transplantation with GSCs (figures from Ko *et al, Stem cells Rev and Rep*, 2011). The transplanted GSCs colonized the seminiferous tubules of recipient mouse testis and expressed *Oct4-GFP* (A) and LacZ (B), respectively. Scale bars indicate 200 μm.

The autologous gPSCs from corresponding GSCs were analysed using GSC- and ESC-specific markers. The GSCs showed positive expression for *Oct4* and *Utf1*, but negative expression for *Nanog*, *Cripto*, and *Fgf4*, while gPSCs expressed *Oct4*, *Nanog*, *Cripto*, and *Fgf4* (Figure 23).

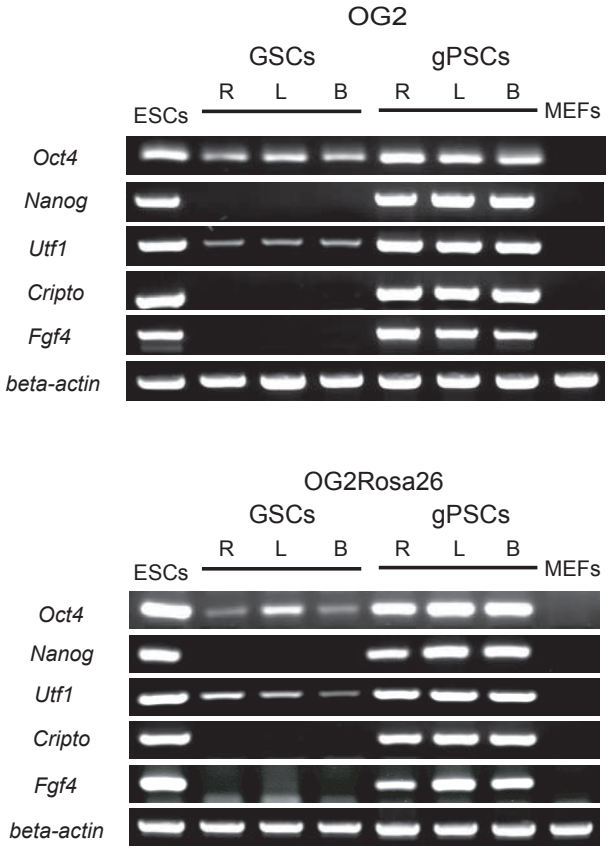

Figure 23. RT-PCR analysis of GSCs and gPSCs (figures from Ko *et al, Stem cells Rev and Rep*, 2011). Analysis of OG2-, OG2Rosa26- GSCs, and gPSCs cells by RT-PCR revealed expression of GSC- and ESC-specific markers in GSCs and gPSCs, respectively. Abbreviation: R = right ear clip; L = left ear clip; B = both ear clips.

Oct4-GFP expression analysis and LacZ staining confirmed the origin of gPSCs generated from autologous OG2 and OG2Rosa26 GSC lines and alkaline phosphatase and SSEA1 staining confirmed pluripotency.

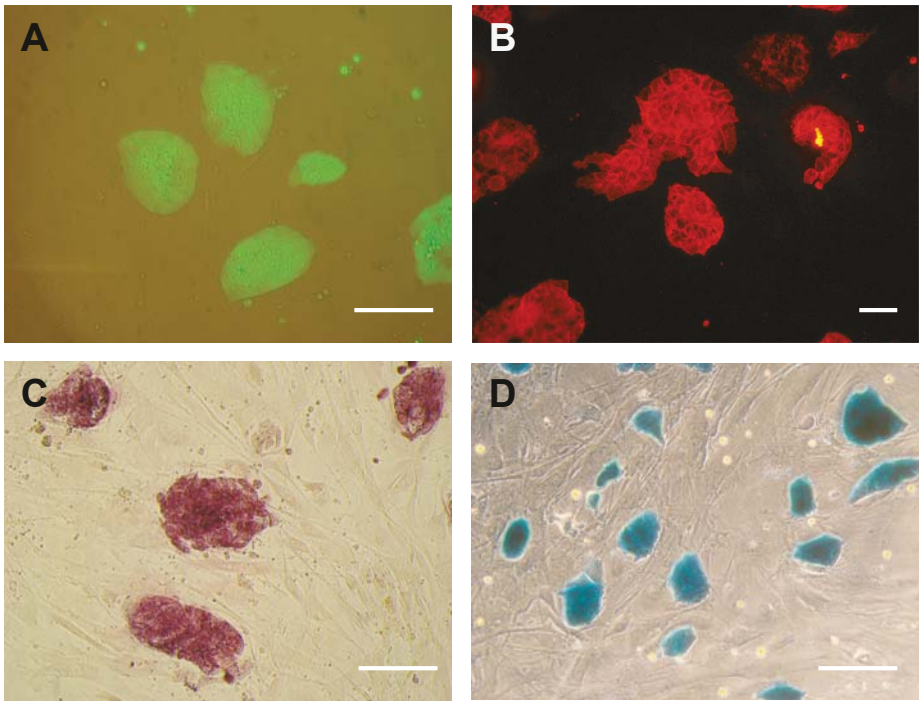

Figure 24. Phenotypical analysis of gPSCs (figures from Ko *et al, Stem cells Rev and Rep,* 2011). gPSCs expressed *Oct4-GFP* (A) and SSEA1 (B). The cells also stained positive for alkaline phosphatase (C) and LacZ (D). Scale bars indicate 200 μm.

Furthermore, micro array analysis was conducted to compare similarities and differences between GSCs and gPSCs that were generated from different mouse backgrounds and experiments. Figures 25 and 26 show the results of pairwise scatter plot analysis between two GSC lines: one with OG2 (C57BL/6) homogeneous genetic background ('GSC') and the other with OG2/LacZ Rosa 26 (C57BL/6 x129sv) heterogeneous genetic background ('GSCr'). A similar expression pattern between GSCs and the corresponding GSCrs was observed. After reprogramming of GSCs into pluripotent gPSCs, there were more differences found between the gPSCs than before the conversion, suggesting a slight difference in the reprogramming process between the cell lines. The heat-map and map of distance analyses using correlation metric shown

in Figure 28 and 29 supports the notion described above. Collectively, unipotent GSCs were clearly distinct from pluripotent ESC and gPSCs, while ESC and gPSCs share similar features (Figure 29).

The hierarchical clustering of samples shown in Figure 28B was performed using the correlation metric and the average linkage method. ESCs and gPSCs were nearly connected, while GSCs cluster differently. Particularly, gPSCr2 outlying from the other gPSCs in the PC1 (Figure 28A) was also remotely linked in the hierarchical clustering.

The heat-map and map of distances analysis of the gene expression data shown in Figure 29 confirm the clustering of gPSCs amongst each other and with the ESCs and a clustering of GSCs among themselves.

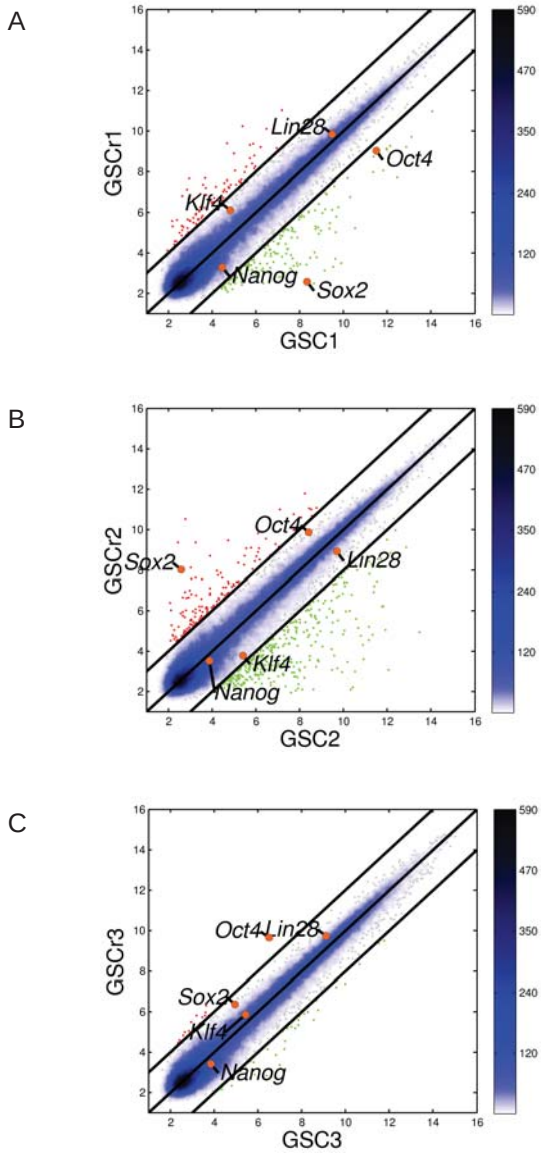

Figure 25. Pairwise scatter plot of GSC versus GSCr. A-C. Pairwise scatter plots of global gene expression profiles were compared between two different types of GSCs; GSC with homogenous genetic background versus GSCr with heterogeneous genetic background. In comparison to cell line number 1 (A) and number 2 (B) of GSC, cell line number 3 (C) shows more similarity between two different GSCs. In Figure 25A and 25B, *Sox2* is divergently expressed, which is not seen in Figure 25C.

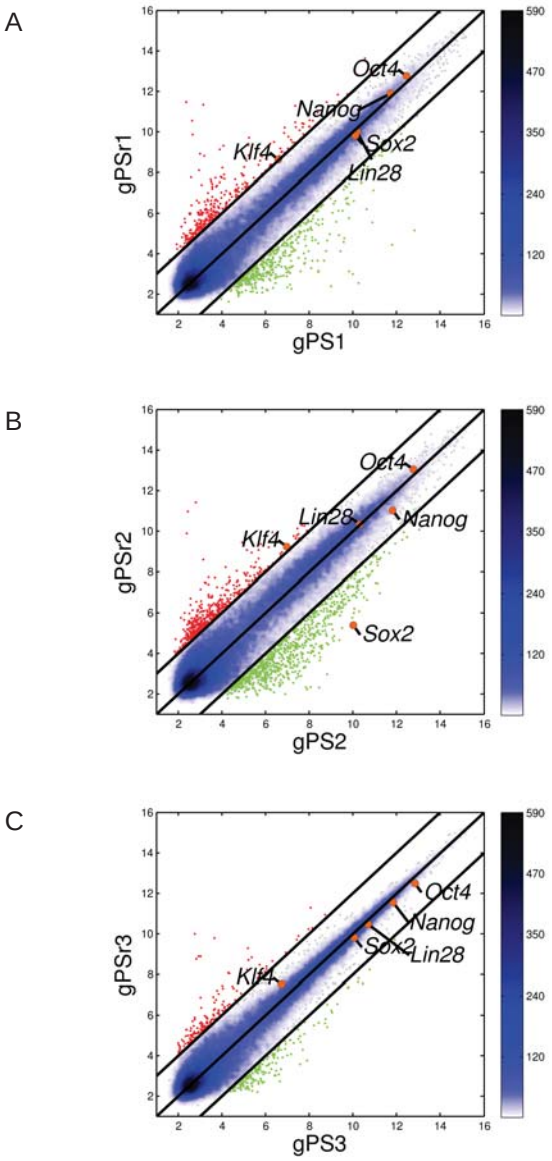

Figure 26. Pairwise scatter plot of gPSCs versus gPSCr. A-C. Pairwise scatter plots of global gene expression profiles were compared between two different types of gPSCs; gPSC with homogenous genetic background versus gPSCr with heterogeneous genetic background. In comparison to cell line number 1 (A) and number 2 (B) of gPSC, cell line number 3 (C) shows more similarity between two different gPSCs, namely gPSC3 and gPSCr3. Notably, Figure 26B reveals the afar expression of *Sox2*. Abbreviation: gPS = germline-derived pluripotent stem cells.

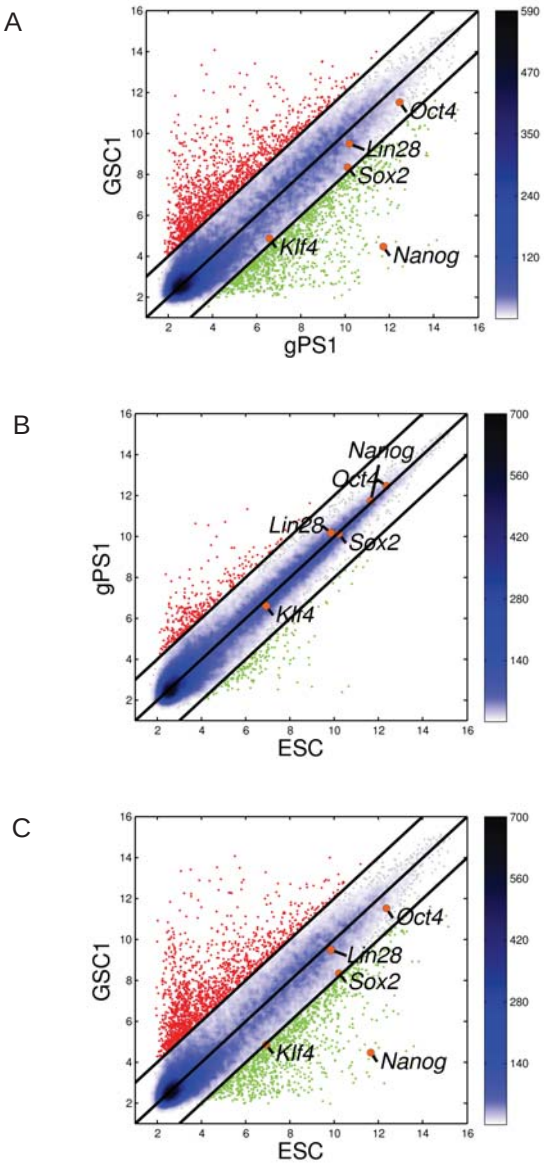

Figure 27. Pairwise scatter plot between GSC, gPSC, and ESC. A-C. gPSC comparison with GSCs (A) revealed some crucial differences between the two cell types, whereas comparison with ESCs (B) showed similarity. ESCs were also compared with GSCs (C) and demonstrated similar results in comparison to the results shown in Figure 27A, indicating the pluripotent feature of gPSCs and ESCs, and the unipotent feature of GSCs. Abbreviation: gPS = germline-derived pluripotent stem cells.

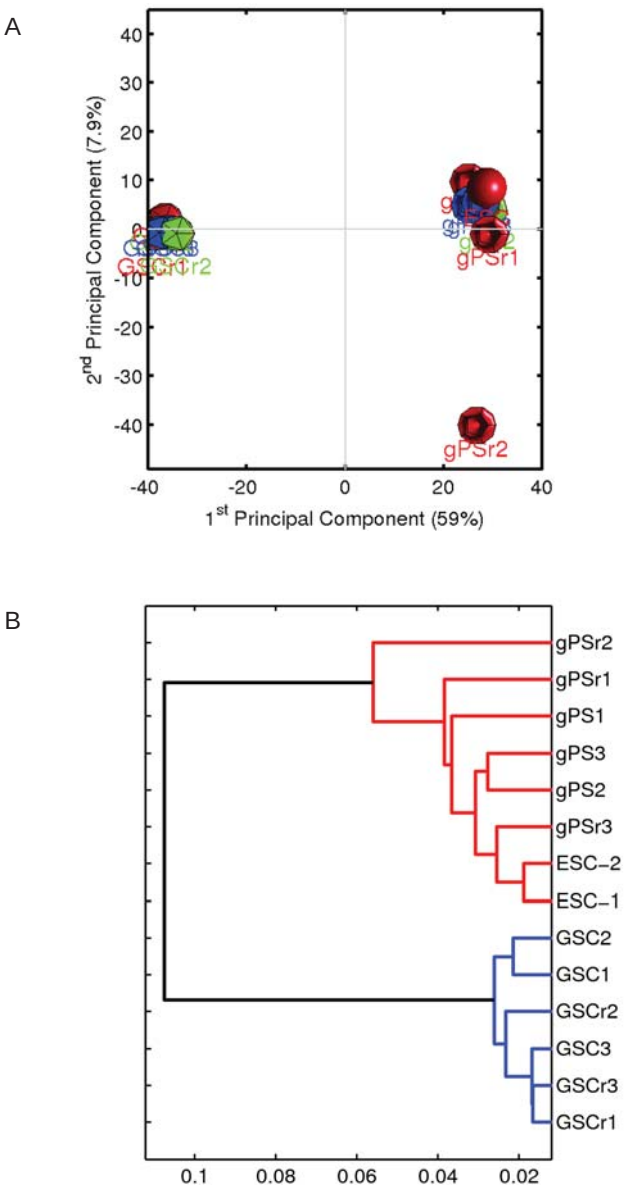

Figure 28. Micro array data using Principal Component Analysis (PCA) and Hierarchical clustering (figure from Ko *et al, Stem cells Rev and Rep,* 2011). Figure A shows that the first principal component (PC1) captures 59% and the second principal component (PC2) captures 7.9% of the gene expression variability. These two PCs combined capture 67% of the gene expression variability. Abbreviation: gPS = germline-derived pluripotent stem cells.

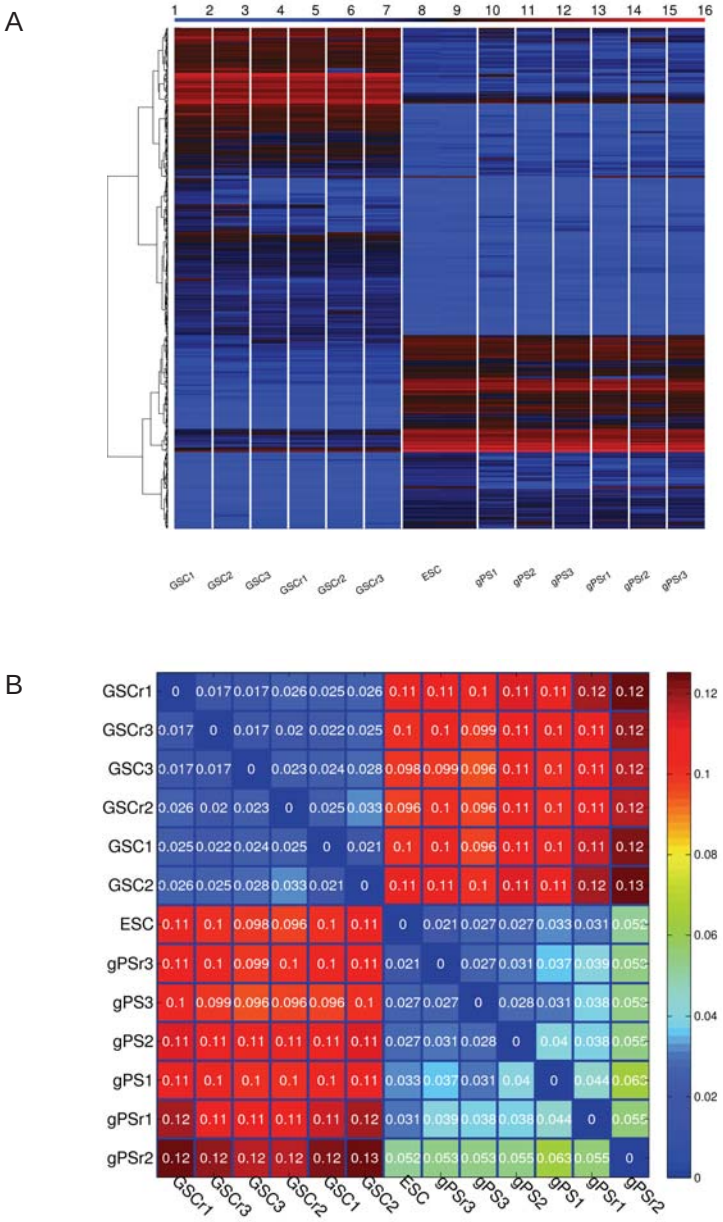

Figure 29. Analysis of heat-map and map of distances. Heap-map of pluripotent and germ cell marker gene expression extracted from the micro array analyses, GSCs demonstrate a different expression patterns than ESCs and gPSCs (A). Map of distances of expression of GSCs, gPSCs, and ESCs (B). Abbreviation: gPS = germline-derived pluripotent stem cells.

5.2.3 Differentiation ability of germline-derived pluripotent stem cells

5.2.3.1 *In vitro* and *in vivo* differentiation ability analysis

The differentiation capacity of gPSCs was examined using various methods *in vitro* and *in vivo*, including *in vitro* differentiation into three germ layers (endoderm, mesoderm, and ectoderm), teratoma formation, chimera formation, and germline contribution.

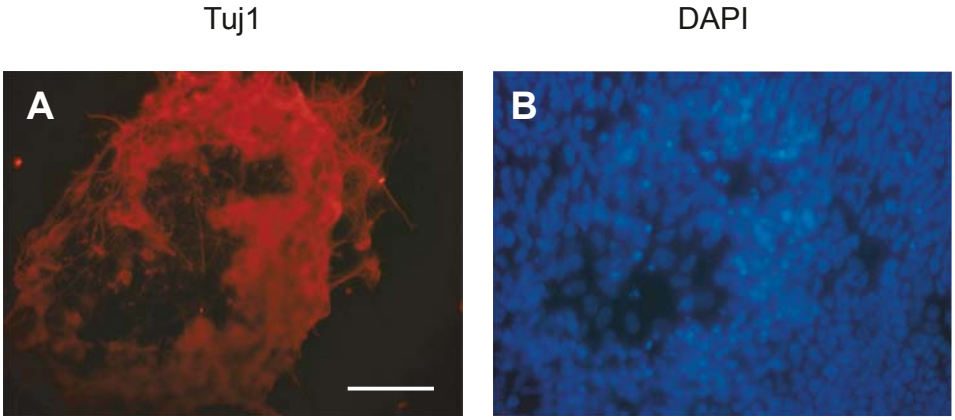

Figure 30. Differentiation of gPSCs into ectoderm lineage (figures from Ko *et al, Stem cells Rev and Rep,* 2011). gPSCs were differentiated into neurons *in vitro*, which was confirmed by the positive staining for the specific neuronal marker Tuj1. Scale bar indicates 200 μm.

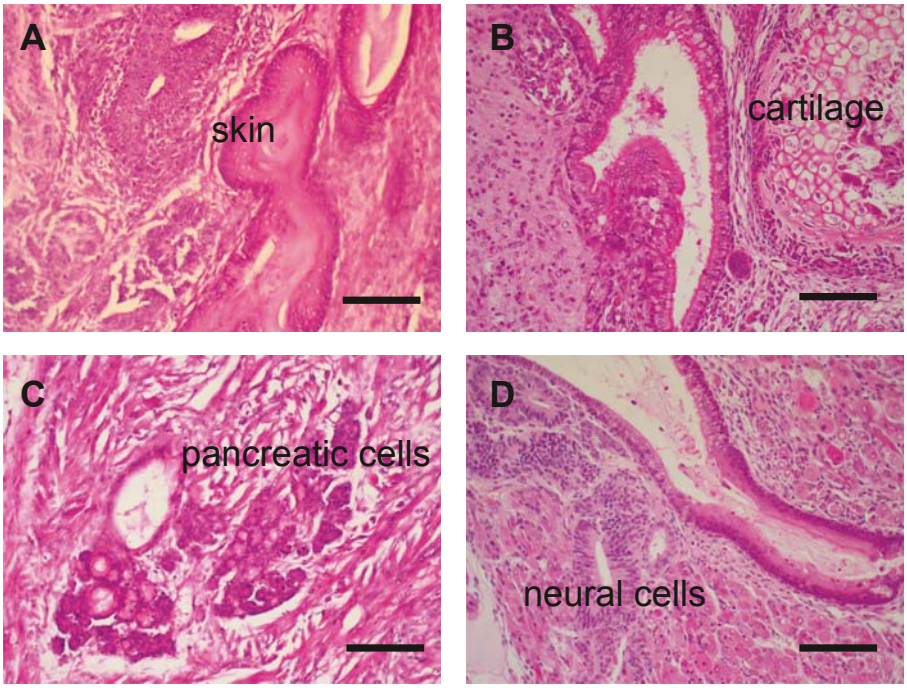

Figure 31. Teratoma formation after injection of gPSCs (figures from Ko *et al, Stem cells Rev and Rep,* 2011). gPSCs were injected into athymic mice and teratomas were formed after several weeks. The teratomas contained cells of the three embryonic germ layers ectoderm (skin, A and neural cells, D), mesoderm (cartilage, B), and endoderm (pancreatic cells, C). Scale bars indicate 50 µm.

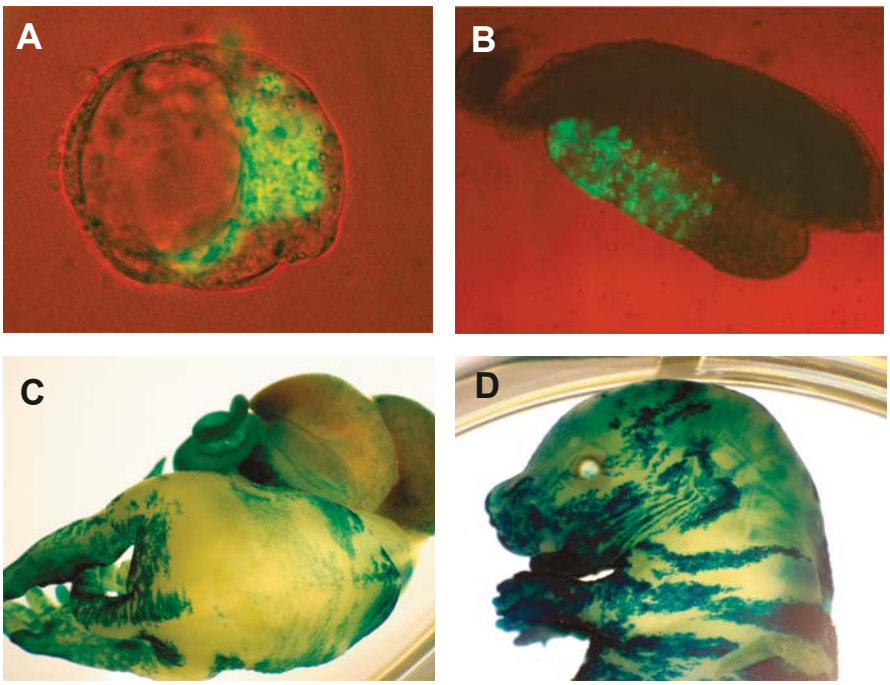

Figure 32. Generation of chimeric embryos and germline transmission (figures from Ko *et al, Stem cells Rev and Rep,* 2011). Blastocyst stage embryos were gener-

ated by aggregation of an eight-cell stage embryo with *Oct4-GFP*-positive gPSCs. The inner cell mass of the blastocyst reveals *Oct4-GFP* expression (A). Moreover, *Oct4-GFP*-positive germ cells were found in female gonads from E13.5 embryos (B). The generation of E13.5 chimeric embryos was proven by LacZ staining (C, D).

5.2.3.2 Differentiation of germline-derived pluripotent stem cells into endothelial cell-like cells

For the differentiation of gPSCs *in vitro*, suspension cultures were used to generate EBs. Five days after EB formation, cells were analyzed for CD31 expression by enzymatic digestion using Accutase. Cell suspensions were subjected to FACS sorting and the isolated CD31-positive cells were subcultured on OP9 cells in the presence of VEGF. Colonies with a uniform cobblestone-like morphology similar to that of endothelial cells formed after 35-45 days. Subsequently, these cells were transferred onto either gelatin- or collagen IV-coated tissue culture dishes for expansion, where they formed a monolayer (Figure 33 and 34) (Kevil and Bullard, 2001). These cells were termed gPSC-derived endothelial-like cells (gPSC-ECs).

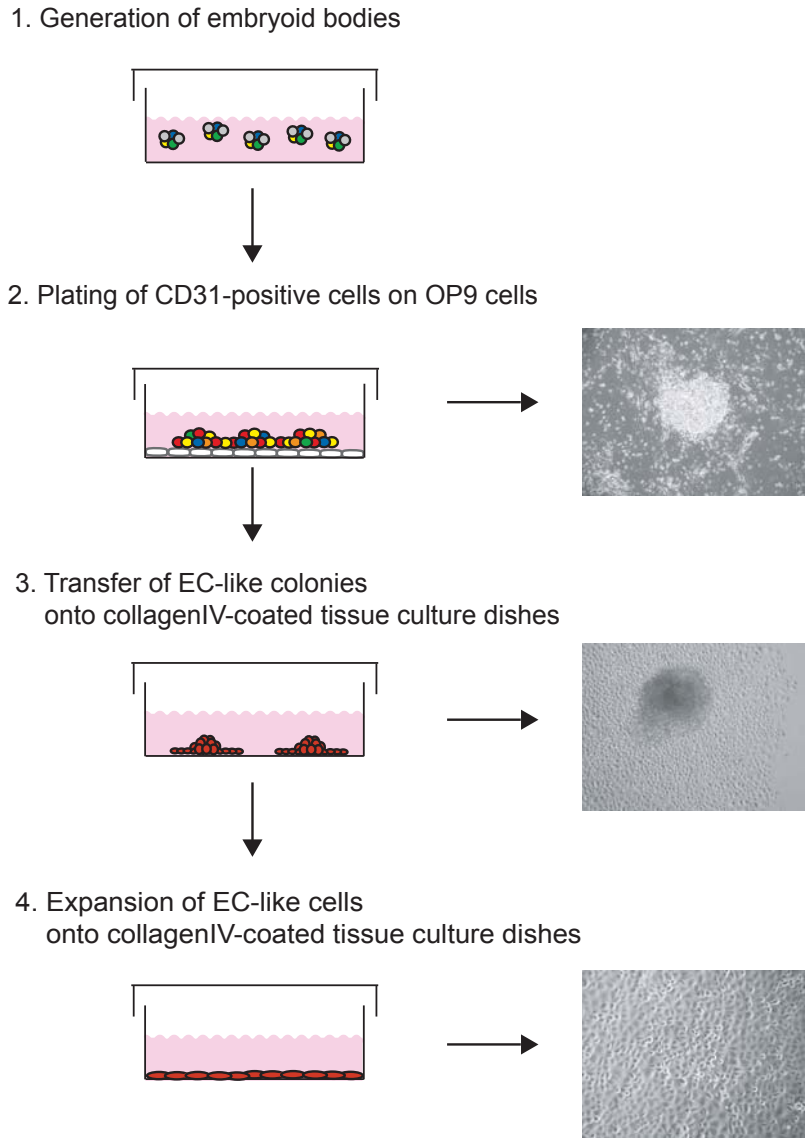

Figure 33. Derivation of EC-like cells from gPSCs. After generation of embryoid bodies, CD31-positive cells were isolated and cultured in the presence of VEGF for differentiation of gPSCs into the endothelial lineage (data were obtained in cooperation with Sarah Yoon Hee Eligehausen, WWU Münster, Germany).

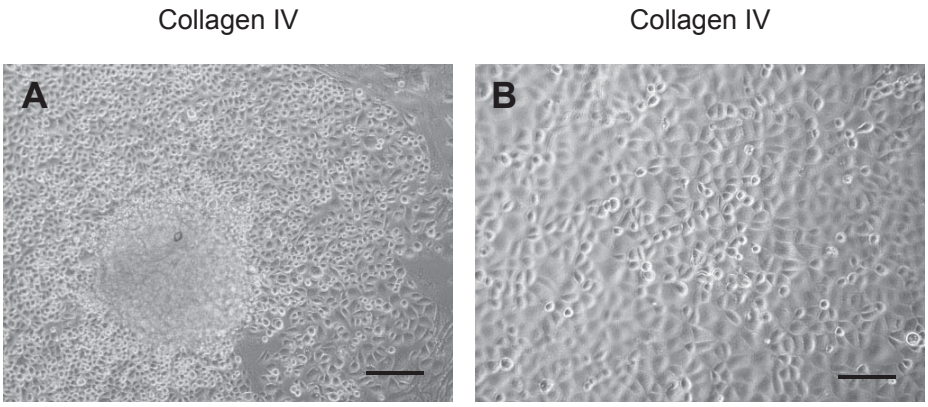

Figure 34. Morphological analysis of gPSC-derived EC-like cells. The cells were grown on collagen IV-coated tissue culture dishes (A, B) and exhibited a cobblestone-like morphology, one of the characteristics of endothelial cells. Scale bars indicate 250 µm (Data were obtained in cooperation with Sarah Yoon Hee Eligehausen, WWU Münster, Germany).

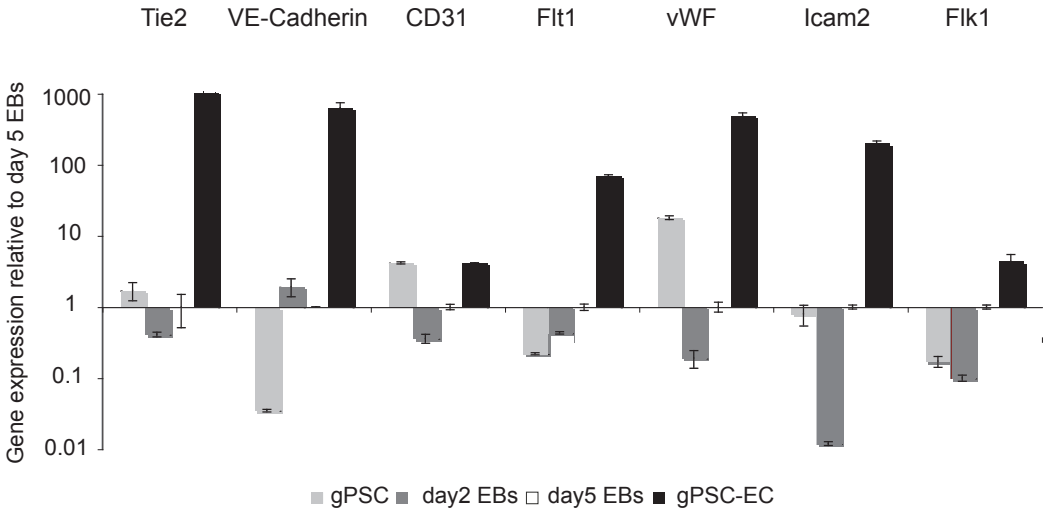

Figure 35. Real-time RT-PCR analysis of gPSC-derived EC-like cells. The cells express endothelial cell-specific marker genes including *Tie2*, *VE-Cadherin*, *CD31*, *Flt1*, *vWF*, *Icam2*, and *Flk1* (Data were obtained in cooperation with Sarah Yoon Hee Eligehausen, WWU Münster, Germany).

Gene expression profiling using real-time RT-PCR was carried out with gPSC, 2-day-old EBs, 5-day-old EBs, and gPSC-EC. Data were normalized relative to val-

ues of gene expression in 5-day-old EBs. The markers included angiopoietin and endothelial growth factor receptors (*Tie2*, *Flk1*, and *Flt1*), junctional adhesive molecules (*VE-Cadherin* and *CD31*), and other endothelial specific antigens (*Icam2* and *vWF*). As shown in Figure 35, the endothelial cell-specific markers *Tie2*, *VE-Cadherin*, *Flt1*, *vWF*, *Flk1*, and *Icam2* exhibited a significantly higher expression in gPSC-EC, than in undifferentiated gPSCs and EBs. Notably, gPSCs expressed *CD31*, whereas *CD31* expression was downregulated during differentiation. The level of *CD31* expression was then restored in gPSC-EC, suggesting the progressive differentiation of gPSCs into the endothelial lineage. This *CD31* expression pattern is consistent with previous studies, which have shown that CD31 protein is expressed on the entire surface of undifferentiated ESCs. During differentiation, CD31 was found to be transiently downregulated and to become restricted to the site of cell-to-cell contacts in differentiated cells (Drake and Fleming, 2000; Li et al., 2005).

Moreover, the similar pattern of *vWF* expression during differentiation, the exclusive expression of *Tie2* in gPSC-EC, and the lack of expression in other cell types all support the endothelial feature of gPSC-derived cells (Mariappan et al., 2009).

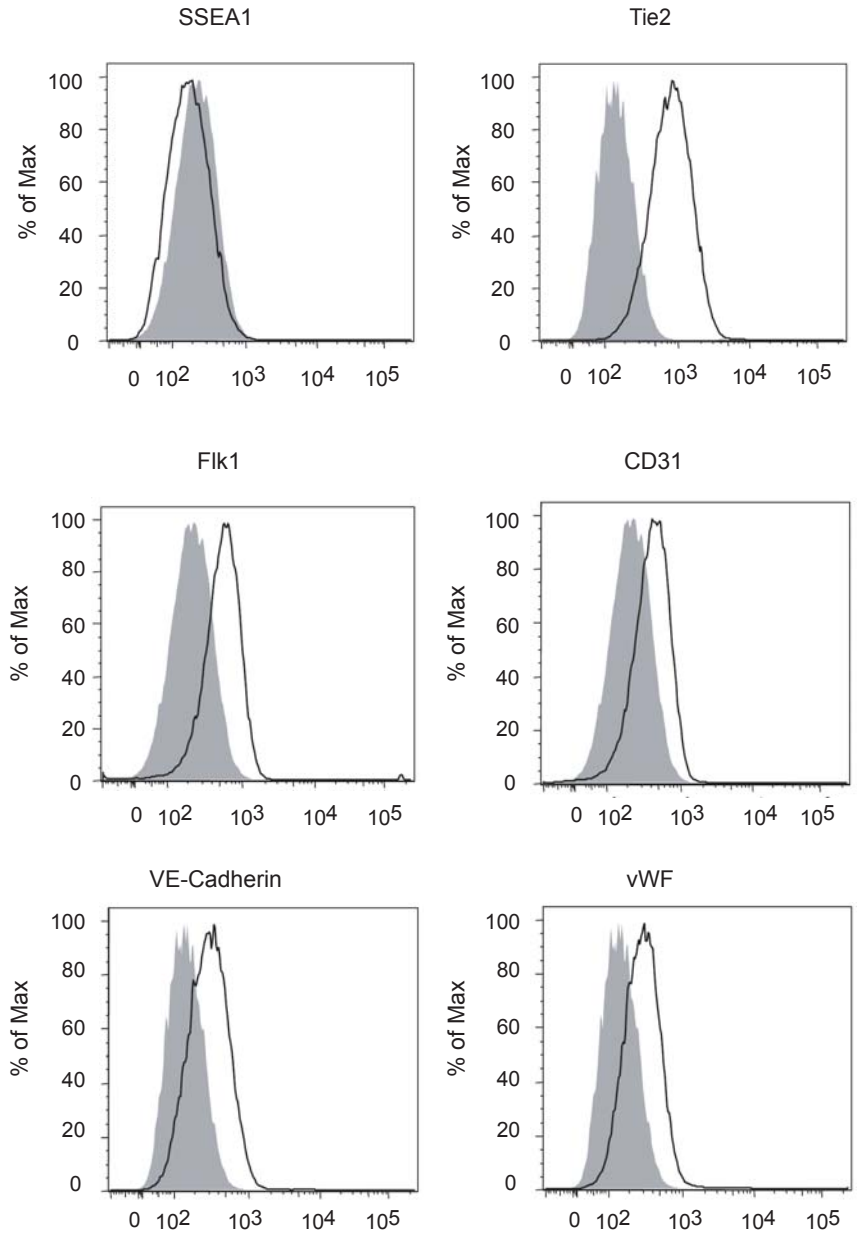

Figure 36. Flow cytometric analyses of gPSC-derived EC-like cells. Cell surface staining of gPSC-derived EC-like cells was performed with antibodies directed to the indicated proteins on the x-axis. Overlays compare the expression of IgG control (gray) versus the indicated proteins (no fills). The y-axis represents the percentage of maximum expression (Data were obtained in cooperation with Sarah Yoon Hee Eligehausen, WWU Münster, Germany).

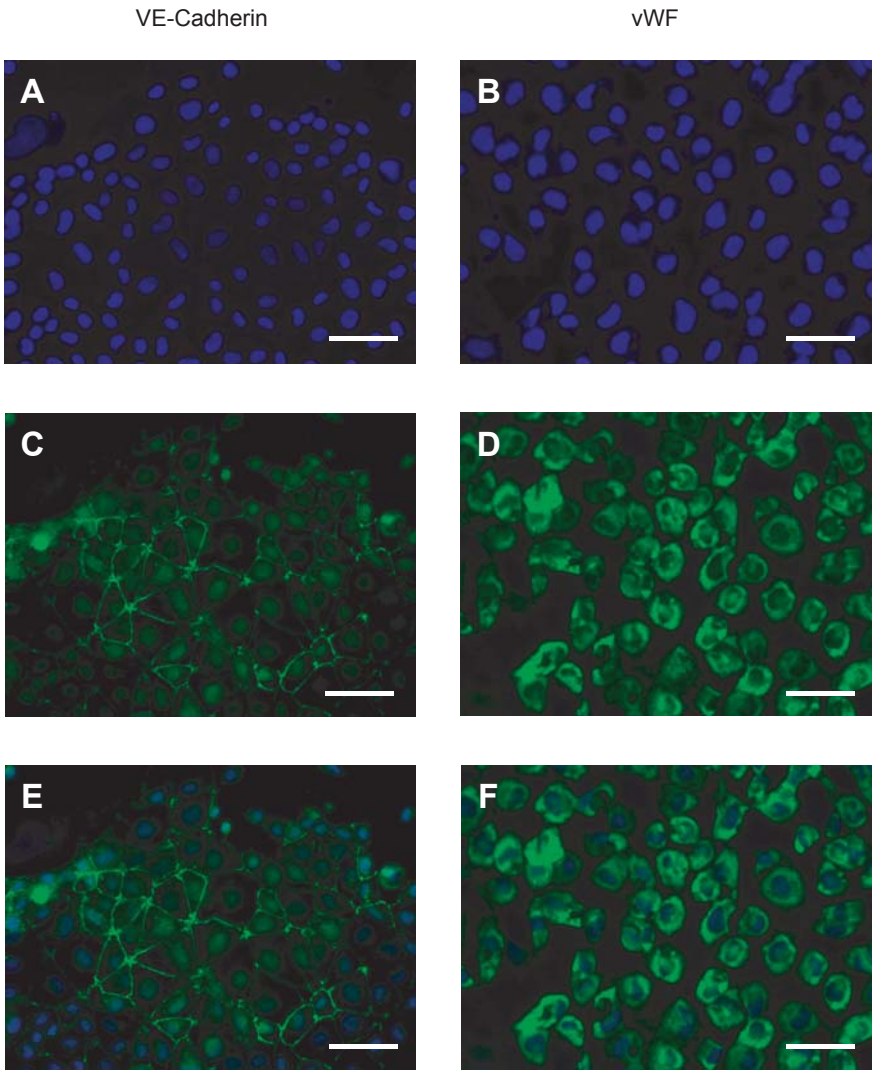

Figure 37. Immunocytochemical analyses of gPSC-derived EC-like cells. The cells were stained with VE-Cadherin (B, E) and vWF (D, F), indicating the endothelial characteristic of gPSC-ECs. Figure 37A and 37C show the DAPI-stained cells. Figure 37E and 37F show the merged images of VE-Cadherin, vWF staining in green and DAPI staining in blue. Scale bars indicate 50 µm (Data were obtained in cooperation with Sarah Yoon Hee Eligehausen, WWU Münster, Germany).

The phenotypical analysis of gPSC-derived cells was performed using flow cytometry analysis. The gPSC-derived cells expressed endothelial cell-specific markers including Tie2, Flk1, CD31, VE-Cadherin, and vWF. The ESC marker SSEA1 was not detected on the cells, excluding the possible existence of undifferentiated gPSCs in *in vitro* culture of gPSC-derived cells (Figure 36).

Consistent with the FACS data, immunofluorescence staining of the cells demonstrated that the endothelial cell-specific marker VE-Cadherin was expressed at the cell adherent junctions and vWF (Figure 37), a glycoprotein synthesized by endothelial cells, was expressed on the gPSC-derived cells.

To examine the functionality of gPSC-derived cells *in vitro*, LDL uptake, and tube formation assays were performed. As shown in Figure 38, the cells incorporated Dil-Ac-LDL, which is one of the characteristics of endothelial cells (Voyta et al., 1984). Moreover, *in vitro* functionality of the cells was assessed by culture on matrigel in the presence of VEGF, which can promote vascular morphogenesis of endothelial cells (Matsumura et al., 1997; Young et al., 2002). As demonstrated in Figure 39, they formed tube-like networks on matrigel, which displayed *Bandeiraea simplicifolia* 1 (BS1)-lectin binding, another characteristic of endothelial cells (Asahara et al., 1999).

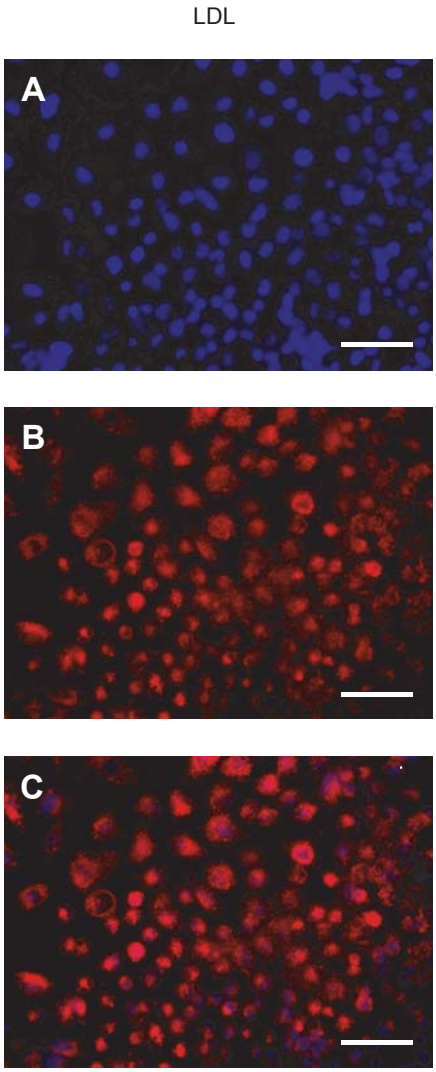

Figure 38. LDL uptake analysis of gPSC-derived EC-like cells. The gPSC derived EC-like cells take up Dil-conjugated acetylated low-density lipoprotein (Dil-Ac-LDL), thereby confirming their *in vitro* functionality. The cells were stained with DAPI (A) and LDL (B). The merged picture (C) shows DAPI staining in blue and LDL uptake in red. Scale bars indicate 50 µm (Data were obtained in cooperation with Sarah Yoon Hee Eligehausen, WWU Münster, Germany).

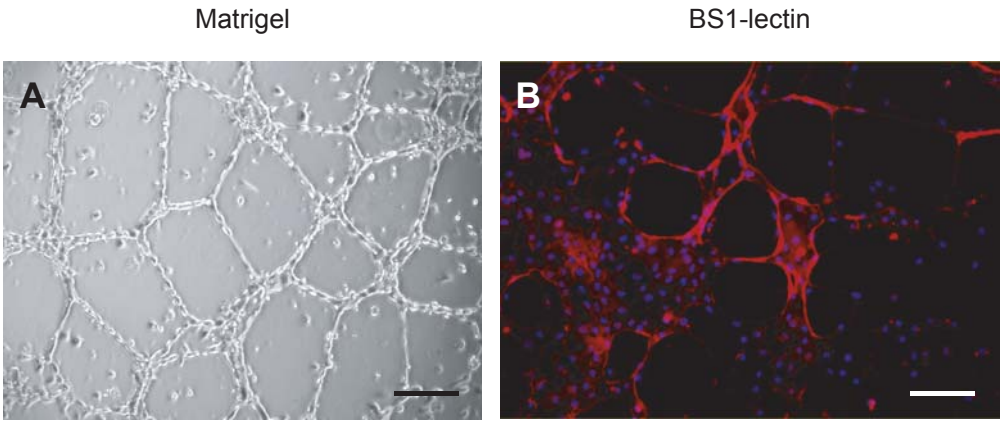

Figure 39. *In vitro* functional analysis of gPSC-derived EC-like cells. Cells form tube-like structures on matrigel (A), which stained with BS1-lectin in red and DAPI in blue (B). Scale bars indicate 250 µm (Data were obtained in cooperation with Sarah Yoon Hee Eligehausen, WWU Münster, Germany).

5.3 *In vitro* differentiation of germline stem cells

5.3.1 Differentiation of germline stem cells into meiotic cells

Since GSCs depict the *in vitro* counterparts of SSC, the established *Oct4-GFP* GSC lines were used to recapitulate spermatogenesis *in vitro*. For stepwise differentiation, GSCs were co-cultured with Sertoli cells and media containing defined factors, which are suggested to promote proliferation and differentiation of GSCs into meiotic cells as shown in Figure 40.

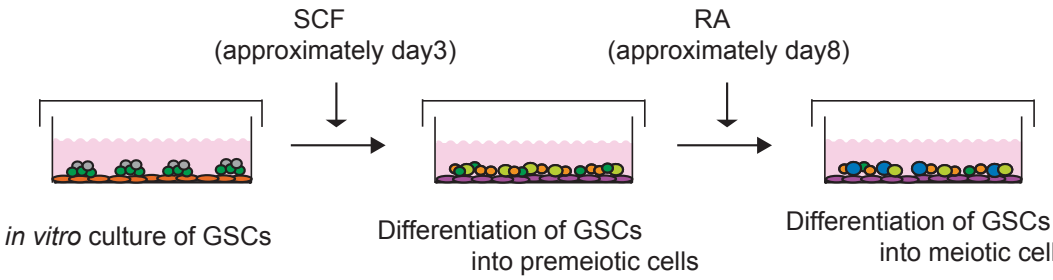

Figure 40. Stepwise induction of differentiation potential of GSCs. GSCs were differentiated to premeiotic cells in response to the addition of steel factor and *in vitro* meiosis was induced by supplementation of retinoic acid.

The time course of c-kit expression at the RNA and protein level was utilized as a first indicator of GSC differentiation. In a previous report, it has been shown that c-kit is expressed in different subtypes of spermatogonia and required for ligand SCF (also known as kit-ligand KL, steel factor) function for the survival and proliferation of differentiating type A spermatogonia (Yoshinaga et al., 1991). Thus, cells were cultured in the presence of SCF to stimulate the differentiation of GSCs into premeiotic cells. Thereafter, cells were treated with RA to induce maturation and progression into the more advanced stages of meiosis. RA has been reported to induce the initiation and completion of meiosis, and its elimination leads to meiotic arrest in RA-mutant mice *in vivo*. RA is therefore considered a major meiotic regulator of spermatogenesis (Anderson et al., 2008; Baltus et al., 2006; Mark et al., 2008).

5.3.2 Characterization of meiotic cells

5.3.2.1 Flow cytometry analysis of *in vitro*-generated cells

The capability of GSCs to differentiate into premeiotic cells was determined by assessing the pattern of c-kit protein expression and *Oct4-GFP* expression in a time-course analysis at day 0, day 3, and day 8 of *in vitro* differentiation. For this, differentiation cultures were enzymatically digested and live cells were separated from dead cells, aggregates, or debris. Subsequently, single cells were gated for analysis (Figure 41). As expected, *Oct4-GFP* expression declined upon differentiation and c-kit expression was significantly up regulated by day 3 of *in vitro* differentiation (Fig-

ure 41A and 41B). After addition of SCF to the medium, c-kit expression was significantly downregulated, suggesting the progressive differentiation of GSCs towards spermatocytogenesis, the premeiotic stage of spermatogenesis by day 8 of *in vitro* differentiation (Figure 41C and 41D), suggesting that the cells had initiated differentiation and subsequently entered meiosis. This result is consistent with a previous report (Yoshinaga et al., 1991), in which expression of c-kit was not found in undifferentiated spermatogonia type A_s, while the onset of expression occurred in differentiating spermatogonia and c-kit downregulation took place upon entry into meiosis.

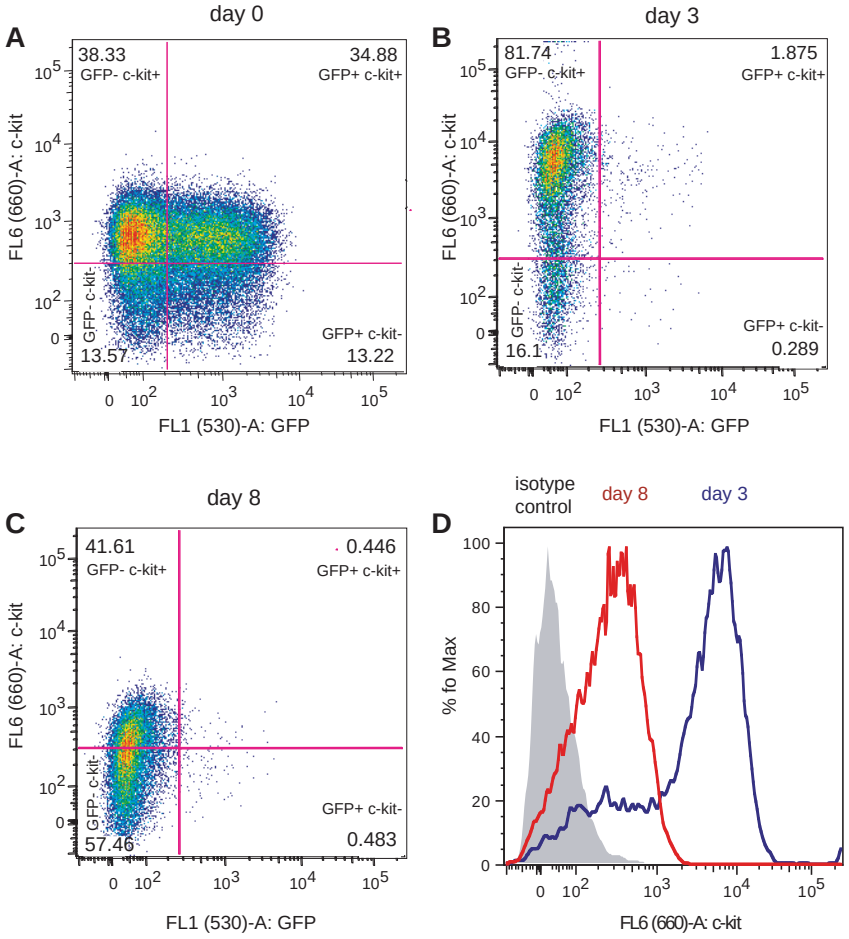

Figure 41. Flow cytometry analysis of *in vitro*-generated cells on different days of culture. *Oct4-GFP* expression and c-kit protein expression levels were determined during *in vitro* differentiation on day 0 (A), day 3 (B), and day 8 (C) and displayed as percentage. Overlays (D) compare the c-kit expression of IgG control (gray) versus cells on day 3 (blue line) of differentiation and day 8 of differentiation (red line).

5.3.2.2 Immunofluorescence staining

After approximately 8 days of differentiation, RA was added to the *in vitro* culture and progression into the more advanced stages of meiosis was monitored. Entry into and progression through meiosis was found to be associated with the formation of synaptonemal complexes- a unique feature of meiosis that occurs in different stages of the first meiotic division- leading to DNA recombination (Inselman et al., 2003). Thus, immunofluorescence staining was performed using an antibody directed to Scp3 (Figure 42).

Figure 42 demonstrates the efficiency of meiotic entry and progression of spermatocyte-like cells on days 8 and 14 of differentiation. Since the majority of meiotic cells were detected in the supernatant of the cultures, all floating cells were collected on day 8, 10, and 14 of differentiation and performed Scp3 and DAPI staining. The Scp3-stained cells were classified into a punctuated or elongated pattern, resembling leptotenema, or zygotenema, pachytenema, and diplotenema in the mouse testis, respectively. Furthermore, semi-quantitative analysis of Scp3-stained cells was carried out to evaluate the time window of meiotic development in the present *in vitro* culture system. The total number of DAPI-stained nuclei and DAPI-positive nuclei with punctuate or elongated Scp3 patterns, respectively, were counted and calculated as percentages (Table 6). The percentage of punctuate-stained cells decreased, while that of elongated-stained cells increased during the time course of differentiation, indicative for meiotic progression of GSCs in the first meiotic division.

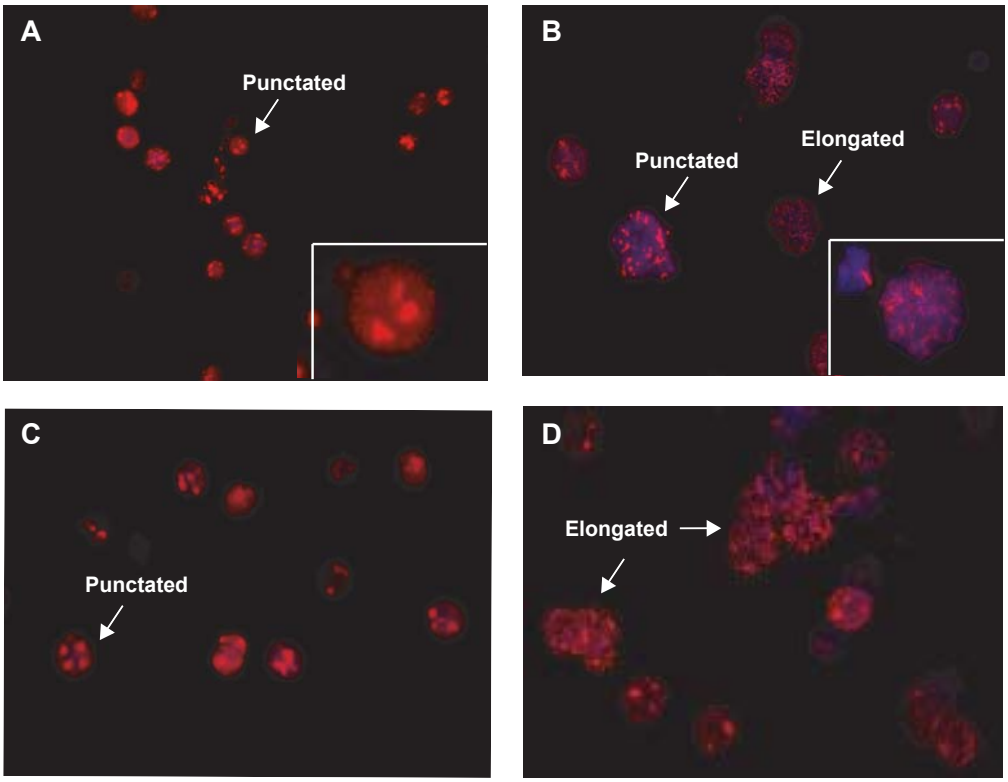

Figure 42. Scp3 staining of *in vitro*-differentiated cells. Scp3 staining was performed on day 8 (A, C) and day 14 (B, D) of *in vitro* differentiation and evaluated as either punctuated or elongated pattern. The insert in Figure 42A and 42B depicts a Scp3-positive cell at higher magnification.

Table 6. Semi-quantitative analysis of *in vitro*-derived spermatocytes

Day of differentiation	Cells with punctuated Scp3-staining pattern	Cells with elongated Scp3-staining pattern	Scp3-negative cells	Total number of DAPI- positive cells
Day 8	205 (27%)	18 (2.3%)	536 (70.7%)	759
Day 10	118 (50.8%)	17 (7.3%)	97 (41.9%)	232
Day 14	130 (49.4%)	104 (39.5%)	29 (11.1%)	263

5.3.2.3 Transmission electron microscopy

The ultrastructure of *in vitro*-generated cells was compared with *in vivo* counterparts by TEM analysis. For morphological analysis and stage determination of *in vitro*-generated spermatogenetic cells, different *in vivo* stages of spermatogenesis were studied.

In Figure 43A and 43B, round spermatid and type B spermatogonia are shown. Type B spermatogonia have rounded and smaller nuclei, which are filled with electron-dense nucleoplasmic material. In contrast, type A spermatogonia have large nuclei and are poor in endoplasmatic reticulum (data not shown). The endoplasmic reticulum has round and elongated cisterns with free ribosome clusters nearby and lies free in the cytoplasm or close to the cell membrane. The elongated cisterns appeared to be interrelated, with a predominance of smooth endoplasmic reticulum over the granular endoplasmic reticulum.

In Figure 43C and 43D, *in vivo* primary spermatocytes are shown. Primary spermatocytes are of a similar size as spermatogonia and have a spherical nucleus with fine granulated chromatin (Figure 43C). The endoplasmic reticulum is reduced in comparison to that of spermatogonia. The size, shape, and internal structure of the mitochondria of these cells recall those of spermatid and spermatogonia shown in Figure 43A and 43B. A characteristic feature of these cells is the presence of the synaptonemal complex, which appears as three parallel electron-dense lines in longitudinal sections. Frequently this structure extends from the nuclear membrane (Figure 43C and 43D).

Furthermore, these cells are characterized by the presence of intercellular bridges (Figure 43E) and a dense multivesicular structure of irregular shape between the nuclear membrane and the plasma membrane, called chromatoid body (Figure 43E and 43F). In the pachytene stage of the meiotic prophase I, matured cells show a larger and more complex region of the Golgi apparatus and an increased number of mitochondria, which have dilated cristae. The mitochondria tend to cluster and electron dense material appeared between them (Figure 43D).

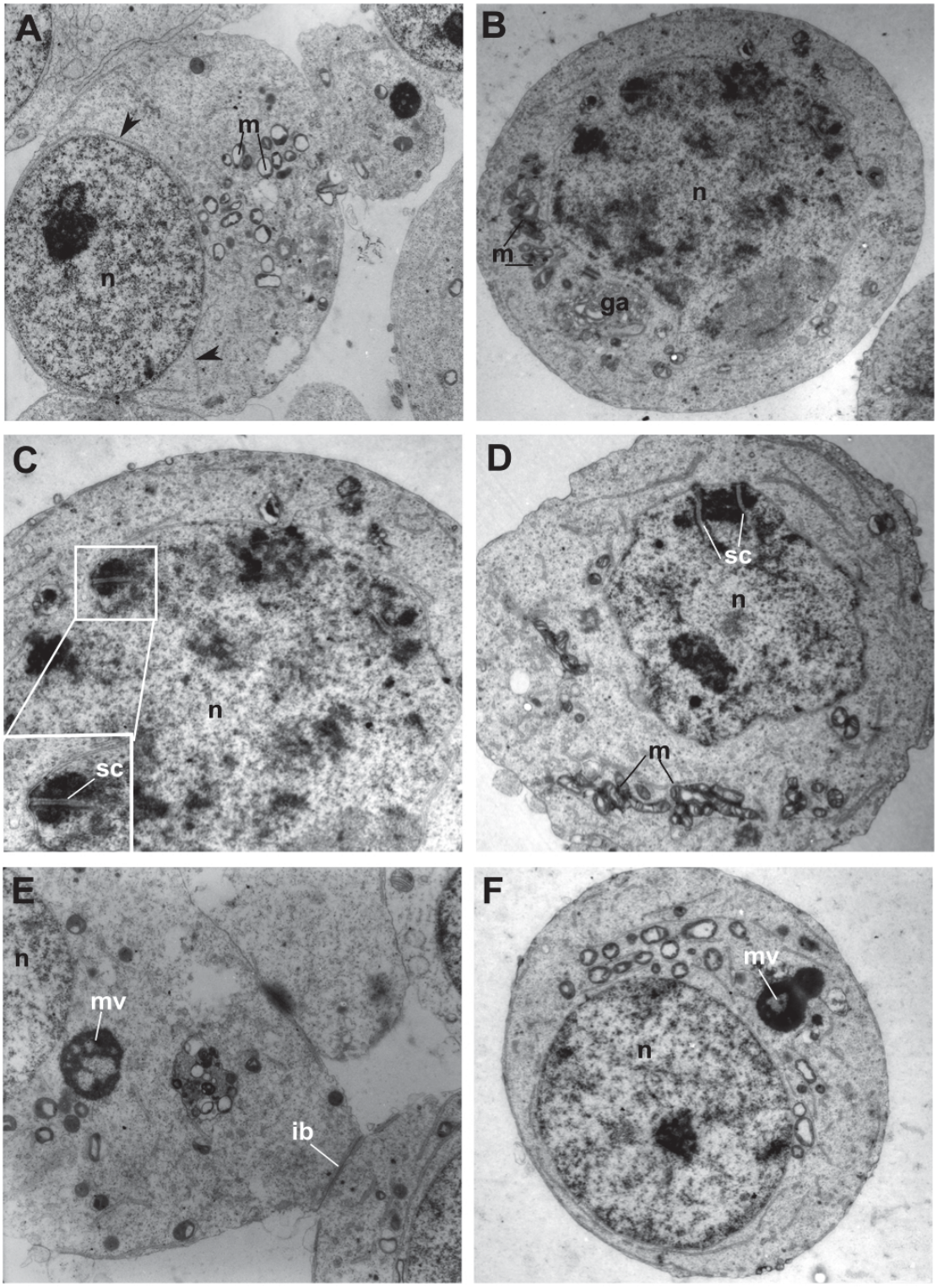
A
m
n
B
n
m
ga
C
n
sc
D
sc
n
m
E
n
mv
ib
F
mv
n

Figure 43. TEM images of different *in vivo* stages of spermatogenetic cells during spermatogenesis. A-F. TEM images showing round spermatid (A), type B spermatogonia (B), and primary spermatocytes (C, D, E, and F). Note the synaptonemal complexes, which appear as electron-dense lines and extend from the nuclear membrane shown in Figure 43C and 43D. Intercellular bridges (E) and dense multivesicular structures of irregular shape between the nuclear membrane and the plasma membrane, called chromatoid body shown in Figure 43E and 43F are characteristic features of this cellular stage. Abbreviation: ga = Golgi apparatus, ib = intercellular bridge, m = mitochondria, mv = multivesicular body, n = nucleus, sc = synaptonemal complex. (A-F: x 6950; insert in C: x 12.210).

In Figure 44A to 44C, *in vivo* spermatid cells of different spermiogenetic stages are shown. Typically the Golgi apparatus depicts the dominant organelle in early spermatids. Figure 44A shows the Golgi phase, the initial phase of spermiogenesis, characterized by the spheroidal nucleus and rough endoplasmatic reticulum, located preferentially around the nucleus. The Golgi apparatus showed lamellae, saccules, and vesicular structures, keeping close to the endoplasmatic reticulum.

As indicated by the acrosomal granule lining part of the nucleus and the cephalic cap developed in the nucleus cranial pole, the spermatid-like cell in Figure 44B mirrors the cephalic cap phase. The characteristic nuclear portion adjacent to the acrosomal vesicle showed an alteration in its contour and this way forms a marginal fossa-like structure (Figure 44C). In both phases, a multivesicular body can be detected in *in vivo* spermatids (Figure 44B).

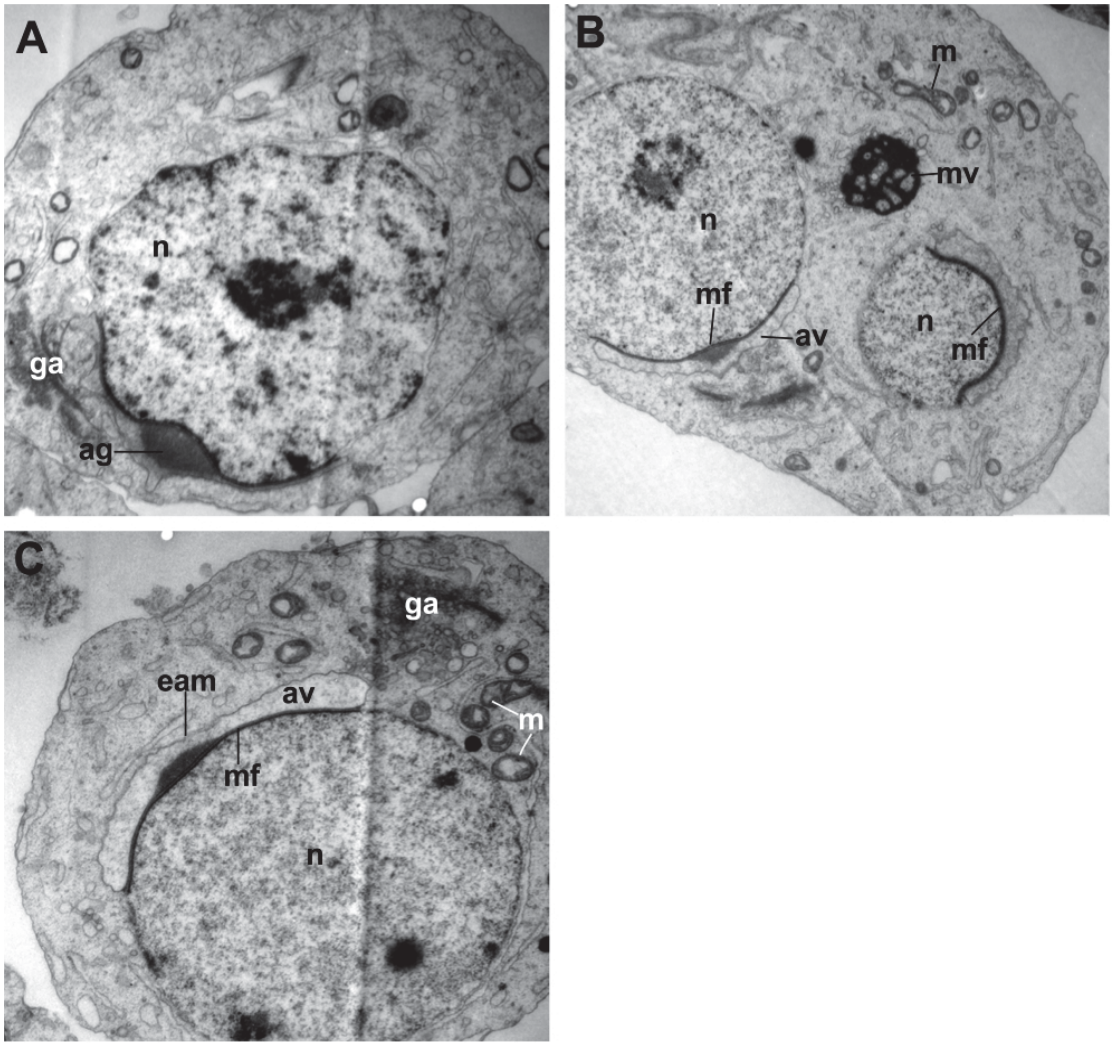

Figure 44. Ultrastructure showing *in vivo* spermiogenetic cells. A: Golgi phase of spermiogenesis. Note Golgi apparatus with lamellae and vesicular structures in close proximity to the endoplasmatic reticulum. B: Spermatid cell in cephalic cap phase indicated by the acrosomal granule lining part of the nucleus. C: Cephalic cap phase of spermatid cells. Note the marginal fossa-like structure. Abbreviation: ag = acrosomal granule, av = acrosomal vesicle, ga = Golgi apparatus, m = mitochondria, mf = marginal fossa, mv = multivesicular body, n = nucleus, (A-C: x 6950).

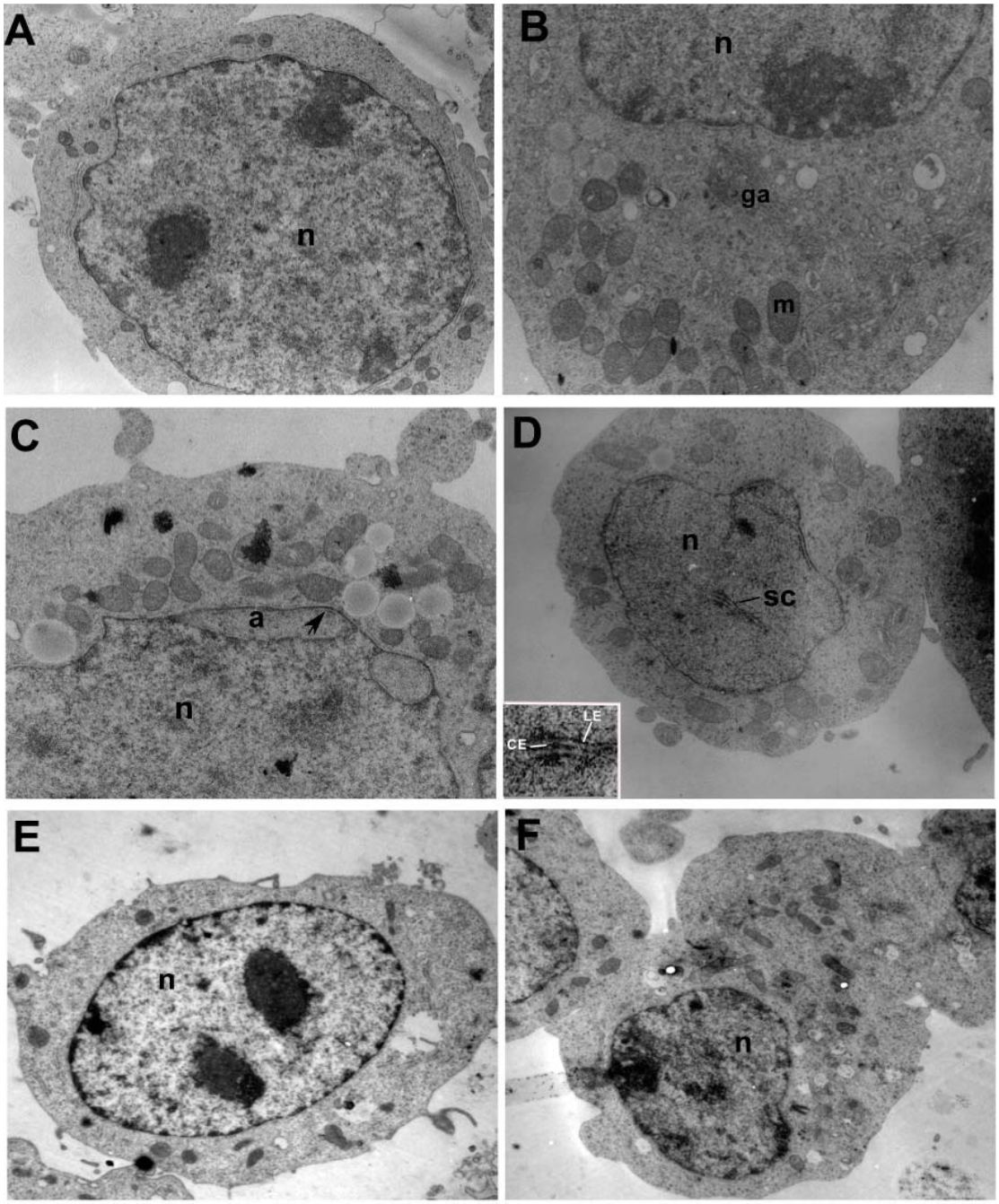
A
n
B
n
ga
m
C
a
n
D
n
sc
LE
CE
E
n
F
n

Figure 45. TEM images of *in vitro*-derived cells, Sertoli cell, and GSC. A-D. TEM images showing the ultrastructure of *in vitro*-derived GSCs. Note the large nucleus (A) and Golgi apparatus as a dominant organelle (B). The characteristic acrosomal granule-like structure is clearly visible in *in vitro*-derived cells (C). In Figure 45D, the synaptonemal complex-like structures are shown. Note the characteristic lateral and central element of the synaptonemal-like structure (insert in D). Control Sertoli cell (E) and GSC (F). Abbreviation: a = acrosomal vesicle, CE = central element, LE = lateral element, ga = Golgi apparatus, m = mitochondria n = nucleus, sc = synaptonemal-like structure. (A, D, E, and F: x 6970; B and C: x 12.210; insert in D: x 12.210).

In comparison to the above outlined *in vivo* cells, the presumptive *in vitro*-differentiated cells have large and irregular nuclei (Figure 45A). Their Golgi apparatus is dominantly made up of lamellae, sacculations, and vesicular structures (Figure 45B). The acrosomal granule-like structure shown in Figure 45C is positioned at the nucleus as it is found in *in vivo* cells. The subacrosomal membrane space between the nuclear membrane and the acrosomal granule-like structure forms a marginal fossa-like structure (Figure 45C, arrowhead).

As shown in Figure 45D, the cells exhibit synaptonemal complex-like structures showing the characteristic lateral and central elements. Mitochondria of all cells show cisternae formation, which are characteristic for mature vesicular mitochondria.

In comparison the ultrastructures of Sertoli cells (Figure 45E) and GSCs (Figure 45F) were analyzed. As shown in Figure 45E and 45F, neither the nuclear ultrastructure, nor the morphology of the Golgi apparatus or mitochondria resemble those of the *in vitro*-derived germ cells.

5.3.2.4 Real-time RT-PCR analysis

To confirm the successful differentiation of GSCs into premeiotic and meiotic stage spermatocytes, gene expression analysis of undifferentiated GSCs and differentiating cultures at various time points during differentiation were performed.

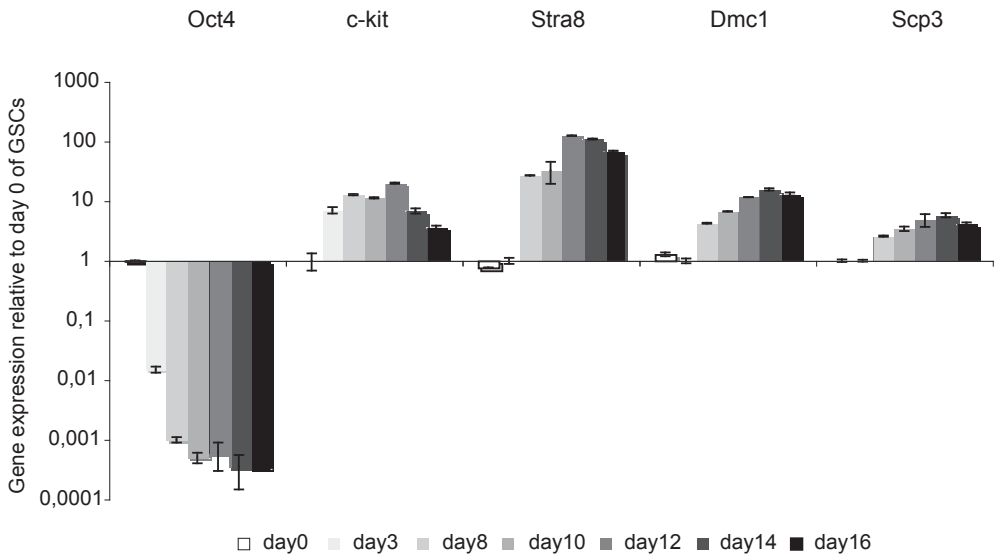

Figure 46. Real-time RT-PCR analysis of *in vitro*-differentiated cells from GSCs. The gene expression analysis of *Oct4-GFP*-GSCs (day 0 of differentiation) and *in vitro*-generated cells on various days of differentiation was performed using the premeiotic marker *Oct4* and the meiotic markers, *c-kit*, *Stra8*, *Dmc1*, and *Scp3*.

As shown in Figure 46, the GSC-specific marker *Oct4* was downregulated during differentiation, whereas the meiotic markers *c-kit*, *Stra8*, *Dmc1*, and *Scp3* were unregulated in *in vitro*-differentiated cells compared with undifferentiated GSCs. The obtained *Oct4* expression pattern is similar to that described in a previous report by (Pesce et al., 1998), in which *Oct4* was detected during postnatal mouse development in type A spermatogonia, but not in type B spermatogonia and primary spermatocytes.

Consistent with previous studies (Prabhu et al., 2006; Schrans-Stassen et al., 1999), which demonstrated that *c-kit* mRNA was detected until late pachytene spermatocytes, whereas the protein was not detected from leptotene spermatocytes onward, in this study the expression of the *c-kit* gene was maintained in the elongated

stage of meiosis I. These observations suggest that GSCs have entered prophase I of meiosis and have undergone meiotic maturation *in vitro*.

5.3.2.5 Round spermatid injection, embryo transfer, and derivation of embryonic stem cells

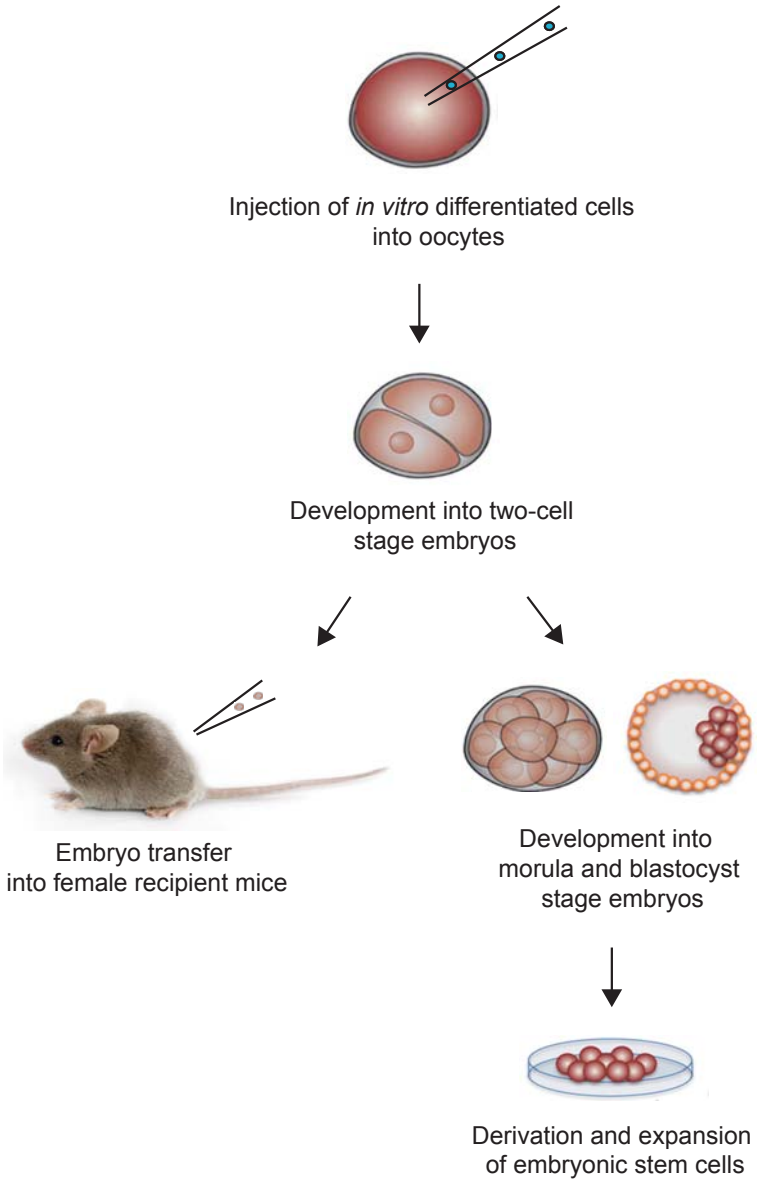

Figure 47. Schematic procedure of ROSI followed by embryo transfer and derivation of ESCs. After injection of *in vitro*-generated cells into oocytes isolated from wild type mice, the two-cell stage embryos were used for either embryo transfer or derivation of ESCs.

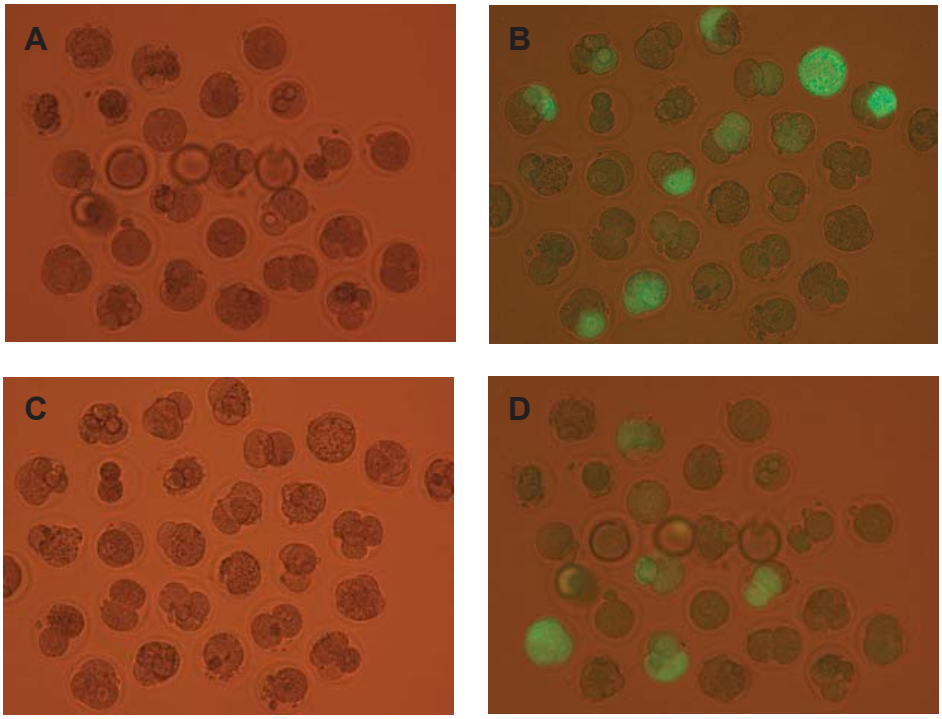

Figure 48. Embryonic development after round spermatid injection. Morphology of mouse embryos followed by ROSI was determined at E3.5. The embryos have different developmental potential determined by GFP expression (A, C) and bright field picture (B, D).

Figure 48 shows various mouse embryos after ROSI. Most embryos arrested at early stage, whereas some developed to the morula or blastocyst stages. Table 7 summarizes the results of embryonic development after ROSI with *in vitro*-differentiated cells.

Table 7. Summarized results of round spermatid injection

Trial	Injected	Survived	Two-cell	Morula +Blastocysts	ET embryos	ET females
1	140	48			27	2
2	120	44		8	ESC derivation	
3	95	84	59	21	82	4
4	73	63			38	2
5	75	61	45	12	51	3
6	92	87	31	19	80	3
7	72	43	12	4	15	1
8	68	55	6		55	3
9	61	57	36	13	36	2
Total	796	542	189	77	384	20
			435	376		
* Ratio			0.434482759	0.204787234		
					Outgrowth	Poor outgrowth
ESC derivation				8	4	1 (green)

Abbreviation: Injected = Total number of oocytes injected; Survived = Total number of oocytes survived; Two-cell = Number of two-cell stage embryos; Morula+Blastocysts = Number of morula and blastocyst stage embryos; ET embryos = Number of transferred two-cell, morula, and blastocyst stage embryos; ET females = Number of recipients

* Ratio: 0.434482759 = two-cell stage embryos/survived oocytes after ROSI, 0.204787234 = embryos developed to morula to blastocyst stage/survived oocytes after ROSI.

To examine the *in vivo* developmental potential of mouse embryos after ROSI, two-cell, morula, and blastocyst stage embryos were transferred to recipient female mice. However, there was neither full-term development of embryos nor offspring production achieved. Finally, four ESC lines were established from eight-morula stage embryos and termed ROSI-derived ESC lines. These lines were maintained under ESC culture conditions described in section 3.2.5.

5.3.2.6 Flow cytometry analysis

To characterize the ROSI-derived ESC lines, FACS analysis was performed using SSEA1 antibody- one of the makers used for ESC characterization. As shown in Figure 49, ROSI-derived ESC lines stained positive for SSEA1 (upper row). SSEA1-positive-stained cells were sorted and subjected to imprinting analysis.

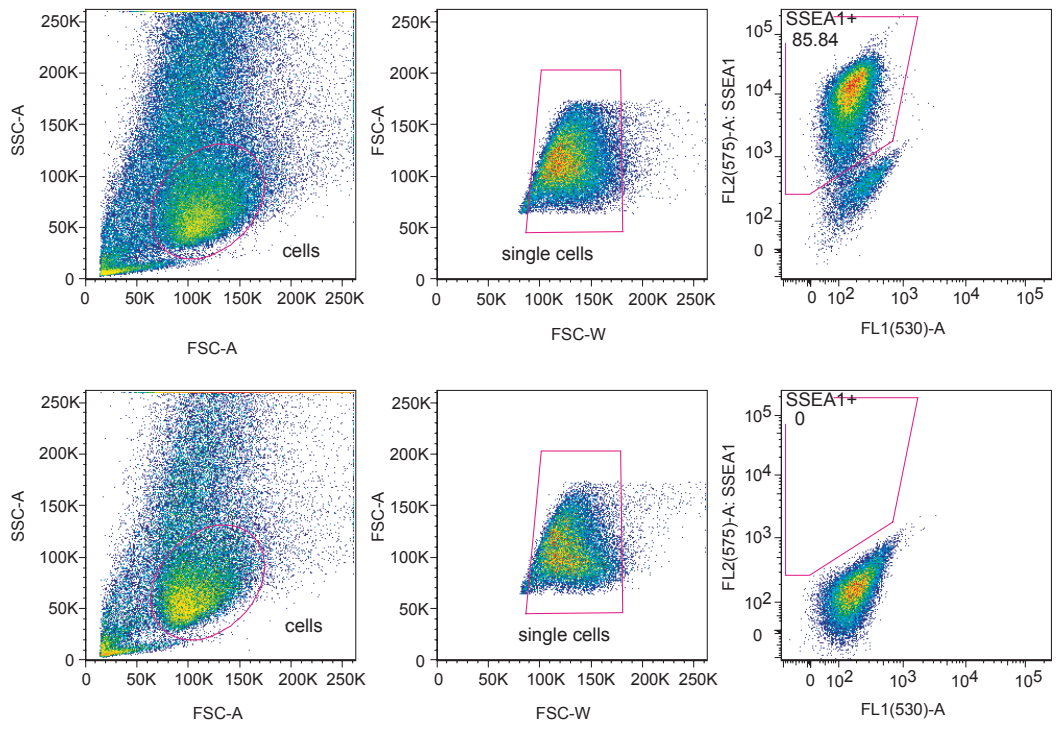

Figure 49. Flow cytometry analysis of SSEA1-stained ROSI-derived ESCs. The ROSI-derived ESCs were stained with ESC marker SSEA1 and flow cytometry analysis showed the positive expression of SSEA1 on the cells (upper raw) in comparison to unstained cells (lower raw).

5.3.2.7 Karyotyping

Karyotype analysis was performed to examine the number of chromosomes in the ROSI-derived ESCs. As demonstrated in Figure 50, chromosome numbers were thirty-nine to forty for all ROSI-derived ESC lines analyzed.

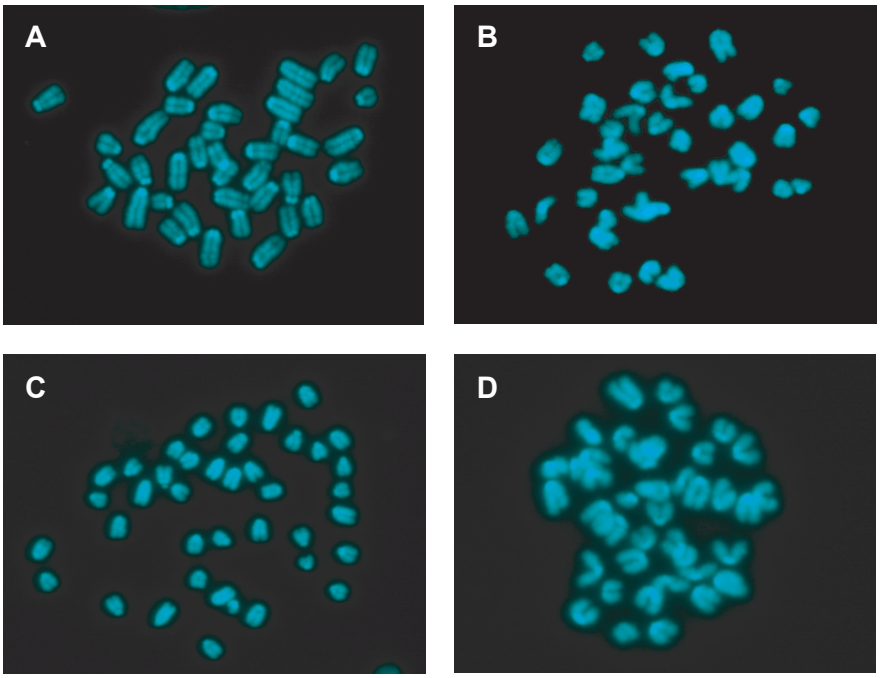

Figure 50. Karyotyping analysis of ROSI-derived ESC line numbers 1 to 4. Representative pictures demonstrate the chromosome spread of ROSI-derived ESC line number 1 (A), 2 (B), 3 (C), and 4 (D).

5.3.2.8 Methylation analysis

Methylation analysis was performed with ROSI-derived ESC lines (Figure 51). The ROSI-derived ESCs show a somatic imprinting pattern for the *H19* gene and show a parthenogenetic imprinting pattern for the *Igf2r* gene.

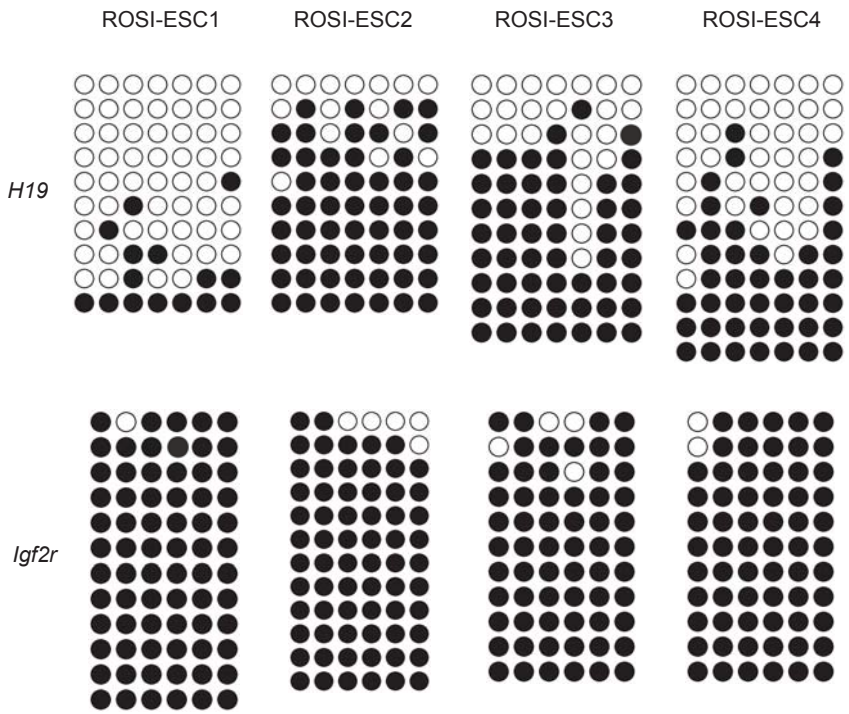

Figure 51. DNA methylation analysis of ROSI-derived ESCs. The imprinting status of ROSI-derived ESC lines numbers 1 to 4 was examined using the bisulfate sequencing method. An open circle represents an unmethylated status; a close circle represents a methylated status. Abbreviation: ROSI-ESC = ROSI-derived ESC line.

5.3.2.9 Characterization of round spermatid injection-derived *Acrosin* embryonic stem cells

In order to examine the ROSI technique, ESCs were derived from ROSI embryos using round spermatids isolated from *Acrosin-EGFP* mice [B6C3-Tg (*Acro3-EGFP*)] (Nakanishi et al., 1999). This ESC line is termed ROSI-derived *Acrosin* ESC line. As shown in Figure 52, the karyotyping analysis demonstrated a normal karyotype containing forty chromosomes, while PCR genotyping analysis detected the *GFP* transgene, confirming that this ESC line has indeed originated from ROSI with the round spermatids from the *Acrosin-EGFP* mouse. The detection of the *Sry* gene indicated the presence of the Y chromosome, which denotes this line as male line. Unfortunately, the four ROSI-derived ESC lines using the *in vitro*-derived round spermatids did not carry the *Oct4-GFP* and *LacZ* transgenes, indicating their parthenogenetic origin.

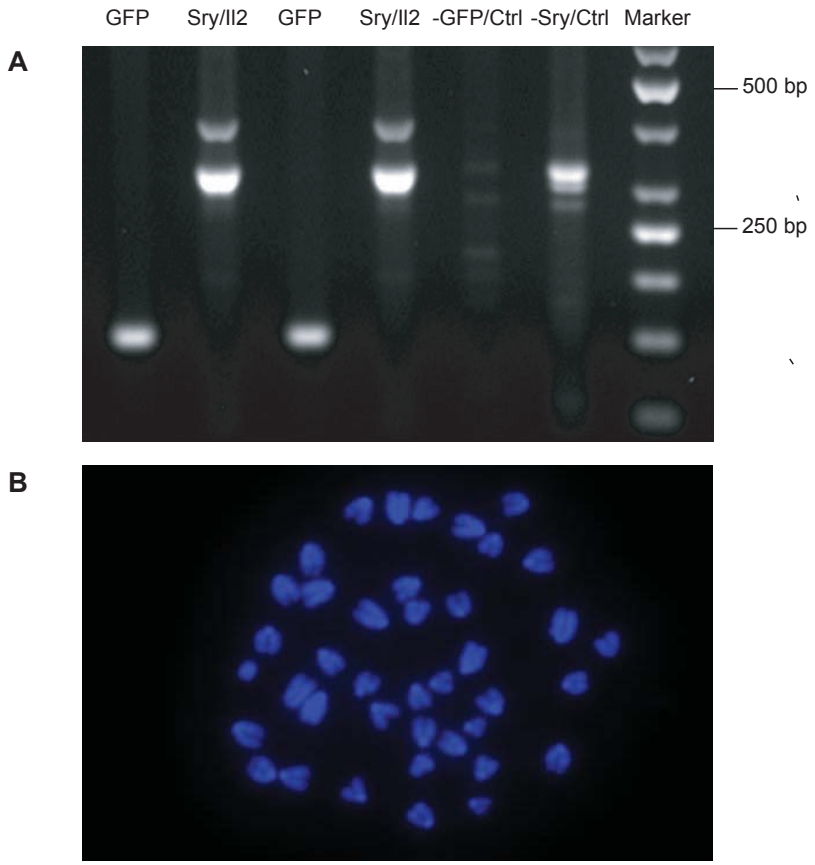

Figure 52. Genotyping analysis and karyotyping analysis of ROSI-derived *Acrosin* ESCs. The ROSI-derived *Acrosin* ESCs have the *GFP* and *Sry* genes with duplicates (A). They have normal number of chromosomes (forty chromosomes) (B). Abbreviation: Ctrl: control.

5.4 Derivation of germline stem cells from OG2 x *Acrosin EGFP* mouse testes

The GSCs were derived from *Acrosin-EGFP* mice and OG2 x *Acrosin-EGFP* mice.

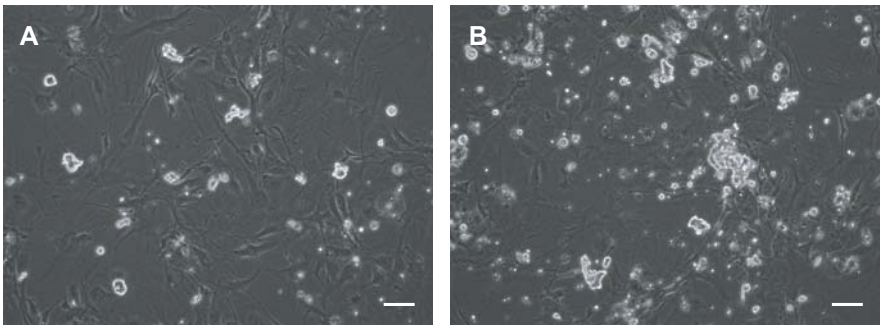

Figure 53. Morphology of *Acrosin* GSCs. GSC colonies derived from *Acrosin-EGFP* mice show a grape-like morphology, typical for GSCs, when they form colonies. The left picture (A) shows GSCs at passage 1 derived from PND 6 mouse testes and the right picture (B) shows GSCs at passage 1 derived from PND 6 and 7 mouse testes. Scale bars indicate 100 μm.

As shown in Figures 53, the GSC colonies appeared as small clusters and formed grape-like colonies, as they grew further. The *Oct4-GFP* expression within GSC colonies was detected (Figure 54). This observation is similar to GSCs derived from different mice as shown in Figure 11.

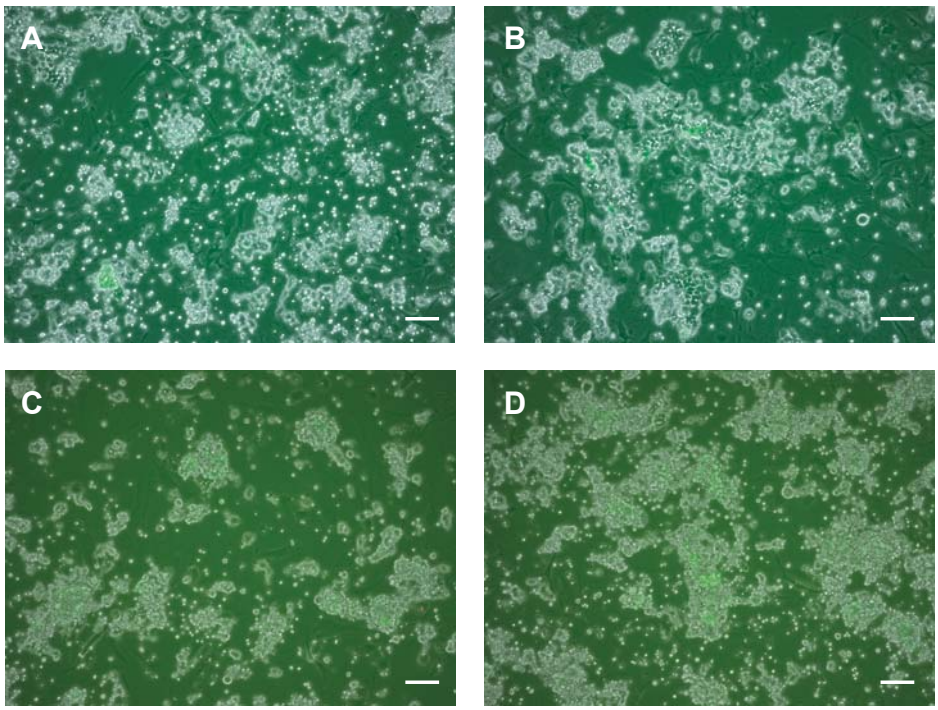

Figure 54. Morphology of OG2 x *Acrosin-EGFP* GSCs. GSC colonies derived from OG2 x *Acrosin-EGFP* mice show a typical grape-like morphology and heterogeneous *GFP* expression within the colonies. The upper pictures (A, B) demonstrate the GSCs at passage 1 derived from PND 7 mouse testes and the lower pictures (C, D) show the GSCs at passage 5 derived from PND 6 mouse testes. Scale bars indicate 100 μm

6. Discussion

6.1 Characteristics of germline stem cells

Several studies have demonstrated the *in vitro* derivation and culture of mouse male GSCs, also called SSCs, under different conditions. The culture conditions varied between the reports in terms of different mouse backgrounds, testis isolation from mice of different age, different medium compositions, presence or absence of feeder cells, and coating of tissue culture dishes with laminin. Albeit all those differences several reports demonstrated the successful *in vitro* cultivation of GSCs (Kanatsu-Shinohara et al., 2005; Kanatsu-Shinohara et al., 2003; Kubota et al., 2004).

In this study, GSCs were generated from adult mouse testes according to previous reports and established as cell lines that could be maintained *in vitro* as long-term cultures without significant loss or alteration of their characteristics at the molecular and cellular level (Ko et al., 2010; Ko et al., 2009; Ko et al., 2011). As shown in Figure 11, the *in vitro* cultured GSCs showed typical grape-like morphology and differential expression of *Oct4-GFP* within colonies. These observations could be correlated by flow cytometry analysis in terms of *Oct4-GFP* and c-kit expression patterns. Figure 12 demonstrates the existence of different subpopulations of GSCs within *in vitro* cultures on MEFs in the presence of defined growth factors. These GSCs can be categorized in four distinct subpopulations according to different expression levels of *Oct4-GFP* and c-kit protein: *Oct4-GFP*-positive and c-kit-positive, *Oct4-GFP*-positive and c-kit-negative, *Oct4-GFP*-negative and c-kit-positive as well as *Oct4-GFP*-negative and c-kit-negative populations.

These cells are not comparable to *in vivo Oct4-GFP*-positive and c-kit-negative GSCs that have been identified as self-renewing A_s cells (single type A spermatogonia) in previous reports (de Rooij, 2001; de Rooij and Russell, 2000; Yoshinaga et al., 1991). Furthermore, in an *in vivo* testicular microenvironment, Sertoli cells surround spermatogenetic cells, while mouse embryonic fibroblasts are used to promote the proliferation of GSCs and to inhibit the differentiation of GSCs in *in vitro* cultures.

The self-renewing type A spermatogonia is the common initial cell type in mouse (A_s) and human (A_{pale}) testicular cell development that differentiate into vari-

ous cell types including subtype A spermatogonia, B spermatogonia, spermatocytes, spermatids, and sperm at later stages depending on the species (de Rooij, 2001; de Rooij and Russell, 2000). The present study aimed at generating human GSCs from testicular biopsies, however all attempts to generate or isolate GSCs failed, irrespective of the culture conditions tested. Table 5 summarizes the different culture methods. We observed overgrowth of human fibroblast-like cells and subsequently formation of very tight colonies, which did not proliferate but rather survived as colonies under different culture conditions. They exhibited distinct characteristics in comparison to human ESCs (WA09/H9) as demonstrated in Figure 13, 14, and 15. The basic problem for establishment of human GSC culture conditions is the lack of markers that could be used to identify human GSCs. The use of human biopsies for experimental purposes bears another problem, namely the difference in the genetic backgrounds of biopsies. Each one might require alternative culture conditions. Similarities and differences between mouse and human GSCs are basically unknown. Mouse GSC culture conditions did not support the culture of human testicular GSCs in any of the attempts. In addition, replating of human testicular cells on mouse feeder cells appears not to be suitable for propagation of human GSCs, even though human ESCs can be grown on mouse feeder cells. The use of human feeder cells might be more supportive. Many open questions remain and have to be addressed to establish suitable *in vitro* conditions for the isolation, identification, culture, and characterization of human GSCs.

6.1.1 Potency and functional analysis of germline stem cells

To determine the potency of the generated GSCs, *in vitro* and *in vivo* experiments were performed. Expression analysis for specific GSC and ESC markers at RNA and protein level confirmed their GSCs identity as shown in Figures 21, 23, and 24. To determine their differentiation potential, GSCs were injected into testis of endogenous germ cell-depleted mice where they reestablished spermatogenesis as demonstrated in Figure 22. In addition, GSCs did not lead to the formation of teratomas upon injection into immunodeficient mice and were thus classified unipotent.

6.1.2 Self-reprogramming ability of germline stem cells into pluripotent cells

In comparison to human GSCs, many studies have been performed on mouse GSCs. One of the most significant features of mouse GSCs is their potential to convert into a pluripotent stage. It has been shown in previous reports, that mouse GSCs generated from *Oct4-GFP* adult mouse testis can be spontaneously converted into ESC-like cells under defined *in vitro* culture conditions (Ko et al., 2010; Ko et al., 2009; Ko et al., 2011). *Oct4* is a known marker for GSCs, but also for pluripotent cells. Once *Oct4-GFP*-poistive GSCs are reprogrammed into pluripotent cells, they exhibit a more intense *Oct4-GFP* signal. Furthermore, as demonstrated by microarray analysis, once the individual GSC lines converted into corresponding pluripotent gPSC lines, additional differences were found amongst the gPSC lines and GSC lines, which might be correlated with the different intensity of *Oct4-GFP* signal in GSCs and gPSCs. The comparative analysis between GSCs of different genetic backgrounds of and gPSCs as shown in Figures 25 and 26 revealed distinct expression of *Sox2* in cells with homogeneous genetic background (GSC, gPSC) and *Sox2* and *Nanog* in cells with heterogeneous genetic background (GSCr, gPSCr). Whether this difference has a considerable effect on the conversion process needs to be further studied. The gPSCr2 revealed a distinct expression pattern between two different types of gPSCs that can be observed in various microarray data displays like principal component analysis, hierarchical clustering, heat-map, or map of distances between samples. This difference might be due to a difference in the sample preparation rather than an exclusive characteristic of the gPSCr2.

6.1.3 Differentiation ability of germline-derived pluripotent stem cells into endothelial-like cells

The directional differentiation of mouse- and human ESCs into endothelial cells has been reported, however, the derivation of endothelial-like cells from gPSCs has not been reported to date (Cho et al., 2007; Li et al., 2007). In the present thesis, endothelial-like cells were generated from gPSCs and characterized *in vitro*.

For the differentiation of gPSCs into endothelial-like cells, embryoid bodies were generated and CD31-positive cells were isolated. CD31 was used in this study as a possible marker for gPSC-derived endothelial-like cells, since in previous reports

CD31 was used as a marker for endothelial cells and CD31-positive cells generated from mouse ESCs could differentiate into endothelial cells *in vitro* (Mariappan et al., 2009; Vittet et al., 1996; Watt et al., 1995).

Figure 34 demonstrates that gPSC-derived cells display a cobblestone-like morphology, which resembles the morphology of *in vivo*-isolated endothelial cells. They clearly differ from smooth muscle cells, which have a more spindle-like shape (Wang et al., 2006). Gene expression analysis, immunofluorescence staining, and FACS analyses revealed that these cells expressed typical endothelial cell markers, such as Tie2, CD31, VE-Cadherin, vWF, Flk1, Flt1, and Icam2 (Garlanda and Dejana, 1997). These cells did not express the smooth muscle cell markers SMA (α-smooth muscle actin) or SM22α, neither at the RNA level nor at protein level (Yamashita et al., 2000). Taken together, these results indicate that the gPSC-derived cells represent cells of the endothelial lineage and not smooth muscle cells, which can also be generated when ESCs are differentiated into the endothelial lineage (Blancas et al., 2008; Yamashita et al., 2000).

In some studies, CD14, CD34, or CD133 have been used as a marker for the identification of endothelial progenitor cells (Asahara et al., 1997; Elsheikh et al., 2005). CD133 has not been used in this study to identify the progenitors of gPSC-derived endothelial cells, since expression of CD133 in mouse endothelial progenitor cells still has not been confirmed (Rafii and Lyden, 2003). The gPSC-derived endothelial-like cells express neither CD14 nor CD34, which indicates that these cells do not exhibit immature endothelial cell features. Moreover, CD34 expression appears to be unstable during culture and not all endothelial cells express CD34, e.g.- those of large vessels (Delia et al., 1993; Fina et al., 1990). As the expression of CD34 on endothelial cells is still controversial, this antigen was not used in the present study as marker for the characterization of gPSC-derived cells.

Furthermore, gPSC-derived cells could take up Dil-ac-LDL from endothelial tubes on matrigel assays, showing their functionality *in vitro*. The LDL uptake and tube formation are related to important functional properties of endothelial cells and some endothelial cells derived from pluripotent cells may lack this functional properties (McCloskey et al., 2006).

Based on the results and observations described above, the gPSC-derived cells are identified as endothelial cell-like cells, which could be used for basic research in

the area of vascular biology and function, as well as for investigations providing proof of concept for the use of pluripotent cell-derived endothelial cells in future therapeutic applications including ischemic diseases.

6.2 *In vitro* spermatogenesis of germline stem cells

Another important feature of GSCs is their ability to produce mature sperm *in vivo*, the process called spermatogenesis. The identity and biological activity of *in vitro* cultured GSCs were confirmed by transplantation of GSCs into infertile mouse testis. GSCs were able to restore spermatogenesis, which showed the full functional capacity of GSCs for generating sperm *in vivo*, suggesting the possibility of generation of mature spermatogenetic cells from GSCs *in vitro*.

In the present study, various types of spermatogenetic cells were generated from established GSCs *in vitro* and characterized using different analysis methods. For *in vitro* spermatogenesis, Sertoli cells were utilized as supporting cells as they are the only somatic cell type in seminiferous tubules of mouse testis, which are in direct contact with spermatogenetic cells of different stages. They provide physical support and secrete essential factors or nutrients to maintain SSCs in balance between self-renewal and differentiation (Oatley and Brinster, 2012).

There are two considerable advantages, which make the *in vitro* differentiation model from GSCs a suitable system to study the initial step of spermatogenesis. First, GSCs are committed to become spermatogenetic cells, not other somatic cell types. Second, the monolayer co-culture method only with Sertoli cells facilitates the generation of spermatogenetic cells and thus the determination of the developmental stage of the cells during a time-course differentiation, the timing of the switch from mitosis to meiosis, and the progression of meiosis based on morphologic changes subsequent to addition of different agents.

The transition of mitosis to meiosis was verified by differential *Oct4-GFP*- and c-kit protein expression and marker gene expression analysis of undifferentiated and differentiated GSCs during the first round of differentiation. Based on the crucial role of the isoform of the c-kit ligand SCF in spermatogenesis described in previous reports (Mauduit et al., 1999b; Mithraprabhu and Loveland, 2009; Sato et al., 2012), the GSCs *in vitro* differentiation cultures revealed the presence of two c-kit ligand

isotypes during the course of the differentiation: the membrane-bound form and the soluble form. As demonstrated in Figure 41, elevated *c-kit* RNA expression levels in GSCs demonstrated the presence of the c-kit receptor in differentiating spermatogonia, while reduced c-kit expression levels following the addition of SCF supported the stage-specific role of c-kit and c-kit ligand interaction in the first wave of spermatogenesis called spermatocytogenesis. Furthermore, the high percentage of c-kit-positive cells with nominal *Oct4-GFP* expression indicated the robustness of the differentiation strategy and the potential of GSC lines to differentiate into premeiotic cells *in vitro*.

Subsequently, the cells were treated with RA for further development. Previous studies have described that in the absence of *Stra8*, which is activated by RA in male mice, germ cells undergo meiotic cessation predominantly at the pachytene stage, indicating that RA is required for DNA replication before cellular entry into and progression through meiosis (Anderson et al., 2008; Baltus et al., 2006; Mark et al., 2008). The progression into a more advanced stage of meiosis I was confirmed by Scp3 staining. A previous report (Henderson and Keeney, 2005) demonstrated that Scp3 protein begins to assemble along each sister chromatid pair at leptotene spermatocytes to form the axial component, which is present until the metaphase I stage, whereas the central component of the synaptonemal complex Scp1 first appears in zygotene spermatocytes. Therefore, Scp3 staining was used as meiotic marker in this study to estimate the differentiation status of GSCs in meiotic prophase I in culture. As shown in Figure 42, *in vitro*-differentiated cells display a primary spermatocyte-like staining pattern, which resembles that of *in vivo* spermatocytes of different stages. Moreover, an increase in the number of elongated Scp3 staining patterns in cells and a decrease in the total number of Scp3-positive cells on later days of differentiation suggests progression of the prophase I of meiosis for a subpopulation of cells. The developmental status of GSCs on different days during differentiation and the generation of primary spermatocyte-like cells from GSCs were also confirmed at the RNA level by additional gene expression analysis for the premeiotic marker *Oct4* and meiotic markers, *c-kit, Stra8, Dmc1*, and *Scp3*. The observed downregulation of *Oct4* and the concomitant up regulation of the tested meiotic genes clearly indicated entry into prophase I of meiosis. In addition, the expression of the *c-kit* gene was maintained in cells with an elongated Scp3 staining pattern, which correlates also with previous studies (Prabhu et al., 2006; Schrans-Stassen et al., 1999).

Presumptive terminally differentiated cells were analyzed using various methods to determine the appearance of haploid round spermatid-like cells from GSCs (data not shown). However, there was no clear evidence of completion of meiosis of *in vitro*-derived cells. Although, there was no marker available to isolate haploid round spermatid-like cells in the present *in vitro* differentiation culture system, on day 18-23 days of *in vitro* differentiation, the cells were isolated and picked mechanically from the culture and ROSI was performed to prove completion of meiosis and generation of haploid round spermatid-like cells, and to determine their *in vivo* functionality by either generation of ESCs or live offspring. We failed to produce live offspring, but we succeeded in deriving ESC lines. The four ROSI-derived ESC lines were karyotypically normal and the imprinting status of the *H19* and *Igf2r* loci was analyzed. *H19* is a paternally repressed and maternally expressed gene, which is fully methylated in GSCs. *Igf2r* is a maternally repressed and paternally expressed gene, which is fully unmethylated in GSCs. Both genes showed the androgenetic imprinting pattern in GSCs. The imprinting status of terminally differentiated cells was not analyzed, since genomic imprinting in male germ cells is accomplished before spermiogenesis, according to a previous report (Kimura and Yanagimachi, 1995b). The somatic imprinting pattern for *H19* in ROSI-derived ESCs is typical for ICSI-derived ESCs, but the parthenogenetic imprinting pattern at the *Igf2r* locus is not. This suggests a high possibility of parthenogenetic origin, consistent with the lack of *Oct4-GFP* and *LacZ* transgenes from the *in vitro*-derived round spermatids. Whether ROSI-derived ESCs have a different imprinting pattern in comparison to ICSI-derived ESCs remains unknown, since the ROSI procedure requires one step more to activate the oocytes (Kimura and Yanagimachi, 1995a), which might lead to the different imprinting status of ROSI-derived ESCs.

The ROSI technique was used for the generation of ESC lines from GSCs-derived presumptive spermatid-like cells and wild type round spermatids isolated from *Acrosin-EGFP* mice. As shown in Figure 52, the ROSI-derived *Acrosin-GFP*-ESCs carried the *GFP* transgene as detected by PCR-analysis and exhibited a normal karyotype. However, the *Oct4-GFP* and *LacZ* genes were not detected in four ROSI-derived ESCs generated from *Oct4*-GSC-derived spermatid-like cells, suggesting that these four ROSI-derived ESC lines originated from parthenogenetic embryos. The functionality of *in vitro*-derived round spermatids could therefore not be demonstrated.

For the detailed analysis and morphological stage determination of *in vitro*-derived germ cells, an extensive ultrastructural analysis of different *in vivo* spermatogenetic and spermiogenetic stages have been conducted. As shown in Figures 43 and 44, cells of different spermatogenetic and spermiogenetic stages show distinct morphological details. The most significant organelle of the *in vitro*-derived cells is the Golgi apparatus, which depicts the main organelle of early spermatids (Martins and Silva, 2001; Mollenhauer et al., 1976) and a characteristic feature of the Golgi phase during spermatid development (Martins and Silva, 2005). The multivesicular body, a typical feature for the early Golgi phase in wild type testicular cells (Figure 44B) have not been found in *in vitro*-differentiated cells in this study. Furthermore, the typical spheroidal shape of the nucleus (Figure 43F) found in early *in vivo* spermatid cells could also not be detected. The *in vitro*-derived cells showed the formation of the acrosomal granule-like structure, indicative for the entrance in the cephalic cap phase as described by Martins and Silva (2005) and which is also detected in *in vivo* spermatid cells (Figure 45C and 44B, 44C). The subacrosomal membrane space between the nuclear membrane and the acrosomal granule-like structure forming a marginal fossa is visible in *in vitro*-derived cells. As shown in Figure 45D, the *in vitro*-differentiated cell exhibits a synaptonemal complex-like structure, which resembles very closely synaptonemal complex structures found in wild type primary spermatocytes (Figure 43C), indicative of primary spermatocyte-like cells *in vitro*.

According to a previous report (Schramm et al., 2011), meiotic chromosome synapsis is an essential step for proper meiotic progression that ensures male and female fertility. A critical step during this process is the assembly of the central element of the synaptonemal complex. Notably, a difference in the diameter of the central element between *in vitro* and *in vivo* cells was observed, whereas the diameter of the lateral element was similar in both cells (Figure 45D and 43C, inserts). This could indicate an incorrect synaptonemal complex-protein assembly and/or protein interaction of the central element in *in vitro*-derived cells. The defective assembly of the synaptonemal complex has deleterious effects on germ cells and could lead to the malformation of acrosomal-like structure, though meiosis has not been completed. Collectively, the identified characteristic features at the ultrastructural level support in part the successful *in vitro* generation of primary spermatocytes.

The mitochondria of *in vitro*-differentiated cells show cisternae formation, which are characteristic for mature vesicular mitochondria (Figure 45B). Mature mi-

tochondria are typical for type A spermatogonia, which are actively dividing cells with high metabolic activity (Martins and Silva, 2001). Meiotic cells to early spermatid cells contain both types of mitochondria, but mature spermatids contain only the immature mitochondria, suggesting that *in vitro*-derived cells need more ATP production to survive in *in vitro* culture, regardless of the cell type during differentiation, than *in vivo* cells. It appears that there is another independent mechanism guiding the transition of mature to immature mitochondria *in vivo*, which cannot occur under *in vitro* conditions. As the major known role of mitochondria is production of energy through ATP production in most cell types, particularly spermatids, immature mitochondria play an important role in the formation of the tail structure. However, it is not yet known, whether they have direct influence on fertility (Rajender et al., 2010). It appears that high cAMP production in *in vitro*-derived cells as a consequence of high ATP production through mature mitochondria leads to incorrect completion of meiosis, eventually leading to an abnormal arrangement of acrosomal-like structures shown in Figure 45C. Indeed, the cAMP level is low in spermatocytes and round spermatids, increases with the progression of spermiogenesis, and is highest in sperm, supporting the presumption described above (Feinberg et al., 1983).

Based on the results and observations shown in the present thesis, a number of factors can be suggested to improve the *in vitro* differentiation model of GSCs.

First, premeiotic, meiotic, and postmeiotic cells differ in cellular and nuclear structure, which reflects the different metabolic requirements of cells during development. For nuclear condensation and elongation, the direct effects of factors produced by Sertoli cells on spermatogenetic cells may be less crucial than the indirect influence of other testicular and somatic cell types. The three-dimensional milieu may provide a microenvironment with individual cell-to-cell contacts, thereby allowing cells to access the paracrine signals more efficiently than in a monolayer co-culture system. The finding from previous studies (Holdcraft and Braun, 2004) that endocrine and paracrine disorders cause impairment in the maintenance of normal spermatogenesis in the mouse testis and that spermatogenesis can occur under the kidney capsule *in vivo* point to an indirect influence of paracrine and autocrine factors in spermatogenesis (Matoba and Ogura, 2011). This concept is also supported by a recent study, in which functional sperm were generated in an organ culture (Sato et al., 2011), while our approach utilized a monolayer *in vitro* system, in which testicular conditioned medium was used to compensate for the co-culture condition.

In addition, the pH of the culture regulates the formation of acrosomes and is affected by metabolites produced during spermatogenesis (Mauduit et al., 1999a; Nakanishi et al., 2001; Panneerdoss et al., 2012). Maintaining the pH of the culture system within an appropriate range could help the progression of differentiation beyond the Golgi phase and lead to the proper formation of the acrosomal cap, which contains components important for fertilization. This appears to be associated with sperm fertilizing capacity, as mutant mice with an abnormally developed acrosome structure are sterile (Xiao et al., 2009; Yao et al., 2002).

To improve the differentiation efficiency and achieve spermatogenesis, the culture conditions might be optimized by prolonging the survival of the initial *in vitro*-derived cells with the help of specific co-culture conditions. Thus, the ultimate goal in generating functional gametes under *in vitro* conditions is the development of culture conditions that more closely mimic the *in vivo* testis environment.

In conclusion**,** the observations and findings presented in this study provide evidences for the generation of primary spermatocyte-like cells from an established mouse GSC line *in vitro*. However, completion of meiosis and production of proper ESCs or live offspring were not achieved. Further optimization of *in vitro* culture systems for the differentiation of GSCs are necessary to support the successful stepwise generation of various spermatogenetic cells *in vitro* and to extend our understanding of the molecular mechanisms underlying the different stages of spermatogenesis.

7. References

Aflatoonian, B., L. Ruban, M. Jones, R. Aflatoonian, A. Fazeli, and H.D. Moore. 2009. In vitro post-meiotic germ cell development from human embryonic stem cells. Hum Reprod. 24:3150-3159.

Anderson, E.L., A.E. Baltus, H.L. Roepers-Gajadien, T.J. Hassold, D.G. de Rooij, A.M. van Pelt, and D.C. Page. 2008. Stra8 and its inducer, retinoic acid, regulate meiotic initiation in both spermatogenesis and oogenesis in mice. Proc Natl Acad Sci U S A. 105:14976-14980.

Asahara, T., T. Murohara, A. Sullivan, M. Silver, R. van der Zee, T. Li, B. Witzenbichler, G. Schatteman, and J.M. Isner. 1997. Isolation of putative progenitor endothelial cells for angiogenesis. Science. 275:964-967.

Asahara, T., T. Takahashi, H. Masuda, C. Kalka, D. Chen, H. Iwaguro, Y. Inai, M. Silver, and J.M. Isner. 1999. VEGF contributes to postnatal neovascularization by mobilizing bone marrow-derived endothelial progenitor cells. EMBO J. 18:3964-3972.

Baltus, A.E., D.B. Menke, Y.C. Hu, M.L. Goodheart, A.E. Carpenter, D.G. de Rooij, and D.C. Page. 2006. In germ cells of mouse embryonic ovaries, the decision to enter meiosis precedes premeiotic DNA replication. Nat Genet. 38:1430-1434.

Blancas, A.A., N.E. Lauer, and K.E. McCloskey. 2008. Endothelial differentiation of embryonic stem cells. Curr Protoc Stem Cell Biol. Chapter 1:Unit 1F 5.

Braydich-Stolle, L., N. Kostereva, M. Dym, and M.C. Hofmann. 2007. Role of Src family kinases and N-Myc in spermatogonial stem cell proliferation. Dev Biol. 304:34-45.

Brinster, C.J., B.Y. Ryu, M.R. Avarbock, L. Karagenc, R.L. Brinster, and K.E. Orwig. 2003. Restoration of fertility by germ cell transplantation requires effective recipient preparation. Biol Reprod. 69:412-420.

Cho, S.W., S.H. Moon, S.H. Lee, S.W. Kang, J. Kim, J.M. Lim, H.S. Kim, B.S. Kim, and H.M. Chung. 2007. Improvement of postnatal neovascularization by human embryonic stem cell derived endothelial-like cell transplantation in a mouse model of hindlimb ischemia. Circulation. 116:2409-2419.

Cooke, H.J., and P.T. Saunders. 2002. Mouse models of male infertility. Nat Rev Genet. 3:790-801.

de Rooij, D.G. 2001. Proliferation and differentiation of spermatogonial stem cells. Reproduction. 121:347-354.

de Rooij, D.G., and L.D. Russell. 2000. All you wanted to know about spermatogonia but were afraid to ask. J Androl. 21:776-798.

Delia, D., M.G. Lampugnani, M. Resnati, E. Dejana, A. Aiello, E. Fontanella, D. Soligo, M.A. Pierotti, and M.F. Greaves. 1993. CD34 expression is regulated reciprocally with adhesion molecules in vascular endothelial cells in vitro. Blood. 81:1001-1008.

Drake, C.J., and P.A. Fleming. 2000. Vasculogenesis in the day 6.5 to 9.5 mouse embryo. Blood. 95:1671-1679.

Draper, J.S., C. Pigott, J.A. Thomson, and P.W. Andrews. 2002. Surface antigens of human embryonic stem cells: changes upon differentiation in culture. J Anat. 200:249-258.

Eddy, E.M. 2002. Male germ cell gene expression. Recent Prog Horm Res. 57:103-128.

Elsheikh, E., M. Uzunel, Z. He, J. Holgersson, G. Nowak, and S. Sumitran-Holgersson. 2005. Only a specific subset of human peripheral-blood monocytes has endothelial-like functional capacity. Blood. 106:2347-2355.

Eminli, S., A. Foudi, M. Stadtfeld, N. Maherali, T. Ahfeldt, G. Mostoslavsky, H. Hock, and K. Hochedlinger. 2009. Differentiation stage determines potential of hematopoietic cells for reprogramming into induced pluripotent stem cells. Nat Genet. 41:968-976.

Feinberg, J., C. Pariset, M. Rondard, M. Loir, M. Lanneau, S. Weinman, and J. Demaille. 1983. Evolution of Ca2+- and cAMP-dependent regulatory mechanisms during ram spermatogenesis. Dev Biol. 100:260-265.

Feng, L.X., Y. Chen, L. Dettin, R.A. Pera, J.C. Herr, E. Goldberg, and M. Dym. 2002. Generation and in vitro differentiation of a spermatogonial cell line. Science. 297:392-395.

Fina, L., H.V. Molgaard, D. Robertson, N.J. Bradley, P. Monaghan, D. Delia, D.R. Sutherland, M.A. Baker, and M.F. Greaves. 1990. Expression of the CD34 gene in vascular endothelial cells. Blood. 75:2417-2426.

Garlanda, C., and E. Dejana. 1997. Heterogeneity of endothelial cells. Specific markers. Arterioscler Thromb Vasc Biol. 17:1193-1202.

Geijsen, N., M. Horoschak, K. Kim, J. Gribnau, K. Eggan, and G.Q. Daley. 2004. Derivation of embryonic germ cells and male gametes from embryonic stem cells. Nature. 427:148-154.

Ginsburg, M., M.H. Snow, and A. McLaren. 1990. Primordial germ cells in the mouse embryo during gastrulation. Development. 110:521-528.

Hanna, J., S. Markoulaki, P. Schorderet, B.W. Carey, C. Beard, M. Wernig, M.P. Creyghton, E.J. Steine, J.P. Cassady, R. Foreman, C.J. Lengner, J.A. Dausman, and R. Jaenisch. 2008. Direct reprogramming of terminally differentiated mature B lymphocytes to pluripotency. Cell. 133:250-264.

Henderson, K.A., and S. Keeney. 2005. Synaptonemal complex formation: where does it start? Bioessays. 27:995-998.

Heng, J.C., B. Feng, J. Han, J. Jiang, P. Kraus, J.H. Ng, Y.L. Orlov, M. Huss, L. Yang, T. Lufkin, B. Lim, and H.H. Ng. 2010. The nuclear receptor Nr5a2 can replace Oct4 in the reprogramming of murine somatic cells to pluripotent cells. Cell Stem Cell. 6:167-174.

Holdcraft, R.W., and R.E. Braun. 2004. Hormonal regulation of spermatogenesis. Int J Androl. 27:335-342.

Inselman, A., S. Eaker, and M.A. Handel. 2003. Temporal expression of cell cycle-related proteins during spermatogenesis: establishing a timeline for onset of the meiotic divisions. Cytogenet Genome Res. 103:277-284.

Irizarry, R.A., B.M. Bolstad, F. Collin, L.M. Cope, B. Hobbs, and T.P. Speed. 2003. Summaries of Affymetrix GeneChip probe level data. Nucleic Acids Res. 31:e15.

Kanatsu-Shinohara, M., K. Inoue, J. Lee, M. Yoshimoto, N. Ogonuki, H. Miki, S. Baba, T. Kato, Y. Kazuki, S. Toyokuni, M. Toyoshima, O. Niwa, M. Oshimura, T. Heike, T. Nakahata, F. Ishino, A. Ogura, and T. Shinohara. 2004. Generation of pluripotent stem cells from neonatal mouse testis. Cell. 119:1001-1012.

Kanatsu-Shinohara, M., K. Inoue, N. Ogonuki, H. Miki, S. Yoshida, S. Toyokuni, J. Lee, A. Ogura, and T. Shinohara. 2007. Leukemia inhibitory factor enhances formation of germ cell colonies in neonatal mouse testis culture. Biol Reprod. 76:55-62.

Kanatsu-Shinohara, M., H. Miki, K. Inoue, N. Ogonuki, S. Toyokuni, A. Ogura, and T. Shinohara. 2005. Long-term culture of mouse male germline stem cells under serum-or feeder-free conditions. Biol Reprod. 72:985-991.

Kanatsu-Shinohara, M., N. Ogonuki, K. Inoue, H. Miki, A. Ogura, S. Toyokuni, and T. Shinohara. 2003. Long-term proliferation in culture and germline transmission of mouse male germline stem cells. Biol Reprod. 69:612-616.

Kevil, C.G., and D.C. Bullard. 2001. In vitro culture and characterization of gene targeted mouse endothelium. Acta Physiol Scand. 173:151-157.

Kim, J.B., B. Greber, M.J. Arauzo-Bravo, J. Meyer, K.I. Park, H. Zaehres, and H.R. Schöler. 2009. Direct reprogramming of human neural stem cells by OCT4. Nature. 461:649-643.

Kim, J.B., V. Sebastiano, G. Wu, M.J. Arauzo-Bravo, P. Sasse, L. Gentile, K. Ko, D. Ruau, M. Ehrich, D. van den Boom, J. Meyer, K. Hubner, C. Bernemann, C. Ortmeier, M. Zenke, B.K. Fleischmann, H. Zaehres, and H.R. Schöler. 2009. Oct4-induced pluripotency in adult neural stem cells. Cell. 136:411-419.

Kim, J.B., H. Zaehres, G. Wu, L. Gentile, K. Ko, V. Sebastiano, M.J. Arauzo-Bravo, D. Ruau, D.W. Han, M. Zenke, and H.R. Schöler. 2008. Pluripotent stem cells induced from adult neural stem cells by reprogramming with two factors. Nature. 454:646-650.

Kimura, Y., and R. Yanagimachi. 1995. Intracytoplasmic sperm injection in the mouse. Biol Reprod. 52:709-720.

Kimura, Y., and R. Yanagimachi. 1995. Mouse oocytes injected with testicular spermatozoa or round spermatids can develop into normal offspring. Development. 121:2397-2405.

Ko, K., M.J. Arauzo-Bravo, J. Kim, M. Stehling, and H.R. Schöler. 2010. Conversion of adult mouse unipotent germline stem cells into pluripotent stem cells. Nat Protoc. 5:921-928.

Ko, K., and H.R. Schöler. 2006. Embryonic stem cells as a potential source of gametes. Semin Reprod Med. 24:322-329.

Ko, K., N. Tapia, G. Wu, J.B. Kim, M.J. Bravo, P. Sasse, T. Glaser, D. Ruau, D.W. Han, B. Greber, K. Hausdorfer, V. Sebastiano, M. Stehling, B.K. Fleischmann, O. Brustle, M. Zenke, and H.R. Schöler. 2009. Induction of pluripotency in adult unipotent germline stem cells. Cell Stem Cell. 5:87-96.

Ko, K., G. Wu, M.J. Arauzo-Bravo, J. Kim, J. Francine, B. Greber, J. Muhlisch, J.Y. Joo, D. Sabour, M.C. Fruhwald, N. Tapia, and H.R. Schöler. 2011. Autologous Pluripotent Stem Cells Generated from Adult Mouse Testicular Biopsy. Stem Cell Rev. 8:435-444.

Kubota, H., M.R. Avarbock, and R.L. Brinster. 2004. Culture conditions and single growth factors affect fate determination of mouse spermatogonial stem cells. Biol Reprod. 71:722-731.

Kubota, H., and R.L. Brinster. 2006. Technology insight: In vitro culture of spermatogonial stem cells and their potential therapeutic uses. Nat Clin Pract Endocrinol Metab. 2:99-108.

Lee, J., and T. Hirano. 2011. RAD21L, a novel cohesin subunit implicated in linking homologous chromosomes in mammalian meiosis. J Cell Biol. 192:263-276.

Lee, J., M. Kanatsu-Shinohara, K. Inoue, N. Ogonuki, H. Miki, S. Toyokuni, T. Kimura, T. Nakano, A. Ogura, and T. Shinohara. 2007. Akt mediates self-renewal division of mouse spermatogonial stem cells. Development. 134:1853-1859.

Li, Z., J.C. Wu, A.Y. Sheikh, D. Kraft, F. Cao, X. Xie, M. Patel, S.S. Gambhir, R.C. Robbins, and J.P. Cooke. 2007. Differentiation, survival, and function of embryonic stem cell derived endothelial cells for ischemic heart disease. Circulation. 116:I46-54.

Li, Z.J., Z.Z. Wang, Y.Z. Zheng, B. Xu, R.C. Yang, D.T. Scadden, and Z.C. Han. 2005. Kinetic expression of platelet endothelial cell adhesion molecule-1 (PECAM-1/CD31) during embryonic stem cell differentiation. J Cell Biochem. 95:559-570.

Maekawa, M., K. Kamimura, and T. Nagano. 1996. Peritubular myoid cells in the testis: their structure and function. Arch Histol Cytol. 59:1-13.

Marh, J., L.L. Tres, Y. Yamazaki, R. Yanagimachi, and A.L. Kierszenbaum. 2003. Mouse round spermatids developed in vitro from preexisting spermatocytes can produce normal offspring by nuclear injection into in vivo-developed mature oocytes. Biol Reprod. 69:169-176.

Mariappan, D., J. Winkler, S. Chen, H. Schulz, J. Hescheler, and A. Sachinidis. 2009. Transcriptional profiling of CD31(+) cells isolated from murine embryonic stem cells. Genes Cells. 14:243-260.

Mark, M., H. Jacobs, M. Oulad-Abdelghani, C. Dennefeld, B. Feret, N. Vernet, C.A. Codreanu, P. Chambon, and N.B. Ghyselinck. 2008. STRA8-deficient spermatocytes initiate, but fail to complete, meiosis and undergo premature chromosome condensation. J Cell Sci. 121:3233-3242.

Martins, M.R., and J.R. Silva. 2001. Ultrastructure of spermatogonia and primary spermatocytes of C57BL6J mice. Anat Histol Embryol. 30:129-132.

Matoba, S., and A. Ogura. 2011. Generation of functional oocytes and spermatids from fetal primordial germ cells after ectopic transplantation in adult mice. Biol Reprod. 84:631-638.

Matsui, Y., K. Zsebo, and B.L. Hogan. 1992. Derivation of pluripotential embryonic stem cells from murine primordial germ cells in culture. Cell. 70:841-847.

Matsumura, T., K. Wolff, and P. Petzelbauer. 1997. Endothelial cell tube formation depends on cadherin 5 and CD31 interactions with filamentous actin. J Immunol. 158:3408-3416.

Mauduit, C., G. Chatelain, S. Magre, G. Brun, M. Benahmed, and D. Michel. 1999. Regulation by pH of the alternative splicing of the stem cell factor pre-mRNA in the testis. J Biol Chem. 274:770-775.

Mauduit, C., S. Hamamah, and M. Benahmed. 1999. Stem cell factor/c-kit system in spermatogenesis. Hum Reprod Update. 5:535-545.

McCloskey, K.E., D.A. Smith, H. Jo, and R.M. Nerem. 2006. Embryonic stem cell-derived endothelial cells may lack complete functional maturation in vitro. J Vasc Res. 43:411-421.

McLaren, A. 2003. Primordial germ cells in the mouse. Dev Biol. 262:1-15.

Mendis-Handagama, S.M. 1997. Luteinizing hormone on Leydig cell structure and function. Histol Histopathol. 12:869-882.

Meng, X., M. Lindahl, M.E. Hyvonen, M. Parvinen, D.G. de Rooij, M.W. Hess, A. Raatikainen-Ahokas, K. Sainio, H. Rauvala, M. Lakso, J.G. Pichel, H. Westphal, M. Saarma, and H. Sariola. 2000. Regulation of cell fate decision of undifferentiated spermatogonia by GDNF. Science. 287:1489-1493.

Mithraprabhu, S., and K.L. Loveland. 2009. Control of KIT signalling in male germ cells: what can we learn from other systems? Reproduction. 138:743-757.

Mollenhauer, H.H., D.J. Morre, and W.J. Vanderwoude. 1976. Endoplasmic reticulum-Golgi apparatus associations in maize root tips. Mikroskopie. 31:257-272.

Molyneaux, K.A., J. Stallock, K. Schaible, and C. Wylie. 2001. Time-lapse analysis of living mouse germ cell migration. Dev Biol. 240:488-498.

Nagano, M., B.Y. Ryu, C.J. Brinster, M.R. Avarbock, and R.L. Brinster. 2003. Maintenance of mouse male germ line stem cells in vitro. Biol Reprod. 68:2207-2214.

Nakanishi, T., M. Ikawa, S. Yamada, M. Parvinen, T. Baba, Y. Nishimune, and M. Okabe. 1999. Real-time observation of acrosomal dispersal from mouse sperm using GFP as a marker protein. FEBS Lett. 449:277-283.

Nakanishi, T., M. Ikawa, S. Yamada, K. Toshimori, and M. Okabe. 2001. Alkalinization of acrosome measured by GFP as a pH indicator and its relation to sperm capacitation. Dev Biol. 237:222-231.

Oatley, J.M., M.R. Avarbock, and R.L. Brinster. 2007. Glial cell line-derived neurotrophic factor regulation of genes essential for self-renewal of mouse spermatogonial stem cells is dependent on Src family kinase signaling. J Biol Chem. 282:25842-25851.

Oatley, J.M., M.R. Avarbock, A.I. Telaranta, D.T. Fearon, and R.L. Brinster. 2006. Identifying genes important for spermatogonial stem cell self-renewal and survival. Proc Natl Acad Sci U S A. 103:9524-9529.

Oatley, J.M., and R.L. Brinster. 2012. The germline stem cell niche unit in Mammalian testes. Physiol Rev. 92:577-595.

Ogawa, T., J.M. Arechaga, M.R. Avarbock, and R.L. Brinster. 1997. Transplantation of testis germinal cells into mouse seminiferous tubules. Int J Dev Biol. 41:111-122.

Okita, K., T. Ichisaka, and S. Yamanaka. 2007. Generation of germline-competent induced pluripotent stem cells. Nature. 448:313-317.

Panneerdoss, S., A.B. Siva, D.B. Kameshwari, N. Rangaraj, and S. Shivaji. 2012. Association of Lactate, Intracellular pH and Intracellular Calcium During Capacitation and Acrosome Reaction: Contribution of Hamster Sperm Dihydrolipoamide Dehydrogenase, the E3 Subunit of Pyruvate Dehydrogenase Complex. J Androl. 33:699-710.

Pellegrini, M., P. Grimaldi, P. Rossi, R. Geremia, and S. Dolci. 2003. Developmental expression of BMP4/ALK3/SMAD5 signaling pathway in the mouse testis: a potential role of BMP4 in spermatogonia differentiation. J Cell Sci. 116:3363-3372.

Pesce, M., X. Wang, D.J. Wolgemuth, and H. Schöler. 1998. Differential expression of the Oct-4 transcription factor during mouse germ cell differentiation. Mech Dev. 71:89-98.

Prabhu, S.M., M.L. Meistrich, E.A. McLaughlin, S.D. Roman, S. Warne, S. Mendis, C. Itman, and K.L. Loveland. 2006. Expression of c-Kit receptor mRNA and protein in the developing, adult and irradiated rodent testis. Reproduction. 131:489-499.

Rafii, S., and D. Lyden. 2003. Therapeutic stem and progenitor cell transplantation for organ vascularization and regeneration. Nat Med. 9:702-712.

Rajender, S., P. Rahul, and A.A. Mahdi. 2010. Mitochondria, spermatogenesis and male infertility. Mitochondrion. 10:419-428.

Resnick, J.L., L.S. Bixler, L. Cheng, and P.J. Donovan. 1992. Long-term proliferation of mouse primordial germ cells in culture. Nature. 359:550-551.

Ryu, B.Y., K.E. Orwig, J.M. Oatley, M.R. Avarbock, and R.L. Brinster. 2006. Effects of aging and niche microenvironment on spermatogonial stem cell self-renewal. Stem Cells. 24:1505-1511.

Saitou, M. 2009. Germ cell specification in mice. Curr Opin Genet Dev. 19:386-395.

Sasaki, H., and Y. Matsui. 2008. Epigenetic events in mammalian germ-cell development: reprogramming and beyond. Nat Rev Genet. 9:129-140.

Sato, T., K. Katagiri, A. Gohbara, K. Inoue, N. Ogonuki, A. Ogura, Y. Kubota, and T. Ogawa. 2011. In vitro production of functional sperm in cultured neonatal mouse testes. Nature. 471:504-507.

Sato, T., T. Yokonishi, M. Komeya, K. Katagiri, Y. Kubota, S. Matoba, N. Ogonuki, A. Ogura, S. Yoshida, and T. Ogawa. 2012. Testis tissue explantation cures spermatogenic failure in c-Kit ligand mutant mice. Proc Natl Acad Sci U S A. 109:16934-16938.

Schmidt, J.A., L.K. Abramowitz, H. Kubota, X. Wu, Z. Niu, M.R. Avarbock, J.W. Tobias, M.S. Bartolomei, and R.L. Brinster. 2011. In vivo and in vitro aging is detrimental to mouse spermatogonial stem cell function. Biol Reprod. 84:698-706.

Schramm, S., J. Fraune, R. Naumann, A. Hernandez-Hernandez, C. Hoog, H.J. Cooke, M. Alsheimer, and R. Benavente. 2011. A novel mouse synaptonemal complex protein is essential for loading of central element proteins, recombination, and fertility. PLoS Genet. 7:e1002088.

Schrans-Stassen, B.H., H.J. van de Kant, D.G. de Rooij, and A.M. van Pelt. 1999. Differential expression of c-kit in mouse undifferentiated and differentiating type A spermatogonia. Endocrinology. 140:5894-5900.

Takahashi, K., K. Tanabe, M. Ohnuki, M. Narita, T. Ichisaka, K. Tomoda, and S. Yamanaka. 2007. Induction of pluripotent stem cells from adult human fibroblasts by defined factors. Cell. 131:861-872.

Takahashi, K., and S. Yamanaka. 2006. Induction of pluripotent stem cells from mouse embryonic and adult fibroblast cultures by defined factors. Cell. 126:663-676.

Vittet, D., M.H. Prandini, R. Berthier, A. Schweitzer, H. Martin-Sisteron, G. Uzan, and E. Dejana. 1996. Embryonic stem cells differentiate in vitro to endothelial cells through successive maturation steps. Blood. 88:3424-3431.

Voyta, J.C., D.P. Via, C.E. Butterfield, and B.R. Zetter. 1984. Identification and isolation of endothelial cells based on their increased uptake of acetylated-low density lipoprotein. J Cell Biol. 99:2034-2040.

Wang, H., S. Yan, H. Chai, G.M. Riha, M. Li, Q. Yao, and C. Chen. 2006. Shear stress induces endothelial transdifferentiation from mouse smooth muscle cells. Biochem Biophys Res Commun. 346:860-865.

Watt, S.M., S.E. Gschmeissner, and P.A. Bates. 1995. PECAM-1: its expression and function as a cell adhesion molecule on hemopoietic and endothelial cells. Leuk Lymphoma. 17:229-244.

Wolgemuth, D.J. 2006. Making the commitment to meiosis. Nat Genet. 38:1362-1363.

Wu, G., L. Gentile, J.T. Do, T. Cantz, J. Sutter, K. Psathaki, M.J. Arauzo-Bravo, C. Ortmeier, and H.R. Schöler. 2011. Efficient derivation of pluripotent stem cells from siRNA-mediated Cdx2-deficient mouse embryos. Stem Cells Dev. 20:485-493.

Xiao, N., C. Kam, C. Shen, W. Jin, J. Wang, K.M. Lee, L. Jiang, and J. Xia. 2009. PICK1 deficiency causes male infertility in mice by disrupting acrosome formation. J Clin Invest. 119:802-812.

Yamashita, J., H. Itoh, M. Hirashima, M. Ogawa, S. Nishikawa, T. Yurugi, M. Naito, and K. Nakao. 2000. Flk1-positive cells derived from embryonic stem cells serve as vascular progenitors. Nature. 408:92-96.

Yan, W. 2009. Male infertility caused by spermiogenic defects: lessons from gene knockouts. Mol Cell Endocrinol. 306:24-32.

Yao, R., C. Ito, Y. Natsume, Y. Sugitani, H. Yamanaka, S. Kuretake, K. Yanagida, A. Sato, K. Toshimori, and T. Noda. 2002. Lack of acrosome formation in mice lacking a Golgi protein, GOPC. Proc Natl Acad Sci U S A. 99:11211-11216.

Ying, Y., X. Qi, and G.Q. Zhao. 2002. Induction of primordial germ cells from pluripotent epiblast. ScientificWorldJournal. 2:801-810.

Yomogida, K., Y. Yagura, Y. Tadokoro, and Y. Nishimune. 2003. Dramatic expansion of germinal stem cells by ectopically expressed human glial cell line-derived neurotrophic factor in mouse Sertoli cells. Biol Reprod. 69:1303-1307.

Yoshinaga, K., S. Nishikawa, M. Ogawa, S. Hayashi, T. Kunisada, and T. Fujimoto. 1991. Role of c-kit in mouse spermatogenesis: identification of spermatogonia as a specific site of c-kit expression and function. Development. 113:689-699.

Young, P.P., A.A. Hofling, and M.S. Sands. 2002. VEGF increases engraftment of bone marrow-derived endothelial progenitor cells (EPCs) into vasculature of newborn murine recipients. Proc Natl Acad Sci U S A. 99:11951-11956.

Zhu, Y., H.L. Hu, P. Li, S. Yang, W. Zhang, H. Ding, R.H. Tian, Y. Ning, L.L. Zhang, X.Z. Guo, Z.P. Shi, Z. Li, and Z. He. 2012. Generation of male germ cells from induced pluripotent stem cells (iPS cells): an in vitro and in vivo study. Asian J Androl. 14:574-579.

Andras Nagy, Marina Gertsenstein, Kristina Vintersten. Richard Behringer. 2002, Manipulating the Mouse Embryo, Third Edition, Cold Spring Harbor Laboratory Press.

Joachim Ude, Michael Koch. 2002, Die Zelle, Atlas der Ultrastruktur, Heidelberg, Berlin, Spektrum.

Neil A. Campbell, Jane B. Reece. 2001 Biology, Sixth Edition, Benjamin-Cummings Publishing Company.

Russell LD, Ettlin RA, Hikim AP, Clegg ED. 1990. Mammalian spermatogenesis. In: Histological and Histopathological Evaluation of the Testis. Florida: Cache River.

Sharpe R. 1994. Regulation of spermatogenesis. In: The Physiology of Reproduction, edited by Knobil E, Neill JD. vol. 1. New York: Raven.

8. Abbreviations

AP	alkaline phosphatase
APC	allophycocyanin
BS	Bandeiraea simplicifolia
BSA	bovine serum albumin
BMP	bone morphogenetic protein
° C	degree Celsius
cDNA	complementary deoxyribonucleic acid
CE	central element
CM	conditioned medium
DAPI	4’-6-Diamidino-2-phenylindole
DMEM	dulbecco’s minimal eagle’s medium
DMEM/F12	dulbecco’s minimal eagle’s medium: Nutrient Mixture F-12
DMSO	dimethyl sulfoxide
DNA	deoxyribonucleic acid
DNase	deoxyribonuclease
dNTP	desoxyribonucleosid triphosphate
dpc	days post coitum
DTT	dithiothreitol
E	embryonic day
EB	embryoid body
ECs	endothelial cells

EDTA	ethylenediaminetetraacetate
EGF	epidermal growth factor
EGCs	embryonic germ cells
ESCs	embryonic stem cells
FACS	fluorescence activated cell sorting
FBS	fetal bovine serum
FGF	fibroblast growth factor
FSH	follicle-stimulating hormone
GDNF	glial cell line-derived neurotrophic factor
GFP	green fluorescence protein
Gfrα1	GDNF family receptor alpha 1
GSCs	germline stem cells
GPI	glycosylphosphatidylinositol
gPSCs	germline-derived pluripotent stem cells
HEPES	4-(2-hydroxyethyl)-1-piperazineethanesulfonic acid
hESCs	human embryonic stem cells
hGH	human growth hormone
min	miniute
h	hour
ICM	inner cell mass
ICSI	intracytoplasmic sperm injection
IGF	insulin-like growth factor
IMDM	iscove’s modified dulbecco’s medium
iPSCs	induced pluripotent stem cells
KO	knockout

KOSR	knockout serum replacement
KSOM	potassium simplex optimized medium
LDL	low-density lipoprotein
LE	lateral element
LIF	leukemia inhibitory factor
MEFs	mouse embryonic fibroblasts
MEM	minimal essential medium
NEAA	non-essential amino acid
PBS	phosphate buffered saline
PC	principal component
PE	phycoerythrin
PFA	paraformaldehyde
PGCs	primordial germ cells
PI3K	phophoinositide 3-kinase
PMSF	phenylmethylsulfonyl fluoride
PND	postnatal day
PVP	polyvinylpyrrolidone
RA	retinoic acid
ROSI	round spermatid injection
RNA	ribonucleic acid
RT	room temperature
RT-PCR	reverse transcriptase polymerase chain reaction
s	second
SC	synaptonemal complex
Scp	synaptonemal complex protein

SFK	src family kinase
SSCs	spematogonial stem cells
SCF	stem cell factor
T	testosterone
TEM	transmission electron microscopy
TGF	transforming growth factor
VEGF	vascular endothelial growth factor
w/v	weight/volume
v/v	volume/volume

9. List of figures

Figure 1. Germ cell development (figure modified from Sasaki *et al*, *Nature Reviews Genetics*, 2008).
Figure 2. Mitotic division of spermatogonia in mouse and primate (figure modified from Oatley and Brinster, *Physiol Rew*, 2012).
Figure 3. Schematic description of spermatogenesis (figure modified from Wolgemuth, *Nature Genetics*, 2006).
Figure 4. Different stage in prophase I of meiosis (figure modified from Lee *et al*, *J Cell Biol*, 2011.
Figure 5. The multiple steps in the mouse spermiogenesis (figure modified from Yan *et al*, *Molecular and cellular Endocrinology*, 2009).
Figure 6. Signaling pathway in spermatogonial stem cells (figure from Oatley *et al*, *Annu. Rev. Cell Dev. Biol*, 2008).
Figure 7. Testicular transplantation (figure modified from Kubota *et al*, *Nat Clin Pract Endocrino Metabol*, 2006).
Figure 8. Schematic illustration of seminiferous tubules in testis (figure modified from Cooke *et al*, *Nature Reviews Genetics*, 2002).
Figure 9. c-kit expression in different type of spermatogenetic cells (figure modified from Yoshinaga *et al*, *Development*, 1991).
Figure 10. Schematic presentation of studies performed on GSCs in this thesis.
Figure 11. Morphology of *Oct4-GFP* GSCs at passage 42.
Figure 12. Flow cytometry analysis of *in vitro* cultured GSCs.
Figure 13. Morphology of human testicular cells grown on gelatin- or collagen IV-coated wells.
Figure 14. Morphology of human testicular cells grown on MEFs.
Figure 15. Morphology of human embryonic stem cells (WA09/H9) grown on MEFs and matrigel-coated wells.
Figure 16. Flow cytometry analysis of the TRA1-81 surface antigen.
Figure 17. Derivation of autologous GSC cell lines and their conversion into gPSC cell lines.

Figure 18. Reprogramming of GSCs into gPSCs (figure from Ko *et al*, *Nature Protocols*, 2010).
Figure 19. Morphology and *Oct4-GFP* expression within GSC colonies (figures from Ko *et al*, *Stem cells Rev and Rep*, 2011).
Figure 20. LacZ staining of GSCs (figures from Ko *et al*, *Stem cells Rev and Rep*, 2011).
Figure 21. RT-PCR analysis of GSCs (figure from Ko *et al*, *Stem cells Rev and Rep*, 2011).
Figure 22. Testicular transplantation with GSCs (figures from Ko *et al*, *Stem cells Rev and Rep*, 2011).
Figure 23. RT-PCR analysis of GSCs and gPSCs (figures from Ko *et al*, *Stem cells Rev and Rep*, 2011).
Figure 24. Phenotypical analysis of gPSCs (figures from Ko *et al*, *Stem cells Rev and Rep*, 2011).
Figure 25. Pairwise scatter plot of GSC versus GSCr.
Figure 26. Pairwise scatter plot of gPSCs versus gPSCr.
Figure 27. Pairwise scatter plot between GSC, gPSC, and ESC.
Figure 28. Micro array data using Principal Component Analysis (PCA) and Hierarchical clustering (figure from Ko *et al*, Stem cells Rev and *Rep*, 2011).
Figure 29. Analysis of heat-map and map of distances.
Figure 30. Differentiation of gPSCs into ectoderm lineage (figures from Ko *et al*, *Stem cells Rev and Rep*, 2011).
Figure 31. Teratoma formation after injection of gPSCs (figures from Ko *et al*, *Stem cells Rev and Rep*, 2011).
Figure 32. Generation of chimeric embryos and germline transmission (figures from Ko *et al*, *Stem cells Rev and Rep*, 2011).
Figure 33. Derivation of EC-like cells from gPSCs.
Figure 34. Morphological analysis of gPSC-derived EC-like cells.
Figure 35. Real-time RT-PCR analysis of gPSC-derived EC-like cells.
Figure 36. Flow cytometric analyses of gPSC-derived EC-like cells.
Figure 37. Immunocytochemical analyses of gPSC-derived EC-like cells.
Figure 38. LDL uptake analysis of gPSC-derived EC-like cells.
Figure 39. *In vitro* functional analysis of gPSC-derived EC-like cells.
Figure 40. Stepwise induction of differentiation potential of GSCs.

Figure 41. Flow cytometry analysis of *in vitro*-generated cells on different days of culture.
Figure 42. Scp3 staining of *in vitro*-differentiated cells.
Figure 43. TEM images of different *in vivo* stages of spermatogenetic cells during spermatogenesis.
Figure 44. Ultrastructure showing *in vivo* spermiogenetic cells.
Figure 45. TEM images of *in vitro*-derived cells, Sertoli cell, and GSC.
Figure 46. Real-time RT-PCR analysis of *in vitro*-differentiated cells from GSCs.
Figure 47. Schematic procedure of ROSI followed by embryo transfer and derivation of ESCs.
Figure 48. Embryonic development after round spermatid injection.
Figure 49. Flow cytometry analysis of SSEA1-stained ROSI-derived ESCs.
Figure 50. Karyotyping analysis of ROSI-derived ESC line numbers 1 to 4.
Figure 51. DNA methylation analysis of ROSI-derived ESCs.
Figure 52. Genotyping analysis and karyotyping analysis of ROSI-derived *Acrosin* ESCs.
Figure 53. Morphology of *Acrosin* GSCs.
Figure 54. Morphology of OG2 x *Acrosin-EGFP* GSCs.

10. List of tables

Table 1. Sequences of oligonucleotide primers for RT-PCR
Table 2. Sequences of oligonucleotide primers for Real-time RT-PCR
Table 3. Sequences of oligonucleotide primers for genotyping
Table 4. Sequences of oligonucleotide primers for DNA methylation analysis
Table 5. Culture of human testicular biopsies under various conditions
Table 6. Semi-quantitative analysis of *in vitro*-derived spermatocytes
Table 7. Summarized results of round spermatid injection

11. Appendix

11.1 Companies

Accutase	PAA Laboratories
Alexa 488-conjugated anti-rat IgG antibody	Invitrogen
Alexa 568-conjugated anti-mouse IgG antibody	Invitrogen
Alkaline phosphatase staining Kit	Chemicon
APC-conjugated anti-c-kit antibody	BD Bioscience
Ascorbic acid	Sigma-Aldrich
Bouin's Solution	Sigma-Aldrich
BSA fraction V solution	Invitrogen
Busulfan	Sigma-Aldrich
Cacodylate	Science services
Collagenase IV	Sigma-Aldrich
Collagen IV	Sigma-Aldrich
Conical tube	SARSTEDT
Cryotube	Nunc
DAPI containing mounting medium	Vector Laboratories
Dimethyl sulfoxide	Sigma-Aldrich
DNase I	Sigma-Aldrich
DMEM	PAA Laboratories
DMEM/F-12	Invitrogen
DTT	Sigma-Aldrich
EGF	Peprotech
EpiTect Bisulfite Kit	Quiagen
Epon-812	Fluka
Eppendorf tube	Eppendorf
Estrogen	Sigma-Aldrich
Ethanol	Sigma-Aldrich
FastRed	Sigma-Aldrich
FBS	Biowest, PAN
FGF2	Peprotech

Follicle-stimulating hormone	Sigma-Aldrich
Gelatin	Sigma-Aldrich
GDNF	Peprotech
D-(+)-glucose solution	Sigma-Aldrich
GlutaMax-I	Invitrogen
glutaraldehyde	Merck
L-glutamine/penicillin/streptomycin	PAA Laboratories
HEPES	Invitrogen
hGH	Prospec
high capacity cDNA Reverse Transcription Kit	Applied Biosystems
Horse serum	Biochrom
Hyaluronidase	Sigma-Aldrich
IGF1	Prospec
Isopropanol	Sigma-Aldrich
Insulin transferrin selenium-A solution	Invitrogen
KO DMEM/Ham’s	Invitrogen
KO serum replacement	Invitrogen
DL-lactic acid	Sigma-Aldrich
lead citrate	Science services
MEM medium	Sigma-Aldrich
MEM vitamins	Invitrogen
β-Mercaptoethanol	PAA Laboratories
Methanol	Sigma-Aldrich
Naphthol phosphate	Sigma-Aldrich
N2 supplement	Invitrogen
Non-essential amino acid	PAA Laboratories
Osmium Tetroxide	Science services
Paraformaldehyde	Sigma-Aldrich
PBS	PAA Laboratories
PE-conjugated anti-SSEA1 antibody	BD Bioscience
PE-conjugated IgM antibody	BD Bioscience
PE-conjugated anti-CD31 antibody	Biozol
PE-conjugated anti-Flk1 antibody	eBioscience

PE-conjugated IgG control antibody	BD Bioscience
Penicillin/streptomycin	PAA Laboratories
Photoflo	Tetenal
Progesterone	Sigma-Aldrich
Rat IgG control antibody	BD Bioscience
Retinoic acid	Sigma-Aldrich
RNeasy mini and micro Kit	Quiagen
Scp3 antibody	Abcam
Sodium pyruvic acid stock solution	PAA Laboratories
SSEA1 antibody	Abcam
StemPro-34 SFM	Invitrogen
Syringe	BD Plastipak
Testosterone	Fluka
Tissue culture plates and dishes	SARSTEDT
Triton X-100	Sigma-Aldrich
TRA1-81 antibody	Chemicon
Trypsin/EDTA	PAA Laboratories
TuJ1 antibody	Chemicon
Uranyl acetate	Science services
VEGF	Prospec
von Willebrand Factor antibody	DAKO